Doctoral Dissertation

博士論文

Theoretical Study of Binary Bose-Einstein Condensates under Synthetic Gauge Fields

（人工ゲージ場下の二成分ボース・アインシュタイン凝縮体の理論的研究）

A Dissertation Submitted for the Degree of Doctor of Philosophy

December 2020

令和２年１２月博士（理学）申請

Department of Physics, Graduate School of Science,
The University of Tokyo

東京大学大学院理学系研究科

物理学専攻

Takumi Yoshino

吉野　匠

Abstract

Bose-Einstein condensates (BECs) in ultracold atomic gas have been studied intensively, since the state of atoms is well controlled by lasers and external electromagnetic fields. Synthetic gauge fields can be induced in a charge-neutral system by mechanical rotation of the system or by using lasers. In a BEC under a synthetic gauge fields, a quantized vortex or a vortex lattice, where multiple quantized vortices are periodically located, are observed. In binary BECs composed of bosonic atoms in two hyperfine states, parallel and antiparallel synthetic gauge fields are induced by the former (mechanical rotation) and the latter (laser) techniques, respectively. In the mean-field theory, vortex lattices appear with various configurations which depend on the ratio of the intercomponent interaction to the intracomponent one. While the ground-state phase diagrams for parallel and antiparallel fields are the same in the mean-field regime, two phase diagrams are significantly different in the quantum Hall regime, where a magnetic field is strong.

In the first part of this thesis, we study the excitation spectra, correlation functions and the quantum depletion of vortex lattices by means of the effective-field theory and the Bogoliubov theory under the lowest-Landau-level (LLL) approximation. We obtain the effective-field theory of vortex lattices in binary BECs by introducing the missing elastic energy term from the symmetry consideration. By renormalizing the coupling constants, we find the effective-field theory for strong magnetic fields so that we can compare it with the Bogoliubov theory. We obtain the analytical expression of the dispersion relations for parallel and antiparallel fields by diagonalizing the effective Hamiltonian and the rescaling relations between them. From the rescaling relations, we clarify that the different excited states for parallel and antiparallel fields are indeed related to each other. By calculating the correlation function, we show that a one-particle density matrix exhibits a quasi-long-range order and that the fraction of depletion increases logarithmically with respect to the number of fluxes. By means of the Bogoliubov theory, we numerically obtain energy spectra with quadratic and linear dispersion relations for parallel and antiparallel fields and confirm the rescaling relations for all the phases. We find that the quantum depletion depends crucially on the direction of synthetic gauge fields and diverges logarithmically with respect to the number of fluxes. By calculating the correction to the ground-state energy due to zero-point fluctuations by the Bogoliubov theory, we show that the transition points shift appreciably due to quantum fluctuations. Furthermore, we show that the variations of an inner angle and an aspect ratio with respect to the ratio of interactions are altered from those obtained by the mean-field theory for rhombic and rectangular lattices, respectively. We find that the quantum fluctuation changes the ground-state phase diagram and leads to the distinction between the phase diagrams for parallel and antiparallel fields which are unique to binary BECs. Moreover, we relate the quantum depletion to shifts of the transition points since the phase diagram is largely modified when the quantum depletion which characterizes the quantum fluctuation is also large.

In the second part of the present thesis, we study the intercomponent entanglement spectrum (ES) and entanglement entropy (EE) of vortex lattices in binary BECs by exploiting the formalisms developed in the first part. By means of the effective-field theory, we show that the ES exhibits a square-root dispersion relation for all the phases and that the rescaling relation holds between the ESs for parallel and antiparallel fields, similarly to the energy spectra. We confirm these predictions through a numerical calculation by

the Bogoliubov theory. We discuss which collective modes contribute to the EE since the ES characterizes the intercomponent entanglement of the excited states. Furthermore, we show that the unusual square-root dispersion relation of the ES is related to the emergence of a long-range interaction in the entanglement Hamiltonian, similarly to the case of two coupled non-chiral Tomonaga-Luttinger liquids studied previously, which may be related to the emergence of the long-range interaction in the subsystem. In particular, we derive the explicit form of the entanglement Hamiltonian for the overlapping triangular lattices. Using the obtained ES, we further show that the leading term of the intercomponent EE is proportional to the volume of the system, as is typical of an extensive partition, and that for the repulsive (attractive) intercomponent interaction, the proportionality constant for parallel (antiparallel) gauge fields is larger than that for antiparallel (parallel) gauge fields. This behavior of the intercomponent EE is qualitatively consistent with the ground-state phase diagrams in the quantum Hall regime. Since both the ground-state phase diagram with the quantum correction and the EE are determined by the excitation spectra, the feature of the EE is reflected in the corrected ground state, so that we can impose a restriction to the corrected ground state although the rigorous ground state is hard to obtain. For instance, we infer that the regime where the ground states similar to the product states appear can be determined from the EE. In a system with a continuous symmetry breaking, the EE is known to have a subleading term that scales logarithmically with respect to the length scale L. By studying an analogous term in the present setup, we show that the subleading term scales logarithmically with respect to the number of fluxes and numerically confirm that the coefficient of the logarithmic term is close to $1/4$. Since the subleading term is obtained from the Nambu-Goldstone modes, we find that the logarithmical contribution to the intercomponent EE is related to the symmetries which are spontaneously broken in the vortex lattices.

List of Publications

This Thesis is based on the following publications.

1. *Collective modes of vortex lattices in two-component Bose-Einstein condensates under synthetic gauge fields*
   Takumi Yoshino, Shunsuke Furukawa, Sho Higashikawa, and Masahito Ueda,
   New Journal Physics **21**, 015001 (2019).

2. *Vortex lattices in binary Bose-Einstein condensates: Collective modes, quantum fluctuations, and intercomponent entanglement*
   Takumi Yoshino, Shunsuke Furukawa and Masahito Ueda,
   in preparation.

The following publications are related but are not claimed in this Thesis.

1. *Intercomponent entanglement entropy and spectrum in binary Bose-Einstein condensates*
   Takumi Yoshino, Shunsuke Furukawa and Masahito Ueda,
   arXiv:2009.02949 (2020).

Abbreviations

BEC	Bose-Einstein condensation
GP	Gross-Pitaevski
LLL	lowest Landau level
ES	entanglement spectrum
EE	entanglement entropy
TLL	Tomonaga-Luttinger liquid

Contents

Chapter 1

Introduction

1.1 Bose-Einstein condensates of ultracold atoms and vortex lattices

Bose-Einstein condensates (BECs) in the ultracold dilute gases of alkali atoms have been created by using laser cooling techniques [1–3]. With the development of atomic, molecular and optical physics, a quantum-state engineering of the BEC has been carried out. For instance, alkali atoms have internal degrees of freedom due to their hyperfine spin states, which can be manipulated by an external fields. Moreover, the atom-atom interaction can be tuned by a field-induced Feshbach resonance. The static and dynamic features of the BECs described in terms of a macroscopic condensate wave function Φ have been studied by a nonlinear Schrödinger equation which is called the Gross-Pitaevskii (GP) equation.

BECs have also been observed in multi-component systems. Two-component (binary) BECs have been created in a mixture of ^{87}Rb atoms in two different hyperfine states [4]. Binary BECs have also been created by using a mixture of two different species of bosons of, e.g., ^{41}K and ^{87}Rb [5]. Furthermore, spinor BECs using atoms with the magnetic quantum numbers $m_F = 0, \pm 1$ and the total spin $F = 1$ have been investigated. Spinor BECs exhibit various phases depending on the coupling constants and the strength of the magnetic field [6]. BECs with three or more components have also been created in experiments [7–9].

A quantized vortex was observed for the first time in a rotating superfluid helium 4 [10]. In BEC, a quantized vortex has been first realized by the phase imprinting technique [11]. Later a single vortex and multiple vortices have been observed by rotating the potential which traps the atoms [12]. When a vortex appears in the two-dimensional system, the vorticity of the superfluid velocity $\mathbf{v} = \hbar\nabla\phi/M$, where ϕ is the phase of the condensate wave function $\Phi = |\Phi|e^{i\phi}$, is nonzero. This fact indicates that the phase ϕ has a singularity at the location of the vortex. By integrating the vorticity over the two-dimensional surface S containing the singularity, we obtain the nonzero circulation $\kappa = \int_S \mathrm{d}\mathbf{S} \cdot \nabla \times \mathbf{v} = \oint_C \mathrm{d}\mathbf{l} \cdot \mathbf{v} = h/M \times m$ ($m \in$ integer), which is quantized in units of h/M. Although atomic gases are charge-neutral, the mechanical rotation of the system creates a synthetic magnetic field because of the equivalence between the Lorentz force and the Coriolis force in the rotating frame of reference. By considering the effective

Hamiltonian in the rotating frame of reference, we find the strength of the magnetic field increases as the angular frequency of the rotation increases.

When the angular frequency of the rotation increases, the BEC establishes an array of singly quantized vortex lines ($|m| = 1$) along the rotation axes rather than a single multiply charged vortex line ($|m| > 1$). The ground state of the vortex lattices for a relatively slowly rotating regime has been studied using the Thomas-Fermi approximation. Here, it is assumed that the intervortex separation is larger than the healing length, which gives a typical length scale of the vortex core. In a rapidly rotating regime which we consider in this thesis, the ground state is given by a wavefunction in the LLL manifold [13]. By rotating the trapping potential for a scalar BEC, the triangular vortex lattice has been observed in both the slowly rotating regime [14, 15] and the rapidly rotating regime [16].

When a system of binary BECs is rotated, parallel synthetic magnetic fields, whose magnitudes and directions are the same between the two components, emerge. Vortex lattices for a binary system present various structures depending on the ratio of the intercomponent interaction to the intracomponent one [17, 18]. In particular, square lattices, which are unique to the binary case, have been observed in a gas of ^{87}Rb atoms [19]. Meanwhile, antiparallel synthetic magnetic fields, whose directions are opposite for the two components, are induced by controlling the phase of the atoms via an atom-light coupling [20]. A geometric vector potential has been realized by utilizing spatially varying internal states, which have been obtained by extending the scheme for creating a spin-orbit coupling in BECs [21]. Antiparallel fields can be naturally induced in the two components because of the zero-sum rule for the geometric potentials. By using the synthetic gauge field technique, vortices have been created in a scalar BEC [22]. While vortex lattices under antiparallel synthetic magnetic fields have not been realized, the ground state has been shown to exhibit a phase diagram equivalent to the case of parallel magnetic fields within a GP mean-field theory [23]. However, for a strong magnetic field, i.e. for a small filling factor, the mean-field theory in general breaks down and the equivalence between the parallel- and antiparallel-field cases no longer holds. Exact diagonalization analyses for small filling factors have shown that for an attractive (repulsive) intercomponent interaction for parallel (antiparallel) magnetic fields, the ground state is well approximated by the product state of a pair of the quantum Hall states [23, 24]. In contrast, for a repulsive (attractive) intercomponent interaction for parallel (antiparallel) magnetic fields, the ground state is a spin-singlet state in which two components are highly entangled.

1.2 Entanglement entropy and spectrum

In condensed-matter systems, quantum entanglement has been utilized to explore a number of interesting properties [25]. Since the entanglement does not appear in the mean-field theory, a number of unique features of a system beyond the mean-field theory can be investigated by examining quantum entanglement. The entanglement of a many-body system is characterized by the entanglement entropy (EE), which is obtained as the von-Neuman entropy of a reduced density matrix on a subsystem. In a variety of quantum many-body systems, the leading term of the EE is proportional to the surface of the subsystem, which is known as the area law. The subleading term of the EE can be often

used to characterize the system. For instance, the subleading term that logarithmically diverges with respect to the surface of subsystem [26] appears in systems with the continuous symmetry breaking. In topologically ordered systems, a constant subleading term called a topological EE emerges [27] and it is used to detect the topological property of a system.

The entanglement spectrum (ES), which is calculated as the eigenspectrum of the reduced density matrix on a subsystem, can characterize the entanglement of the system in more detail. In topological systems in two dimensions, the ES exhibits a linear dispersion relation analogous to the edge-state energy spectrum and this fact has been proved analytically for fractional quantum Hall states [28,29]. For two coupled non-chiral Tomonaga-Luttinger liquids (TLL), the ES between two components features a square-root dispersion relation when the energy spectrum of the bulk is partially gapless [29]. This interesting feature is related with the long-range interaction in the entanglement Hamiltonian of the subsystem. For binary BECs, the intercomponent ES exhibits a square-root dispersion relation when the two components are coupled by the Rabi coupling; the ES is gapful when there is no intercomponent tunneling. These ES are also related to long-range interactions in the entanglement Hamiltoinan [30].

1.3 Issues of binary BECs

The excitation spectra for parallel and antiparallel fields are different due to the difference of the time-dependent GP equations between the two cases. It is an interesting question to ask whether the relation between the excited states for parallel and antiparallel fields which are completely different due to the distinction between the two fields exists while the ground-state phase diagrams of vortex lattices in binary BECs for parallel and antiparallel fields are equivalent in the mean-field regime. It is also important to understand the excited state in antiparallel fields since the antiparallel fields become accessible recently due to the development of the technology.

It is also an interesting question to ask how quantum fluctuations change the ground-state phase diagram, since the phase diagrams for parallel and antiparallel fields are equivalent in the mean-field theory while they are not in the quantum Hall regime. We would like to find out how quantum fluctuations correct the phase diagram in the mean-field theory and create the difference in the phase diagrams between parallel and antiparallel fields. Such a distinction in the phase diagrams between the parallel and antiparallel fields is unique in the binary system.

The ground-state phase diagram for an arbitrary filling factor has not been obtained rigorously yet. However it is hard to obtain it since the ground-state energy with the quantum correction is determined by both the ground and excited states. It is an interesting question to ask how the ground state are restricted by the intercomponent EE, which are easier to calculate and which excited states largely contribute to the intercomponent entanglement. We would like to find out whether the long-range interaction appears in the entanglement Hamiltonian since it may be related with the emergence of the long-range interaction in the subsystem. Finally, whether the logarithmic contribution of the intercomponent EE which appears in a system with a continuous symmetry breaking, also appears in the vortex lattices is important since it may relate the symmetries which

are spontaneously broken and their numbers with the EE.

1.4 Purpose of this thesis

The purpose of this thesis is to study the excited states, the ground state with the quantum correction and the intercomponent entanglement for vortex lattices in binary BECs.

First, to consider the relation between the excited states for parallel and antiparallel fields, we formulate the Bogoliubov theory and the effective-field theory of vortex lattices to study the excitation spectra. By obtaining the dispersion relations for parallel and antiparallel fields, we clarify the relation between them by deriving the rescaling relations which can be compared by the two methods. In particular, we note that a missing term in the effective-field theory, which is important for interlaced triangular lattices, is identified. Furthermore, the issue of the violation of the rescaling relations, which remained an open question in the previous research [31], is resolved by renormalization which is a prescription proposed to correct the effective-field theory.

By obtaining the quantum correction to the ground-state energy by the Bogoliubov theory, we investigate the ground-state phase diagram with the quantum correction by discussing how the transition points shift from the original points given by the mean-field theory. We explicitly find the phase diagram by taking the quantum correction into account. We also find that the quantum fluctuations leads to the distinction between the ground-state phase diagrams for parallel and antiparallel fields. Since the existence of the two types of magnetic fields are unique to the binary system, the result is also unique to such a system. Furthermore, since the quantum fluctuation is measured by the quantum depletion, we obtain its value and find that large shifts of the transition point are related to large values of the quantum depletion.

We obtain the intercomponent EE to discuss the behavior of the ground-state phase diagram with the quantum correction since both the EE and the corrected phase diagram are calculated by using the excitation spectra. Previous exact-diagonalization studies for the quantum Hall regime have shown that the product state with a small intercomponent EE appears for parallel (antiparalell) fields with an attractive (repulsive) intercomponent interaction and the spin-singlet state with a large intercomponent EE appears for parallel (antiparalell) fields with a repulsive (attractive) intercomponent interaction [23, 24]. If a similar behavior of the intercomponent EE is found in vortex lattices, we can restrict their ground-state phase diagram and expect that the restriction can be used in a wide intermediate regime between the mean-field regime and the quantum Hall regime since the vortex lattices appear when the strength of the magnetic field is lowered. In order to consider which excited states have a large contribution to the intercomponent EE, we calculate the ES whose value increases when two components are disentangled. We also discuss the ES with a square-root dispersion relation of the vortex lattices in the binary system which is expected from the gapless excitation spectra, since the ES in the cases of two coupled non-chiral TLLs and binary BECs where a gapless excitation spectrum appears has a fractional-power or gapped dispersion relation. Then, we derive an effective long-range interaction in the entanglement Hamiltonian. Finally, we obtain an additional logarithmic term in the intercomponent EE, which has appeared as a consequence of the

continuous symmetry breaking in the binary BECs. We show that it actually appears as vortex lattices of binary BECs break the $U(1) \times U(1)$ gauge symmetry and the translational symmetries. Since the subleading term of the intercomponent EE originates from the Nambu-Goldstone mode, we find that the symmetries which are spontaneously broken are related with the EE.

1.5 Organization of this thesis

This thesis is constituted by reviews and the original works on vortex lattices, and organized as follows.

In Chap. 2, we review binary BECs and synthetic gauge fields in ultracold atomic gases. In Sec. 2.1, we review the ground state of binary BECs. We discuss that the two components are separated or mixed depending on the value of the ratio of the intercomponent interaction to intracomponent one. In Sec. 2.2, we review binary BECs under parallel synthetic gauge fields. We explain that rotating neutral-charged atomic gases experience a synthetic magnetic field because of the equivalence between the Coriolis force and the Lorentz force. In analyzing the low-energy properties of a rotating system, we introduce the LLL approximation, in which the state is expanded in terms of the basis states of the LLL. This approximation is valid for a sufficiently strong magnetic field. Then we describe the mean-field theory for rapidly rotating binary BECs, in which the two components experience parallel synthetic magnetic fields. We present the ground-state phase diagram of vortex lattices under the LLL approximation with various vortex structures which depend on the ratio of the intercomponent interaction to the intracomponent one. In Sec. 2.3, we discuss the binary BECs under antiparallel synthetic magnetic fields. Using a minimal model, we explain that the synthetic gauge field is induced by the spatially dependent interaction of atoms and lasers. Then we review an experimental realization of antiparallel fields in the ultracold atomic system [20]. We argue that the phase diagram of vortex lattices for antiparallel fields are equivalent to the phase diagram for parallel fields by showing that the equivalence of the energy functionals for parallel and antiparallel fields. In Sec. 2.4, we review the ground-state phase diagrams of the binary bosonic system under parallel and antiparallel magnetic fields in the regime where the mean-field theory breaks down. These phase diagrams are presented in the plane spanned by the ratio of the coupling constants for inter- and intra-component interactions and the filling factor. We also explain that the ground states with a repulsive (attractive) intercomponent interaction for parallel fields is similar to the ground states with an attractive (replusive) intercomponent interaction for antiparallel fields.

In the following chapters, we present our original works.

In Chap. 3, we develop an effective-field theory of the vortex lattices for the binary system. In Sec. 3.1, we review the mean-field description of a vortex lattice for a scalar BEC. We separate the short-distance structure of vortices from a large-scale structure of a vortex lattice in order to introduce the renormalized coupling constant. In Sec. 3.2, we derive an effective-field theory of vortex lattices in binary BECs by extending the derivation for a scalar case. After introducing the setup of our system, we obtain an effective Hamiltonian by keeping leading terms in the derivative expansion. Then we introduce an elastic energy from a symmetry consideration. Here, we identify a

missing term which is important in discussing interlaced triangular lattices. We discuss the renormalization of the coupling constants by generalizing the argument in Sec. 3.1 to the binary system. The renormalization is crucial in order for the effective-field theory to be consistent with the Bogoliubov theory under the LLL approximation. We present the renormalization factors for inter- and intracomponent interactions in terms of the ratio of the coupling constants. In Sec. 3.3, we diagonalize the Hamiltonian obtained from the effective-field theory to obtain analytic forms of the dispersion relations. We then find rescaling relations between the dispersion relations for parallel and antiparallel fields. From rescaling relations, we relate the excited states in parallel and antiparallel fields for all the phase as the ground states for the two cases are equivalent in the mean-field theory. We also discuss that the quadratic and linear dispersion relations for parallel (antiparallel) fields are related to the in- and anti- (anti- and in-) phase oscillations, respectively, by the equation of motion. For the following chapters, we also calculate the correlation function which demonstrate a quasi-long-range order from the one-particle density matrix and the depleted density which logarithmically increases with respect to the number of the fluxes.

In Chap. 4, we formulate the Bogoliubov theory for vortex lattices in binary BECs under the LLL approximation. In Sec. 4.1, we formulate the Bogoliubov theory in the LLL approximation for a binary system. After introducing the LLL magnetic Bloch state, which is a complete orthogonal basis of the LLL manifold, we show that a periodic pattern of zeros of the basis state can be shifted by controlling the value of a wave vector so as to reproduce the displacement of vortex lattices in binary BECs. Then we employ the Bogoliubov approximation to obtain the Bogoliubov Hamiltonian in the LLL approximation. By diagonalizing the Bogoliubov Hamiltonian, we calculate the excitation spectrum and the quantum correction to the ground-state energy and we express the fraction of depletion in terms of the eigenvector. In Sec. 4.2, we present numerical results. We present the excitation spectra with quadratic and linear dispersion relations for both parallel and antiparallel synthetic gauge fields. We discuss the criterion to determine the type of the Nambu-Goldstone modes and the experiments observing the oscillation of the vortex lattices in scalar and binary BECs. We confirm the rescaling relations which are obtained in the previous chapter. Then we determine the elastic constants introduced in the effective-field theory by fitting the analytical expressions of the excitation spectra to the numerical results, so that all the parameters are determined. For all the phases, we obtain the quantum depletion and confirm its divergence with respect to the number of quantum fluxes. Finally we obtain the ground-state energy by taking the quantum correction into account and minimize it with respect to an inner angle and an aspect ratio for rhombic and rectangular lattices, respectively. We show that transition points shift appreciably and an inner angle and an aspect ratio in terms of the ratio of coupling constants vary due to the quantum correction. We discuss that quantum fluctuations lead to the distinction in the phase diagrams between parallel and antiparallel fields; we note here that these phases are equivalent in the mean-field theory. We point out such a result is unique to the binary system as the parallel and antiparallel fields only appear in such a system. We also relate a shift in the transition points to the quantum depletion.

In Chap. 5, we study the intercomponent ES and EE for vortex lattices of binary BECs. In Sec. 5.1, we review the ES and EE in condensed-matter systems. We discuss that the EE for a d-dimensional system with continuous symmetry breaking exhibits an

additional term which scales logarithmically with respect to L^{d-1}, where L is the length scale of the system. We also briefly review the studies of the ES for topological systems and spontaneously symmetry-broken systems. The low-energy regime of the ES has been found to be proportional to the dispersion relation of the edge state for topological systems. Meanwhile, the ES for two non-chiral TLLs has been found to show a square-root dispersion relation due to the emergence of the long-range interaction in the entanglement Hamiltonian. In Sec. 5.2, we calculate analytical forms of the intercomponent ES and EE for vortex lattices by means of the effective-field theory derived in Chap. 3. We obtain an analytical expression of the ES and find a rescaling relation between the ESs for parallel and antiparallel fields. Then, we find that a long-range interaction appears by calculating the entanglement Hamiltonian in a real space and its analytical expression for overlapping triangular lattices. We show that the leading contribution of the intercomponent EE is proportional to the area and its subleading term logarithmically decreses with respect to the area of the system. In Sec. 5.3, we obtain the intercomponent ES and EE using the Bogoliubov theory. After the formulation of the ES and EE, we present a numerical result of the ES, which shows a square-root dispersion relation, and confirm the rescaling relation. By calculating the intercomponent EE for all the phases, we find that its value for parallel (antiparallel) fields is larger than the other in the case of the repulsive (attractive) intercomponent interaction. The behavior of the EE is qualitatively consistent with what is expected in the quantum Hall regime. We discuss the ground-state phase diagram with the quantum correction from the standpoint of the intercomponent EE since both the quantum correction and the intercomponent EE arise from the same excitation spectra. Then we discuss which excited states have a large contribution to the EE from the ES. We find that the ES is consistent with the behavior of the EE. We also obtain the square-root dispersion of the ES as expected from the ladder system and relate it with the emergence of the long-range interaction which may appear in the subsystem at absolute zero. Finally we consider the logarithmic contribution of the intercomponent EE which arise from the Nambu-Goldstone modes, so that the obtained EE is related with the continuous symmetry breaking.

In Chap. 6, we conclude the thesis by giving a summary and future prospects.

The relations between chapters are depicted in Fig. 1.1.

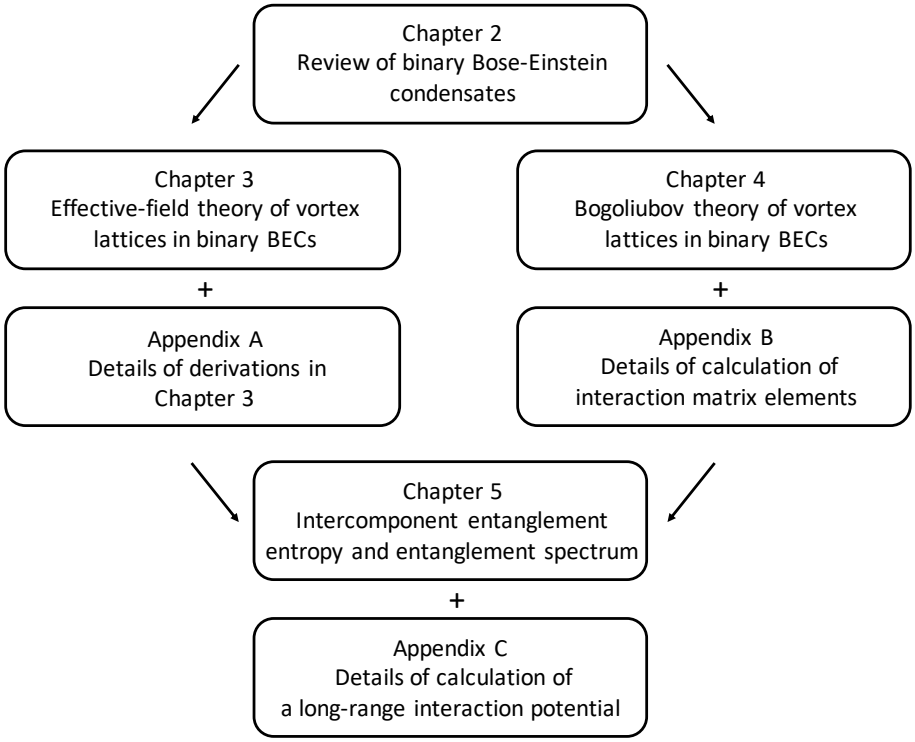

Figure 1.1: Relations between chapters.

Chapter 2

Review of binary Bose-Einstein condensates

In this chapter, we review binary (i.e., two-component) BECs. In Sec. 2.1, we consider binary BECs which are not subjected to the synthetic gauge fields. In Sec. 2.2, we discuss the ground-state phase diagram and the experimental realization of binary BECs under the parallel synthetic gauge fields. In Sec. 2.3, we discuss the synthetic gauge fields created by the laser using the minimal model and review an experiment which observed the spin Hall effect induced by the antiparallel magnetic fields in a cold-atom system. In Sec. 2.4, we review the quantum Hall state of binary BECs.

2.1 Binary Bose-Einstein condensates

Two-component BECs without rotation have been studied on the basis of the mean-field theory [32]. The solution of the Gross-Pitaevski (GP) equation shows a rich ground-state structure depending on the parameters of the system. In particular, the two components go under phase separation owing to the intercomponent interaction. We consider a binary system whose components are labeled by 1 and 2. We assume that the coupling constant of an intracomponent interaction for each component is given by g_i, $(i = 1, 2)$ and that for intercomponent interaction by g_{12}. By using the Thomas-Fermi approximation for the Schrödinger equation for the trapped binary BECs, the two components are mixed when $g_1 g_2 - g_{12}^2 > 0$. Otherwise, when $g_1 g_2 - g_{12}^2 < 0$, two components are separated so that the symmetry of the ground state is broken while the symmetry is restored in the mixed case [33–35]. In this thesis we only consider the parameters which create the mixed BECs.

The two-component BECs have been observed experimentally by using the different spin states of ^{87}Rb [36,37] and ^{87}Na [38]. In the case of ^{87}Rb, the separation of the BECs is weak since the coupling constants g_1, g_2 and g_{12} are nearly equal. In contrast, the values of the coupling constants satisfy $g_1 g_2 - g_{12}^2 < 0$ for ^{23}Na, so that the two components are separated and form spin domains.

2.2 Binary Bose-Einstein condensates under parallel synthetic gauge fields

In this section, we discuss the vortex lattices in binary BECs under the parallel synthetic magnetic fields. In Sec. 2.2.1, we show that the synthetic magnetic field is induced by rotating the system. In Sec. 2.2.2, we introduce the LLL approximation, which is validated when the magnetic field is sufficiently strong. In Sec. 2.2.3, we obtain the mean-field theory for the binary BECs and apply the LLL approximation. In Sec. 2.2.4, we review that the various configurations of vortex lattices appear as the ground-state phase diagram. We also see that the square lattices are observed in experiment.

2.2.1 Rotating Bose gas

We consider a particle of mass M in the two-dimensional xy plane [39]. The Schrödinger equation of the particle is given by

$$i\hbar\frac{\partial}{\partial t}\psi(\mathbf{r},t)=\left[-\frac{\hbar^2}{2M}\left(\frac{\partial^2}{\partial x^2}+\frac{\partial^2}{\partial y^2}\right)+V(\mathbf{r},t)\right]\psi(\mathbf{r},t), \tag{2.1}$$

where $V(\mathbf{r},t)$ is a time-dependent potential. The Schrödinger equation (2.1) is rewritten in the polar coordinate $(x,y)=(r\cos\theta,r\sin\theta)$ as

$$i\hbar\frac{\partial}{\partial t}\psi(r,\theta,t)=\left[-\frac{\hbar^2}{2M}\left(\frac{1}{r}\frac{\partial}{\partial r}r\frac{\partial}{\partial r}+\frac{1}{r^2}\frac{\partial^2}{\partial\theta^2}\right)+V(r,\theta,t)\right]\psi(r,\theta,t). \tag{2.2}$$

When the system is rotating with an angular velocity vector $\mathbf{\Omega}=\Omega(0,0,1)$ by the time dependent potential $V=V(r,\theta-\Omega t)$, the Schrödinger equation in the rotating frame of reference is given by

$$i\hbar\frac{\partial}{\partial t}\psi(r,\theta,t)=\left[\frac{\mathbf{p}^2}{2M}+V(r,\theta)-\Omega\ell_z\right]\psi(r,\theta,t), \tag{2.3}$$

where $\mathbf{p}=-i\hbar\nabla$ and ℓ_z is the angular momentum operator in the z direction written as

$$\ell_z=xp_y-yp_x=-i\hbar\left(x\frac{\partial}{\partial y}-y\frac{\partial}{\partial x}\right)=-i\hbar\frac{\partial}{\partial\theta}. \tag{2.4}$$

To derive Eq. (2.3), we utilize the fact that the Schrödinger equation in the rotating frame of reference is given by the new degrees of freedom introduced as $(\theta',t'):=(\theta-\Omega t,t)$. Since the derivatives with respect to t and θ are given by

$$\frac{\partial}{\partial\theta}=\frac{\partial}{\partial\theta'},\quad \frac{\partial}{\partial t}=\frac{\partial}{\partial t'}-\Omega\frac{\partial}{\partial\theta'}, \tag{2.5}$$

the left-hand side of Eq. (2.2) is rewritten as

$$i\hbar\frac{\partial}{\partial t}\psi=\left(i\hbar\frac{\partial}{\partial t'}+\Omega\ell_z\right)\psi. \tag{2.6}$$

and the right-hand side of Eq. (2.2) is rewritten by simply replacing θ by θ'. By omitting the primes on θ and t, which indicate the rotating frame of reference, we obtain Eq. (2.3).

From Eq. (2.3), we obtain the Hamiltonian in the rotating frame of reference H_Ω as

$$H_\Omega = \frac{\mathbf{p}^2}{2M} + V(\mathbf{r}) - \Omega\ell_z = \frac{(\mathbf{p} - M\boldsymbol{\Omega}\times\mathbf{r})^2}{2M} + \tilde{V}(\mathbf{r}), \tag{2.7}$$

where

$$\tilde{V}(\mathbf{r}) = V(\mathbf{r}) - \frac{1}{2}M(\boldsymbol{\Omega}\times\mathbf{r})^2. \tag{2.8}$$

This is analogous to the Hamiltonian of a particle with a charge q under the magnetic field $\mathbf{B} = B(0,0,1)$ in the z direction given as

$$H = \frac{(\mathbf{p} - q\mathbf{A}(\mathbf{r}))^2}{2M} + V(\mathbf{r}), \tag{2.9}$$

with the vector potential $\mathbf{A}(\mathbf{r}) = \frac{1}{2}(\mathbf{B}\times\mathbf{r})$ in the symmetric gauge. From Eqs. (2.7) and (2.9), we find the effective magnetic field $B = 2M\Omega/q$ is induced, where q is the fictitious charge of a particle. The reduction of the potential $\tilde{V}$ in Eq. (2.8) by the mechanical rotation corresponds to the centrifugal force due to a rotation in classical mechanics.

For a gas of N particles, a synthetic gauge field appears by rotating the gas. As the interaction for each pair of particles, we assume the rotationally invariant interaction term that depends only on the distance between the two particles $U(\mathbf{r}_i, \mathbf{r}_j) = U(|\mathbf{r}_i - \mathbf{r}_j|)$, where $\mathbf{r}_i$ is the position of the i th particle. A similar discussion for Eq. (2.7) is followed by the Hamiltonian for identical N particles in the rotating frame of reference of the form,

$$H_\Omega = \sum_{i=1}^{N}\left[\frac{\mathbf{p}_i^2}{2M} + V(\mathbf{r}_i)\right] + \sum_{i<j} U(|\mathbf{r}_i - \mathbf{r}_j|) - \boldsymbol{\Omega}\cdot\mathbf{L}, \tag{2.10}$$

where $\mathbf{L} = \sum_{i=1}^{N}\mathbf{r}_i\times\mathbf{p}_i$ is the total angular momentum. This Hamiltonian can also be written as

$$H_\Omega = \sum_{i=1}^{N}\frac{[\mathbf{p}_i - q\mathbf{A}(\mathbf{r}_i)]^2}{2M} + \sum_{i=1}^{N}\tilde{V}(\mathbf{r}_i) + \sum_{i<j} U(|\mathbf{r}_i - \mathbf{r}_j|). \tag{2.11}$$

When the trapping potential in the xy plane is the harmonic potential $V(\mathbf{r}) = \frac{1}{2}M\omega^2 r^2$, where ω is the trapping frequency, the effective potential $\tilde{V}$ is given by

$$\tilde{V}(\mathbf{r}) = \frac{1}{2}M(\omega^2 - \Omega^2)r^2. \tag{2.12}$$

Since the effective potential vanishes if the rotation speed is fast enough $\Omega \simeq \omega$, we effectively obtain a system without the trapping potential but with a uniform synthetic magnetic field. In ultracold atoms, the interaction is described by a contact interaction $U(\mathbf{r}_i - \mathbf{r}_j) = g\delta(\mathbf{r}_i - \mathbf{r}_j)$. As a gas is tightly confined in the z direction by a harmonic trapping potential of frequency ω_z, the ground state in the z direction is given by the Gaussian ground state $\psi_z(z) = \exp(-z^2/2d_z^2)/(\pi d_z^2)^{1/4}$ with $d_z = \sqrt{\hbar/M\omega_z}$. Therefore the interaction parameter g is renormalized as $g = g_{3\mathrm{D}}\int dz|\psi_z(z)|^4 = g_{3\mathrm{D}}/\sqrt{2\pi}d_z$. We find that the effective coupling constant is given by

$$g = g_{3\mathrm{D}}\sqrt{\frac{M\omega_z}{2\pi\hbar}}, \quad g_{3\mathrm{D}} = \frac{4\pi\hbar^2 a_s}{M}, \tag{2.13}$$

where g_{3D} is the coupling constant in the three-dimensional case and a_s is the s-wave scattering length.

2.2.2 Lowest-Landau-level approximation

From Eq. (2.7), we find the Hamiltonian in the rotating frame of reference for a particle trapped in a harmonic potential with trapping frequency ω as

$$\hat{h}_\Omega = \hat{h} - \Omega \hat{l}_z, \tag{2.14}$$

with

$$\hat{h} = \frac{1}{2M}(\hat{p}_x^2 + \hat{p}_y^2) + \frac{M\omega^2}{2}(\hat{x}^2 + \hat{y}^2), \quad \hat{l}_z = \hat{x}\hat{p}_y - \hat{y}\hat{p}_x, \tag{2.15}$$

where $\hat{x}$ and $\hat{p}$ are the position and momentum operators, respectively, satisfying the canonical commutation relations $[\hat{x}, \hat{p}_x] = [\hat{y}, \hat{p}_y] = i\hbar$ and $[\hat{x}, \hat{p}_x] = [\hat{y}, \hat{p}_x] = 0$ and $\hat{l}_z$ is the angular momentum operator in the z direction. The Hamiltonian is diagonalized in terms of the creation and annihilation operators

$$\hat{a}_x = \sqrt{\frac{M\omega}{2\hbar}}\left(\hat{x} + i\frac{\hat{p}_x}{M\omega}\right), \quad \hat{a}_y = \sqrt{\frac{M\omega}{2\hbar}}\left(\hat{y} + i\frac{\hat{p}_y}{M\omega}\right), \tag{2.16}$$

satisfying the commutation relations $[\hat{a}_x, \hat{a}_x^\dagger] = [\hat{a}_y, \hat{a}_y^\dagger] = 1$ and $[\hat{a}_x, \hat{a}_y] = [\hat{a}_x, \hat{a}_y^\dagger] = 0$. Using $\hat{a}_x$ and $\hat{a}_y$, Eq. (2.15) is rewritten as

$$\hat{h} = \hbar\omega(\hat{a}_x^\dagger \hat{a}_x + \hat{a}_y^\dagger \hat{a}_y + 1), \quad \hat{l}_z = i\hbar(\hat{a}_x \hat{a}_y^\dagger + \hat{a}_x^\dagger \hat{a}_y). \tag{2.17}$$

Furthermore, since $\hat{h}$ and $\hat{l}_z$ are commutable ($[\hat{h}, \hat{l}_z] = 0$), these two operators can be diagonalized simultaneously. By introducing

$$\hat{a}_\pm = \frac{1}{\sqrt{2}}(\hat{a}_x \mp i\hat{a}_y), \tag{2.18}$$

we find that

$$\hat{h} = \hbar\omega(\hat{a}_+^\dagger \hat{a}_+ + \hat{a}_-^\dagger \hat{a}_- + 1), \quad \hat{l}_z = \hbar(\hat{a}_+^\dagger \hat{a}_+ - \hat{a}_-^\dagger \hat{a}_-). \tag{2.19}$$

From the expression of $\hat{l}_z$ in Eq. (2.19), we find that the creation operators $\hat{a}_\pm^\dagger$ correspond to the modes rotating anti-clockwise (+) and clockwise (-), respectively. Let n_+ and n_- be the eigenvalues of $\hat{a}_+^\dagger \hat{a}_+$ and $\hat{a}_-^\dagger \hat{a}_-$, respectively. Then the eigenenergy of Eq. (2.14) is obtained as

$$\epsilon = \hbar[(\omega - \Omega)n_+ + (\omega + \Omega)n_- + \omega], \tag{2.20}$$

where the corresponding energy spectrum is presented in Fig. 2.1. When the rotation frequency Ω approaches the trapping frequency ω, we find that the energy levels are highly degenerate and that they are equally separated by $2\hbar\omega$ as the Landau levels in a magnetic field. Therefore the low-energy physics is dominated by the states in the energy level $n_- = 0$, which we call the lowest Landau level (LLL).

We find that the eigenfunctions of Eq. (2.14) are given by

$$\psi_{n_+,n_-}(z, z^*) = \frac{1}{\sqrt{n_+! n_-!}}(\hat{a}_+^\dagger)^{n_+}(\hat{a}_-^\dagger)^{n_-}\Phi_0(z, z^*), \tag{2.21}$$

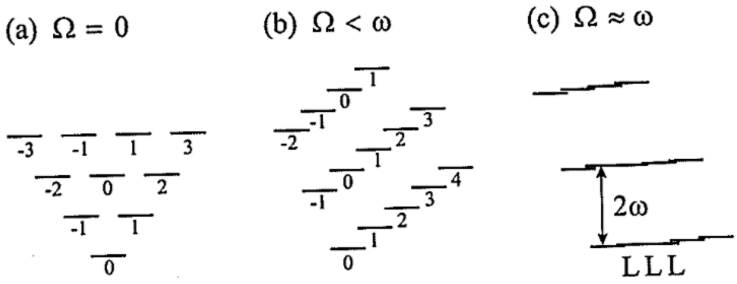

Figure 2.1: Energy spectrum of (2.20) for (a) $\Omega = 0$, (b) $\Omega < \omega$, and (c) $\Omega \simeq \omega$. The number below each level shows the angular momentum n_+. When the system is rapidly rotating as in the case (c), the ground state is approximated by a superposition of $n_- = 0$ states and the energy gap between the ground state and the first excited state is $2\hbar\omega$. Reproduced from Fig. 18 of Ref. [13]. Copyright © 2009 by the American Physical Society.

where

$$\Phi_0(z, z^*) = \frac{1}{\sqrt{\pi}} e^{-\frac{|z|^2}{2}}, \tag{2.22}$$

is the most localized LLL state described by a Gaussian wave function. Here $z = (x+iy)/\ell$ is a complex coordinate and $\ell = \sqrt{\hbar/2M\Omega}$ is an effective magnetic length. Then the LLL states with $n_- = 0$ are given by

$$\phi_m(z, z^*) = \frac{1}{\sqrt{m!}} (\hat{a}_+^\dagger)^m \Phi_0(z, z^*) = \frac{z^m}{\sqrt{\pi m!}} e^{-\frac{|z|^2}{2}} \quad (m = 0, 1, 2, \dots), \tag{2.23}$$

where we replace n_+ to m. Using Eq. (2.23) as a basis, we can express an arbitrary single-particle state in the LLL manifold as

$$\phi_{\rm LLL}(z, z^*) = \sum_{m \geq 0} c_m \phi_m(z, z^*) = f(z) e^{-\frac{|z|^2}{2}}, \tag{2.24}$$

where $f(z) = \sum_{m\geq 0} c_m z^m / \sqrt{\pi m!}$ is an analytic function of z. We can factorize the function $f(z)$ as $f(z) = C \prod_{m\geq 0}(z - z_m)$, where C is a constant. Since the wave function vanishes at $z = z_m$, these zeros correspond to the positions of vortices.

2.2.3 Mean-field theory

We consider N identical bosons in the rotating frame of reference. From Eq. (2.10), we have the Hamiltonian in the second-quantized form as

$$H = \int {\rm d}^3\mathbf{r}\ \hat{\psi}^\dagger(\mathbf{r}) \left[-\frac{\hbar^2}{2M}\nabla^2 + V(\mathbf{r}) - \Omega \ell_z + \frac{g}{2}\hat{\psi}^\dagger(\mathbf{r})\hat{\psi}(\mathbf{r}) \right] \hat{\psi}(\mathbf{r}), \tag{2.25}$$

where $\ell_z = -i\hbar[\mathbf{r} \times \nabla]_z$ is the angular momentum operator in the z direction and $\hat{\psi}(\mathbf{r})$ is the bosonic field operator satisfying the canonical commutation relations $[\hat{\psi}(\mathbf{r}), \hat{\psi}^\dagger(\mathbf{r}')] =$

$\delta(\mathbf{r}-\mathbf{r}')$ and $[\hat{\psi}(\mathbf{r}),\hat{\psi}(\mathbf{r}')]=[\hat{\psi}^\dagger(\mathbf{r}),\hat{\psi}^\dagger(\mathbf{r}')]=0$. Furthermore, the total number of particles is given by $N=\int d\mathbf{r}\ \hat{\psi}^\dagger(\mathbf{r})\hat{\psi}(\mathbf{r})$. As for the interaction term, we assume a contact interaction (2.13).

From Eq. (2.25), we have the Heisenberg equation of motion for $\hat{\psi}(\mathbf{r})$ as

$$i\hbar\frac{\partial}{\partial t}\hat{\psi}(\mathbf{r})=[\hat{\psi}(\mathbf{r}),H]=\left[-\frac{\hbar^2}{2M}\nabla^2+V(\mathbf{r})-\Omega\ell_z+g\hat{\psi}^\dagger(\mathbf{r})\hat{\psi}(\mathbf{r})\right]\hat{\psi}(\mathbf{r}). \tag{2.26}$$

Since the system forms a BEC in which a large number of particles occupy a single-particle state at sufficiently low temperatures, we can replace the bosonic field operator $\hat{\psi}(\mathbf{r})$ by a mean field $\psi(\mathbf{r})$ representing a macroscopic wave function subject to the normalization $\int d\mathbf{r}|\psi(\mathbf{r})|^2=N$. By the mean-field approximation, we obtain the time-dependent GP equation given as

$$i\hbar\frac{\partial}{\partial t}\psi(\mathbf{r},t)=\left(-\frac{\hbar^2}{2M}\nabla^2+V(\mathbf{r})-\Omega\ell_z+g|\psi(\mathbf{r})|^2\right)\psi(\mathbf{r},t). \tag{2.27}$$

By assuming a stationary solution of the form $\psi(\mathbf{r},t)=\psi(\mathbf{r})e^{-i\mu t/\hbar}$, we find the time-independent GP equation as

$$\left(-\frac{\hbar^2}{2M}\nabla^2+V(\mathbf{r})-\Omega\ell_z+g|\psi(\mathbf{r})|^2\right)\psi(\mathbf{r})=\mu\psi(\mathbf{r}), \tag{2.28}$$

where μ is a chemical potential. We find the GP ground state which minimizes the chemical potential μ for the solution. By replacing $\hat{\psi}(\mathbf{r})$ by $\psi(\mathbf{r})$ in $H-\mu N$, we obtain the GP energy functional as

$$E_\Omega=\int \mathrm{d}^3\mathbf{r}\ \left[\psi^*(\mathbf{r})\left(-\frac{\hbar^2}{2M}\nabla^2+V(\mathbf{r})-\Omega\ell_z-\mu\right)\psi(\mathbf{r})+\frac{g}{2}|\psi(\mathbf{r})|^4\right]. \tag{2.29}$$

By assuming that the potential is a harmonic potential $V(\mathbf{r})=\frac{1}{2}M\omega^2r^2$, the energy functional (2.29) is rewritten as

$$E_\Omega=\int \mathrm{d}^3\mathbf{r}\ \left\{\frac{|[-i\hbar\nabla-q\mathbf{A}(\mathbf{r})]\,\psi(\mathbf{r})|^2}{2M}+\frac{M}{2}(\omega^2-\Omega^2)r^2|\psi(\mathbf{r})|^2-\mu|\psi(\mathbf{r})|^2+\frac{g}{2}|\psi(\mathbf{r})|^4\right\}. \tag{2.30}$$

When the rotation frequency Ω and the trapping frequency ω are close to each other, the trapping potential vanishes and the wave function can be given by the LLL states. We further assume that the scale of the interaction energy gn, where n is the particle density, is much smaller than the single-particle energy gap $\hbar\Omega$ i.e. $gn\ll\hbar\Omega$, so that a particle is not excited out of the LLL manifold by the interaction term. If the mean field $\psi(\mathbf{r})$ is approximated by the LLL wave function (2.24), it is called the LLL approximation [40] and we call this regime the "mean-field LLL regime"[1] [41]. From Eq. (2.24), we find that the mean-field ground state $\psi(\mathbf{r})$ has vortices located at zero points z_m . The ground state of Eq. (2.30), which is similar to the Ginzburg-Landau energy functional for type-II superconductors, has been found to be a triangular vortex lattice known as the Abrikosov lattice [42].

[1]This regime is sometimes called the "mean-field quantum Hall regime". Here, we do not use this term to distinguish it from the regime of bosonic quantum Hall states where the mean-field theory is violated.

2.2.4 Vortex lattices in binary BECs

We consider a two-dimensional Bose gas with two hyperfine spin states labeled as $\alpha = \uparrow, \downarrow$. The GP energy functional for this binary system is given by

$$E = \int \mathrm{d}^2\mathbf{r} \left[\sum_{\alpha=\uparrow,\downarrow} \left\{ \psi_\alpha^*(\hat{h} - \Omega \hat{l}_z - \mu)\psi_\alpha \right\} + \sum_{\alpha,\beta=\uparrow,\downarrow} \frac{g_{\alpha\beta}}{2} |\psi_\alpha|^2 |\psi_\beta|^2 \right], \tag{2.31}$$

with

$$\hat{h} = -\frac{\hbar^2}{2M}\nabla^2 + \frac{1}{2}M\omega^2 r^2, \quad \hat{l}_z = -i\hbar[\mathbf{r} \times \nabla]_z, \tag{2.32}$$

where ψ_α is the condensate wave function for the component α. We assume that the coupling constants for intracomponent and intercomponent interactions are given by $g = g_{\uparrow\uparrow} = g_{\downarrow\downarrow}$ and $g_{\uparrow\downarrow} = g_{\downarrow\uparrow}$, respectively. Since the gas is confined in the z direction by the harmonic potential, the coupling constants are renormalized as discussed in the previous section. We also assume that the number of particles in each component is the same. The parallel synthetic magnetic fields are caused by the mechanical rotation.

Mueller and Ho [17] obtained the ground state of a rapidly rotating binary BECs in the mean-field theory by minimizing the GP energy functional (2.31) under the LLL approximation. By assuming that BECs are subjected to a sufficiently shallow effective potential, they minimized the interaction part by using trial wave functions ψ_α ($\alpha = \uparrow, \downarrow$) involving the Jacobi theta function, which has periodic zeros apart from the Gaussian factor. In (a)-(e) of Fig. 2.2, the five equilibrium vortex-lattice configurations are shown by black and grey dots representing the vortex cores of the two components. In the last figure of Fig. 2.2, the parameters specifying the structure of the vortex lattices in the complex plane are presented, where $\tau = x + iy$, η is the inner angle and a and b parametrizes the displacement of vortex cores between two components. In Fig. 2.3, the phase diagram of vortex lattices for the binary system is shown by presenting the parameters η, a and $|\tau|$ as a function of the ratio of the intercomponent interaction to the intracomponent one $\alpha = g_{\uparrow\downarrow}/g$. In Ref. [18], the behavior of the slowly rotating BECs has been numerically studied. Various vortex-lattice configurations consistent with the rapidly rotating case [17] have been found.

The vortex lattices of binary BECs have been observed by the JILA group in 2004 [19]. They prepared a single-component triangular vortex lattice by using the $|1\rangle = |F = 1, m_F = -1\rangle$ state of ^{87}Rb as observed in Fig. 2.4 (a). Then they excited about 80% of atoms to $|2\rangle = |F = 2, m_F = 1\rangle$ by a short pulse and waited until the number of each component became the same by deexcitation. In Fig. 2.4 (b), the image of one of the two components for binary BECs is displayed. They observed the square lattices. In Fig. 2.4 (c) and (d), six peaks and four peaks are obtained by the two-dimensional Fourier transformation of the images of the triangular vortex lattice and the square vortex lattice, respectively. In particular, Fig. 2.4 (d) is clear evidence of creation of square lattices.

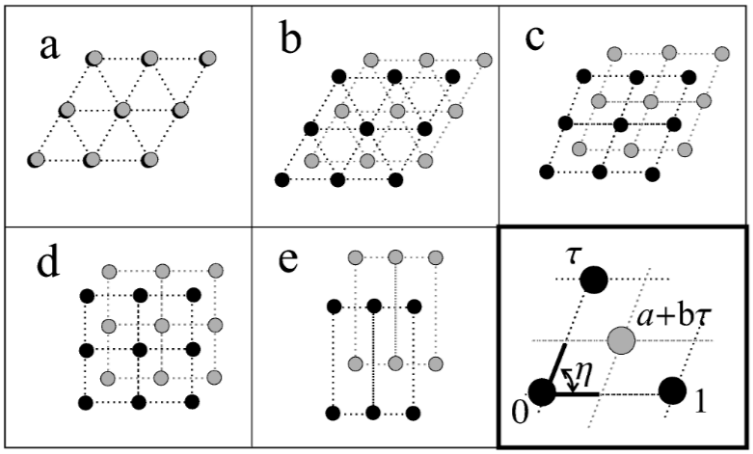

Figure 2.2: Vortex lattice structures of rapidly rotating binary BECs. Vortices of two different components are indicated by black and grey circles. (a) Overlapping triangular lattices. (b) Interlaced triangular lattices. (c) Rhombic lattices. (d) Square lattices. (e) Rectangular lattices. The right bottom panel depicts the geometry of the lattices. Vortices of the first and second components are located at $m+n\tau$ and $(a+m)+(b+n)\tau$, respectively, in the complex plane, where m and n are integers. All configurations have $a = b$. Reproduced from Fig. 1 of Ref. [17]. Copyright © 2002 by the American Physical Society.

2.3 Binary Bose-Einstein condensates under antiparallel synthetic gauge fields

In this section, we review the binary BECs under antiparallel synthetic gauge fields. In Sec. 2.3.1, we use the minimal model to explain that synthetic gauge fields are created by lasers. In Sec. 2.3.2, we review an experiment in which the antiparallel magnetic fields has successfully been created in the atomic gas of ^{87}Rb. In Sec. 2.3.3, we explain that within the mean-field theory, the phase diagram of the vortex lattices for antiparallel fields is equivalent to that for parallel fields.

2.3.1 Creation of synthetic gauge fields by using lasers

In this section, we consider the minimal model of generating the synthetic gauge fields by lasers [43]. The two basis states of the two-dimensional Hilbert space $\{|g\rangle, |e\rangle\}$ associated with the internal degrees of freedom of an atom represent the ground state and the excited state of an atom, respectively. We assume that two states are coupled by space-dependent external fields. The general form of the Hamiltonian of a particle is given by

$$H = \left(\frac{\hat{p}^2}{2M} + V\right)\hat{1} + \hat{U}, \tag{2.33}$$

where M is the mass, $\hat{p} = -i\hbar\nabla$ is the momentum operator and $\hat{1}$ is the identity operator of the internal Hilbert space. The potential V does not depend on the internal state of the particle and the internal states are coupled by the coupling operator $\hat{U}$, which is

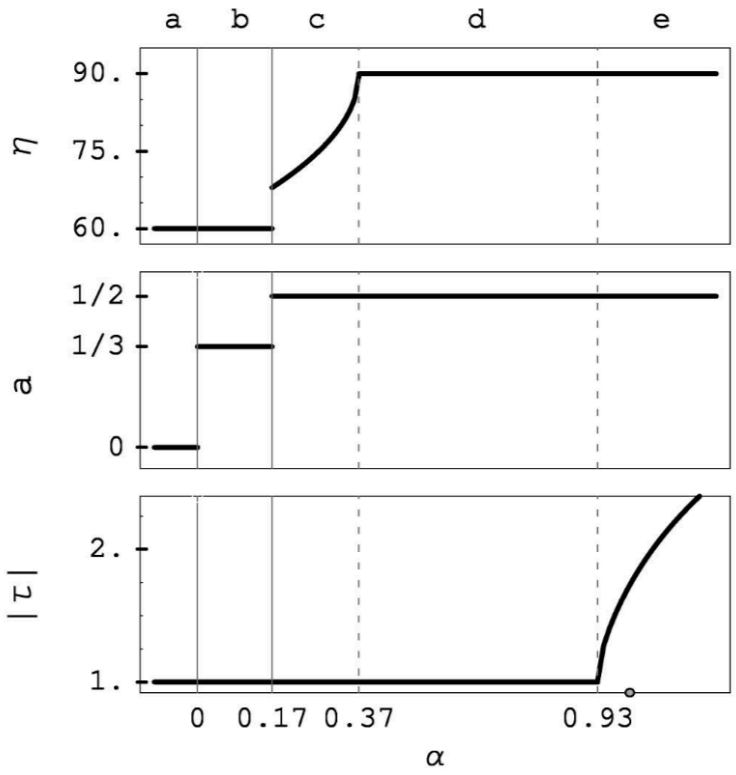

Figure 2.3: Parameters of vortex lattices η, a and $|\tau|$ as a function of $\alpha = g_{\uparrow\downarrow}/g$. The configurations of vortex lattices are illustrated in Fig. 2.2, where $\tau = |\tau|e^{i\eta}$. Vertical solid and dashed lines indicate the first and second-order phase transitions, respectively. The open circle on the horizontal axis denotes $\alpha = 1$. Reproduced from Fig. 2 of Ref. [17]. Copyright © 2002 by the American Physical Society.

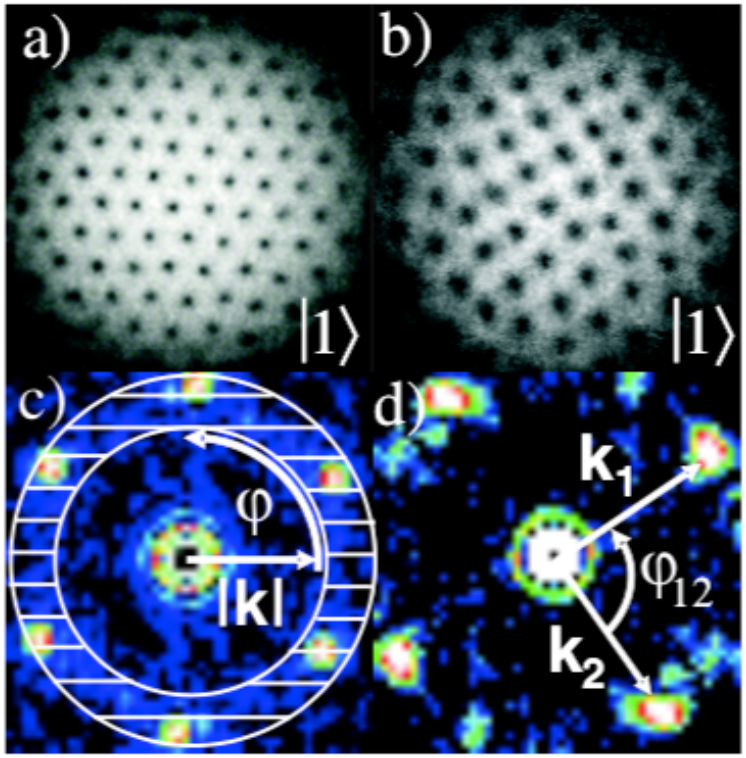

Figure 2.4: (a) Triangular vortex lattice observed in a scalar BEC. (b) Square vortex lattice observed in the $|1\rangle$ component of binary BECs. (c) Reciprocal space of the triangular lattices by two-dimensional Fourier transformation of (a). The center peak is at the Γ point. Six peaks emerge in an equiangular configuration at every 60°. (d) Reciprocal space of the square lattice. Four peaks clearly indicate the formation of square vortex lattices. Reproduced from Fig. 1 of Ref. [19]. Copyright © 2004 by the American Physical Society.

written in the matrix form as

$$U = \frac{\hbar\Omega}{2}\begin{pmatrix} \cos\theta & e^{-i\phi}\sin\theta \\ e^{i\phi}\sin\theta & -\cos\theta \end{pmatrix}, \tag{2.34}$$

where Ω is the generalized Rabi frequency characterizing the coupling strength, θ is the mixing angle and ϕ is the phase angle. In the case of a two-level atom in a monochromatic laser field, $\Omega\cos\theta$ is the detuning of a laser, $\Omega\sin\theta$ is the strength of the atom-laser coupling and ϕ is the laser phase. The parameters V, Ω, θ and ϕ depend on the position vector $\mathbf{r}$, so that the dynamics of the particle is governed by them.

To analyze the Hamiltonian (2.33), we introduce a useful basis in terms of the eigenvectors of the matrix U, which are given by

$$|\chi_1\rangle = \begin{pmatrix} \cos(\theta/2) \\ e^{i\phi}\sin(\theta/2) \end{pmatrix}, \quad |\chi_2\rangle = \begin{pmatrix} -e^{-i\phi}\sin(\theta/2) \\ \cos(\theta/2) \end{pmatrix}, \tag{2.35}$$

with eigenvalues $\hbar\Omega/2$ and $-\hbar\Omega/2$, respectively. These states called "dressed states" are spatially dependent since the matrix U depends on $\mathbf{r}$. From the orthogonality of these normalized states, we find that $i\langle\chi_j|\nabla\chi_j\rangle$ is real and the relation $\langle\nabla\chi_2|\chi_1\rangle = -\langle\chi_2|\nabla\chi_1\rangle$ is satisfied.

In terms of these dressed states, the full state vector of the particle is given as

$$|\Psi(\mathbf{r},t)\rangle = \sum_{j=1,2}\psi_j(\mathbf{r},t)|\chi_j(\mathbf{r})\rangle. \tag{2.36}$$

We derive the equation of motion for ψ_1 assuming that ψ_2 is negligible. Since both $\psi_j(\mathbf{r},t)$ and $|\chi_j\rangle$ are spatially dependent, we find $\nabla[\psi_j|\chi_j\rangle] = [\nabla\psi_j]|\chi_j\rangle + \psi_j[|\nabla\chi_j\rangle]$. By acting the momentum operator on the state, we obtain

$$\mathbf{P}|\Psi\rangle = \sum_{j,l=1}^{2}[(\delta_{j,l}\mathbf{P} - \mathbf{A}_{jl})\psi_l]|\chi_j\rangle, \tag{2.37}$$

with

$$\mathbf{A}_{jl} = i\hbar\langle\chi_j|\nabla\chi_l\rangle. \tag{2.38}$$

Since we assume ψ_2 is negligible, we obtain the time-dependent Schrödinger equation for ψ_1 by projecting the Schrödinger equation $i\hbar|\dot{\Psi}\rangle = H|\Psi\rangle$ onto the dressed state $|\chi_1\rangle$. This assumption is called the adiabatic approximation. In this approximation, the Schrödinger equation for ψ_1 is given by

$$i\hbar\frac{\partial\psi_1}{\partial t} = \left[\frac{(\mathbf{P}-\mathbf{A})^2}{2M} + V + \frac{\hbar\Omega}{2} + W\right]\psi_1. \tag{2.39}$$

Here, the two geometric potentials $\mathbf{A}(\mathbf{r})$ and $W(\mathbf{r})$ are related to the spatial dependence of the dressed state as

$$\mathbf{A}(\mathbf{r}) = i\hbar\langle\chi_1|\nabla\chi_1\rangle = \frac{\hbar}{2}(\cos\theta - 1)\nabla\phi, \tag{2.40}$$

$$W(\mathbf{r}) = \frac{\hbar^2}{2M}|\langle\chi_2|\nabla\chi_1\rangle|^2 = \frac{\hbar^2}{8M}[(\nabla\theta)^2 + \sin^2\theta(\nabla\phi)^2]. \tag{2.41}$$

We see that Eq. (2.39) is analogous to the Schrödinger equation for a charged particle with the scalar potential $W(\mathbf{r})$ and the vector potential $\mathbf{A}(\mathbf{r})$. A synthetic magnetic field appears when the effective magnetic field

$$\mathbf{B}(\mathbf{r}) = \nabla \times \mathbf{A}(\mathbf{r}) = \frac{\hbar}{2}(\nabla \cos\theta) \times \nabla\phi, \tag{2.42}$$

is nonzero. From the analytical expression of $\mathbf{B}$ in Eq. (2.42), we obtain a nonzero magnetic field when both the gradient of the mixing angle θ and that of the phase angle ϕ are nonzero and when they are not parallel to each other. The second geometric potential $W(\mathbf{r})$ is a scalar potential creating a force on the particle. When we adiabatically eliminate $|\chi_1\rangle$ instead of $|\chi_2\rangle$, the Schrödinger equation for ψ_2 is obtained. In this case, the same scalar potential $W(\mathbf{r})$ and the vector potential with a reversed sign, $-\mathbf{A}(\mathbf{r})$, are obtained in the equation for ψ_2.

2.3.2 Experimental realization

The antiparallel synthetic magnetic fields are applied to the pseudospin-1/2 ^{87}Rb BECs with the atomic mass m by coupling two states via the two laser beams ("Raman lasers") with wavelength λ [20]. Two beams parallel to the x axis propagate in opposite directions and couples the states $|f = 1, m_F = 0, -1\rangle = |\uparrow, \downarrow\rangle$ with strength Ω. We introduce the single-photon recoil energy as $E_R = \hbar^2 k_R^2/2m$, where $\hbar k_R = 2\pi\hbar/\lambda$ is the momentum. For a resonant Raman coupling, the Hamiltonian of a single particle is given by

$$H = \frac{\hbar^2 \mathbf{k}^2}{2m} I + \frac{\hbar\Omega}{2}\sigma_1 - \frac{\hbar^2 k_R k_x}{m}\sigma_3 + E_R I, \tag{2.43}$$

where $\hbar\mathbf{k}$ is the vector of the momentum operator and I and σ_i $(I = 1, 2, 3)$ are the identity matrix and the Pauli matrices for the pseudospin degrees of freedom, respectively. The eigenenergy of the Hamitonian $E_\pm$ is given by

$$E_\pm = \varepsilon_\pm(k_x) + \frac{\hbar^2(k_y^2 + k_z^2)}{2m}, \tag{2.44}$$

with

$$\varepsilon_\pm(k_x) = \frac{\hbar^2 k_x^2}{2m} + E_R \pm \sqrt{\left(\frac{\hbar\Omega}{2}\right)^2 + \left(\frac{\hbar^2 k_R k_x}{m}\right)^2}. \tag{2.45}$$

Since the wavenumber k_x which minimizes the lower dispersion relation $E_-(k_x)$ is calculated from $\partial\varepsilon_\pm(k_x)/\partial k_x = 0$, we find that two ground states have the nonzero wavenumber $k_x = \pm q$ with $q = k_R[1 - (\hbar\Omega/4E_R)^2]^{1/2}$ and they represent the dressed states $\uparrow'$ and $\downarrow'$, respectively. We assume $\hbar\Omega < 4E_R$. By performing the Taylor expansion of $\varepsilon_-(k_x)$ about the minima $\pm q$, the dispersion relation is rewritten as

$$\varepsilon_-(k_x) = -\frac{(\hbar\Omega)^2}{16E_R} + \frac{1}{2m^*}(\hbar k_x \mp \hbar q)^2 + \cdots, \tag{2.46}$$

where $m^* = 2m/[1-(\hbar\Omega/4E_R)^2]$ is an effective mass. From Eq. (2.46), we find a synthetic magnetic field depending on the dressed state and the scalar potential independent of the

dressed state. Since the scalar potential is compensated by an additional potential in the experiment, we omit this term in the following. The effective Hamiltonian is obtained as

$$H = \frac{(\mathbf{p}I - A\mathbf{e}_x\sigma_3)^2}{2m^*} + \cdots, \tag{2.47}$$

with

$$A = \hbar k_R[1 - (\hbar\Omega/4E_R)^2]^{1/2}, \tag{2.48}$$

where I and σ_3 are the 2×2 identity matrix and the z component of the Pauli matrix, respectively, in terms of dressed states. The antiparallel synthetic magnetic fields are obtained when the strength Ω is spatially dependent: $\Omega = \Omega(y)$.

To prepare the binary BECs from an ultracold atomic gas with $N \simeq 5 \times 10^4$ atoms, the energy level of $|F = 1, m_F = 0, \pm 1\rangle$ states are shifted by a bias magnetic field. The energy shifts due to the linear and quadratic Zeeman effects are proportional to m_F and $(m_F)^2$, respectively. Therefore the degeneracy of the levels are lifted by the linear Zeeman effect and the $|F = 1, m_F = 1\rangle$ state is eliminated while the $|F = 1, m_F = -1\rangle$ state approachs the $|F = 1, m_F = 0\rangle$ state by the quadratic Zeeman effect in order to prepare the binary system. The energy difference between the remaining two levels is $\Delta E = 2\pi\hbar \times 15$ MHz. Two Raman lasers with frequencies ω and $\omega + \delta\omega$ couple the two hyperfine states $|F = 1, m_F = 0, -1\rangle$ to the same highly excited state, producing an effective coupling between $|F = 1, m_F = 0, -1\rangle$. The spin-dependent Lorentz force has been observed from the shear of the gas and the antiparallel magnetic fields are confirmed from the observation of the spin current.

2.3.3 Equivalence of parallel and antiparallel fields within a mean-field regime

When the filling factor $\nu \equiv N/N_\mathrm{v}$, where N is the number of particle and N_v is the number of quantized vortices, is large ($\nu \gg 1$), the magnetic field is so weak that the system is well described by GP mean-field theory as in Eq. (2.30). Since the energy functional for the system in antiparallel magnetic fields is given by

$$E[\psi_\uparrow, \psi_\downarrow] = \int d^2\mathbf{r} \left[\psi_\uparrow^* \mathcal{K}(B)\psi_\uparrow + \psi_\downarrow^* \mathcal{K}(-B)\psi_\downarrow + \sum_{\alpha,\beta} \frac{g_{\alpha\beta}}{2}|\psi_\alpha|^2|\psi_\beta|^2\right], \tag{2.49}$$

with the single-particle Hamiltonian in the symmetric gauge given by

$$\mathcal{K}(\pm B) = \frac{1}{2M}\left[\left(-i\hbar\frac{\partial}{\partial x} \pm \frac{qB}{2}y\right)^2 + \left(-i\hbar\frac{\partial}{\partial y} \mp \frac{qB}{2}x\right)^2\right], \tag{2.50}$$

we find the GP energy functionals for the cases of parallel and antiparallel magnetic fields are connected to each other as [23]

$$E_\mathrm{antiparallel}[\psi_\uparrow, \psi_\downarrow] = E_\mathrm{parallel}[\psi_\uparrow, \psi_\downarrow^*]. \tag{2.51}$$

We can prove the equivalence of the energy functionals for parallel and antiparallel fields by performing the partial integrations twice as

$$\int d^2\mathbf{r}\ \psi_\downarrow^* \mathcal{K}(-B)\psi_\downarrow = \int d^2\mathbf{r}\ \psi_\downarrow \mathcal{K}(B)\psi_\downarrow^*, \tag{2.52}$$

and replacing $\psi_\downarrow$ to $\psi_\downarrow^*$ for parallel fields. Since the ground-state wave function is determined by minimizing the energy functional, Eq. (2.51) implies that the ground-state phase diagram of vortex lattices in the mean-field theory under the antiparallel magnetic fields is equivalent to that for parallel magnetic fields as shown in Fig. 2.2. Later, we use this fact in formulating the Bogoliubov theory of the vortex lattices for antiparallel fields.

2.4 Binary Bose-Einstein condensates in the quantum Hall regime

In the mean-field theory, we have seen that the ground-state phase diagrams of the vortex lattices in binary BECs for parallel and antiparallel fields are equivalent. However, in the quantum Hall regime, where the magnetic field is so strong that the mean-field theory breaks down, the ground-state phase diagrams for parallel and antiparallel fields are different. The strength of the magnetic field for a binary system is given by the total filling factor $\nu = (N_\uparrow + N_\downarrow)/N_\mathrm{v}$, where N_α ($\alpha = \uparrow, \downarrow$) denotes the numbers of particles in the component α and N_v is the number of magnetic flux quanta piercing through each component. By the exact diagonalization, the ground-state phase diagrams in the space of the total filling factor and the ratio of the intercomponent interaction $g_{\uparrow\downarrow}$ to the intracomponent interaction g for parallel and antiparallel fields are presented in Fig. 2.5 [24] and Fig. 2.6 [23], respectively. The authors of Refs. [24] and [23] found that the product states given by a pair of various quantum Hall states, where two components are disentangled, are robust for an attractive (repulsive) intercomponent interaction in parallel (antiparallel) fields. In contrast, the spin-singlet quantum Hall (pairing) states, in which two components are highly entangled, appear for the repulsive (attractive) intercomponent interaction in parallel (antiparallel) fields.

Therefore it is interesting to discuss the quantum correction to the ground state for parallel and antiparallel fields by calculating the Lee-Huang-Yang correction based on the Bogoliubov theory as a step to go beyond the mean-field theory. We expect that the intercomponent EE is large in the regime where the spin-singlet states appear, while we expect that the intercomponent EE is small in the regime where the product states appear. The intercomponent EE of vortex lattices in binary BECs is expected to show similar behavior since the vortex lattices turn into the quantum Hall states by increasing the strength of the magnetic fields. We address these problems in Chap. 5.

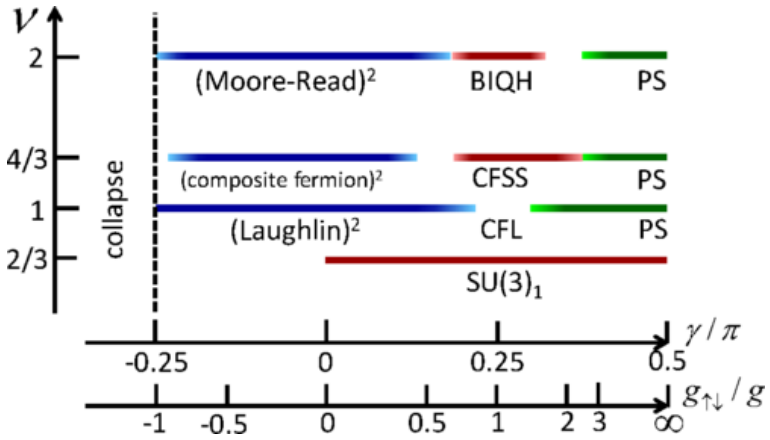

Figure 2.5: Ground-state phase diagram for parallel fields in terms of the total filling factor ν and the ratio $g_{\uparrow\downarrow}/g = \tan\gamma$ of the intercomponent coupling constant $g_{\uparrow\downarrow}$ to the intracomponent one g. We assume $g > 0$. For an attractive intercomponent interaction, the product states of a pair of nearly uncorrelated quantum Hall states appear. The quantum Hall (QH) states (Laughlin, composite Fermion and Moore-Read states) depend on the filling factor ν. In contrast, various spin-singlet QH states appear in the region of repulsive intercomponent interactions, such as a $SU(3)_1$ state at $\nu = 2/3$, a composite Fermion spin-singlet state (CFSS) at $\nu = 4/3$ and a bosonic integer quantum Hall (BIQH) state at $\nu = 2$. Furthermore, a gapless spin-singlet composite Fermi liquid (CFL) appears at $\nu = 1$. At larger $g_{\uparrow\downarrow}/g$, a phase separation (PS) occurs. The shaded bars indicate the regimes of the different phases. The phase boundaries are not precisely given due to the finite-size effect or ambiguity in setting the condition. Reproduced from Fig. 1 of Ref. [24]. Copyright © 2017 by the American Physical Society.

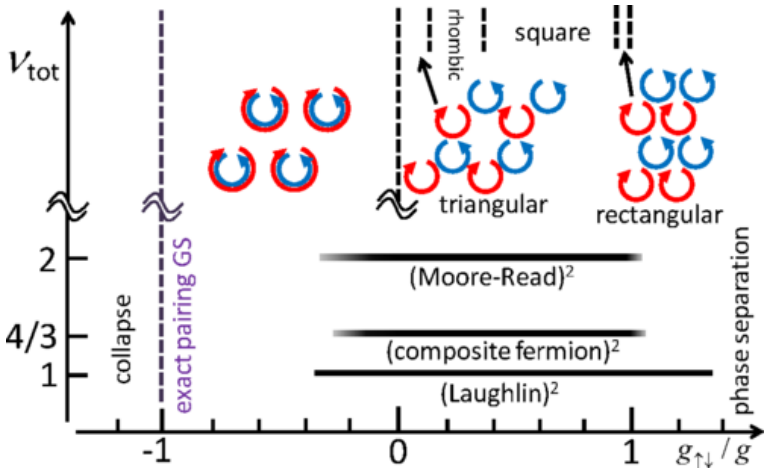

Figure 2.6: Ground-state phase diagram for antiparallel fields in terms of the total filling factor ν and the ratio $g_{\uparrow\downarrow}/g$ of the intercomponent coupling constant $g_{\uparrow\downarrow}$ to the intercomponent one g. We assume $g > 0$. In the mean-field regime with a large filling factor, vortex lattices appear. For small ν, various quantum spin Hall states given by product states of a pair of nearly independent quantum Hall states such as the Laughlin state at $\nu = 1$, the composite Fermion state at $\nu = 4/3$ and the Moore-Read state at $\nu = 2$ appear. For $\nu = 1$, the range of the phase is determined by an appropriate extrapolation to the thermodynamic limit while the ranges of the phases for $\nu = 4/3$ and 2 are not determined precisely due to the finite-size effect. At $g_{\uparrow\downarrow}/g = -1$, an exact pairing ground state is obtained and beyond this point the system collapses in the thermodynamic limit. At a large $g_{\uparrow\downarrow}/g$, the phase separation occurs. Reproduced from Fig. 1 of Ref. [23]. Copyright © 2014 by the American Physical Society.

Chapter 3

Effective-field theory of vortex lattices in binary BECs

In this chapter, two different excited states in parallel and antiparallel fields in contrast to the ground states in the mean-field theory are related by the rescaling relations. In Sec. 3.1, we start by reviewing a mean-field description of vortex lattices for a scalar BEC [44]. In particular, we highlight the importance of renormalization of the coupling constant. In Sec. 3.2, we derive a low-energy effective-field theory of vortex latices in binary BECs. We introduce a new term for the elastic energy and renormalization factors for coupling constants of intercomponent and intracomponent interactions. In Sec. 3.3, we calculate the excitation spectra and obtain rescaling relations between the dispersion relations for parallel and antiparallel fields. We also discuss oscillation modes which correspond to quadratic and linear dispersion relations.

3.1 Mean-field description of vortex lattices

3.1.1 System and formalism

We consider a system of a three-dimensional scalar BEC rotating at an angular velocity Ω with a rotation axis along the z-axis. A BEC is trapped in a harmonic potential $V(\mathbf{r}) = \frac{1}{2}M(\omega^2 r_\perp^2 + \omega_z^2 z^2)$, where $\mathbf{r}_\perp = (x, y, 0)$, M is the mass of an atom, and $\omega_\perp$ and ω_z are the trapping frequency in the xy plane and z-axis, respectively. We assume that the vortices are rectilinear and they form a triangular lattice. At a large rotation rate, in which the number of quantized vortices N_v satisfy $N_\mathrm{v} \gg 1$, the angular velocity Ω is close to the angular frequency

$$\Omega_v = \frac{\pi\hbar n_v}{M}, \tag{3.1}$$

where $n_v = N_\mathrm{v}/A$ is the two-dimensional density of vortices. We obtain the mean angular velocity Ω_v from the condition of quantization of vorticity $\oint_{\mathcal{C}} d\vec{\ell} \cdot \mathbf{v} = N_\mathrm{v}(\mathcal{C})h/M$, where $\mathbf{v}$ is the superfluid velocity and $N_\mathrm{v}(\mathcal{C})$ is the number of vortices inside the contour $\mathcal{C}$. By substituting $\mathbf{v} = \Omega\mathbf{e}_z \times \mathbf{r}$, where $\mathbf{e}_z$ is the unit vector along the z-axis, into the condition of the quantization of vorticity, we find the angular velocity Ω_v in Eq. (3.1). In terms of the magnetic length given by $\ell = \sqrt{\hbar/2M\Omega_v}$, the area of the unit cell is given by

$2\pi\ell^2 = 1/n_v$. We note that the mean angular velocity Ω_v is usually smaller than the angular velocity Ω.

We separate the short-distance structure of vortices from the large-scale structure to consider the large-scale property of the vortex lattice. The order parameter is written as

$$\psi(\mathbf{r}) = e^{i\Phi(\mathbf{r})} f(\mathbf{r}) \sqrt{n(\mathbf{r})}, \tag{3.2}$$

where $f(\mathbf{r})$ is a rapidly varying periodic real function vanishing at each vortex core, $\sqrt{n(\mathbf{r})}$ is a slowly varying real envelope function and $\Phi(\mathbf{r})$ is the phase factor. We normalize f^2, so that its average over each unit cell of the lattice is equal to unity: $\int \mathrm{d}^2\mathbf{r} f^2/2\pi\ell^2 = 1$. Here, $n(\mathbf{r})$ is the density profile of the system, which varies slowly in the unit cell of the vortex lattice. The phase $\Phi(\mathbf{r})$ varies by an integer multiple of 2π around each vortex.

In the laboratory frame, the mean-field energy of the BEC is given by

$$E = \int \mathrm{d}^3\mathbf{r} \left[\frac{\hbar^2}{2M} |\nabla\psi(\mathbf{r})|^2 + V(\mathbf{r}) n(\mathbf{r}) f^2(\mathbf{r}) + \frac{g}{2} n^2(\mathbf{r}) f^4(\mathbf{r}) \right], \tag{3.3}$$

where a coupling constant of the interaction term g is given by $g = 4\pi a_s \hbar/M$ using an s-wave scattering length a_s. By substituting Eq. (3.2) in Eq. (3.3), the kinetic term of Eq. (3.3) given by K is rewritten as

$$K := \int \mathrm{d}^3\mathbf{r} \frac{\hbar^2}{2M} |\nabla\psi(\mathbf{r})|^2 = \int \mathrm{d}^3\mathbf{r} \frac{\hbar^2}{2M} \left[(\nabla\sqrt{n})^2 f^2 + (\nabla\Phi)^2 n f^2 + n(\nabla f)^2 + \frac{1}{2}\nabla f^2 \cdot \nabla n \right]. \tag{3.4}$$

We now replace f^2 in the first term on the right-hand side of Eq. (3.4) by its average, which is unity because the variation of the density n across the unit cell of a vortex lattice is small. This approximation will be used repeatedly in a later part. In the second term of Eq. (3.4), we keep f^2 since the phase Φ varies rapidly in the unit cell. For the fourth term, we integrate it by parts to obtain $-\int d^3r f^2 \nabla^2 n$. Then by replacing f^2 by its average in a unit cell, we find that this surface term vanishes since both the density and its derivative vanish at large distance. We thus find that the kinetic term is rewritten as

$$K = \int \mathrm{d}^3\mathbf{r} \frac{\hbar^2}{2M} \left[(\nabla\sqrt{n})^2 f^2 + (\nabla\Phi)^2 n f^2 + n(\nabla f)^2 \right]. \tag{3.5}$$

We determine the unit cell in the xy plane in such a way that a vortex j locates at the center of the cell $\mathbf{R}_j$. The superfluid velocity $\hbar\nabla\Phi/M$ around a vortex j is given by the sum of a rate of a solid body rotation $\mathbf{\Omega}_v \times \mathbf{R}_j$ which is determined by the vortex density and the position of the vortex and a local velocity around the vortex $\hbar\nabla\phi_j/M$, where ϕ_j is the azimuthal angle with respect to the center of the cell j:

$$\hbar\nabla\Phi/M \simeq \mathbf{\Omega}_v \times \mathbf{R}_j + \hbar\nabla\phi_j/M, \tag{3.6}$$

with $\mathbf{\Omega}_v = \Omega_v \mathbf{e}_z$. By substituting the superfluid velocity into the second term of the kinetic term of Eq. (3.5), we obtain

$$\int \mathrm{d}^3\mathbf{r} \frac{\hbar^2}{2M} (\nabla\Phi)^2 n f^2 = \sum_j \int_j \mathrm{d}^3\mathbf{r}\, n f^2 \left[\frac{\hbar^2 (\nabla\phi_j)^2}{2M} + \frac{1}{2} M \Omega_v R_j^2 + \hbar\mathbf{\Omega}_v \cdot (\mathbf{R}_j \times \nabla\phi_j) \right], \tag{3.7}$$

where $\int_j \mathrm{d}^3\mathbf{r}$ indicates the integration over the unit cell j and the sum $\sum_j$ represents the summation over all cells. The last term in Eq. (3.7) remains nonvanishing when the density n varies in the unit cell. By introducing ρ as $\mathbf{R}_j = \mathbf{r}_\perp - \rho$ in the unit cell j, the second term on the right-hand side of Eq. (3.7) is given as

$$\frac{1}{2}I\Omega_v^2 + \frac{1}{2}M\Omega_v^2 \sum_j \int_j \mathrm{d}^3\mathbf{r}\; nf^2(\rho^2 - 2\mathbf{r}_\perp \cdot \rho), \tag{3.8}$$

where $I = \int \mathrm{d}^3\mathbf{r} M n f^2 r_\perp^2$ is the total moment of inertia of the system. Using the moment of inertial I again, the trapping potential term in the xy plane is written as

$$\int \mathrm{d}^3\mathbf{r}\; \frac{M}{2}\omega_\perp^2 r_\perp^2 nf^2 = \frac{1}{2}I\omega_\perp^2. \tag{3.9}$$

The total energy is given by

$$\begin{aligned} E = \frac{1}{2}I(\omega_\perp^2 + \Omega_v^2) + \int \mathrm{d}^3\mathbf{r}\; \left[\frac{\hbar^2(\nabla\sqrt{n})}{2M} + \frac{M}{2}n\omega_z^2 z^2\right] + \sum_j \int_j \mathrm{d}^3\mathbf{r}\; n(\mathbf{r})\left[\frac{\hbar^2(\nabla f)^2}{2M}\right. \\ \left. + f^2\left(\frac{\hbar^2(\nabla\phi_j)^2}{2M} + \frac{1}{2}M\Omega_v^2(\rho^2 - 2\rho\cdot\mathbf{r}_\perp) + \hbar\boldsymbol{\Omega}_v\cdot(\mathbf{R}_j\times\nabla\phi_j)\right) + \frac{g}{2}nf^4\right]. \end{aligned} \tag{3.10}$$

In the rotating frame of reference, the total energy of the system rotating at the angular velocity Ω is given by $E' = E - \Omega L$, where L is the angular momentum along the z-axis given by

$$L = \int \mathrm{d}^3\mathbf{r}\; \psi^*(\mathbf{r}\times\mathbf{p})_z\psi = \int \mathrm{d}^3\mathbf{r}\; n(\mathbf{r})f^2(\mathbf{r})\hbar[\mathbf{r}\times\nabla\Phi(\mathbf{r})]_z. \tag{3.11}$$

By substituting Eq. (3.6) in Eq. (3.11) and using ρ again, we find

$$L = I\Omega_v + \sum_j \int_j \mathrm{d}^3\mathbf{r}\; nf^2[\hbar(\mathbf{r}_\perp\times\nabla\phi_j)_z - M\Omega_v\rho\cdot\mathbf{r}_\perp]. \tag{3.12}$$

3.1.2 Structure of vortices

We determine the structure of a vortex in the unit cell and obtain the total energy of the vortex lattices on a long-distance scale. To calculate the integral over the unit cell, we introduce the Wigner-Seitz approximation, which replaces the hexagonal unit cell into a circle of radius $\sqrt{2}\ell$, so that the area is invariant. The vortex is located at the center of the circle and we assume that f is cylindrically symmetric in the cell. We also assume that the vortex spacing is smaller than the characteristic length in the z direction. Then we can neglect $\partial f/\partial z$ in Eq. (3.10) and f depends only on transverse coordinates x, y and the average local density. From $\mathbf{R}_j = \mathbf{r}_\perp - \rho$, we find $(\nabla\phi_j)^2 = 1/\rho^2$ and $\hbar(\rho\times\nabla\phi_j)_z = \hbar$. Therefore the angular momentum in the Wigner-Seitz approximation is given by

$$L = I\Omega_v + \sum_j \int_j \mathrm{d}^3\mathbf{r}\; nf^2(\hbar - M\Omega_v\rho\cdot\mathbf{r}_\perp). \tag{3.13}$$

To calculate the third term on the right-hand side of Eq. (3.13), we expand the spatially dependent mean density $n(\mathbf{r})$ about the center of cell j as $n(\mathbf{R}_j+\rho) \simeq n(\mathbf{R}_j) + \rho\cdot\nabla n(\mathbf{R}_j)$. We find

$$\begin{aligned}\sum_j \int_j \mathrm{d}^3\mathbf{r}\; nf^2 \rho\cdot\mathbf{r}_\perp &\simeq \frac{1}{2}\sum_j \nabla_j\cdot[\mathbf{R}_j n(\mathbf{R}_j)]\int_j \mathrm{d}^3\mathbf{r}\;\left\langle\rho^2\right\rangle \simeq \frac{1}{2}\int \mathrm{d}^3\mathbf{r}\;\nabla\cdot[\mathbf{r}n(\mathbf{r})]\left\langle\rho^2\right\rangle \\ =&\frac{1}{2}\int \mathrm{d}^3\mathbf{r}\;\nabla\cdot[\mathbf{r}n(\mathbf{r})\left\langle\rho^2\right\rangle] - \frac{1}{2}\int \mathrm{d}^3\mathbf{r}\;\mathbf{r}n(\mathbf{r})\cdot\nabla\left\langle\rho^2\right\rangle,\end{aligned} \tag{3.14}$$

where $\langle g\rangle = \int_j \mathrm{d}^3\mathbf{r}\; gf^2/\int_j \mathrm{d}^3\mathbf{r}$ is the average of an arbitrary function g within the unit cell j. The details of the calculation are given in App. A.1.1. When the density is zero at large distance, the first term in the last expression in Eq. (3.14) vanishes. Furthermore, when $\langle\rho^2\rangle$ does not depend on position, the second term also vanishes owing to $\nabla\langle\rho^2\rangle = 0$ and the last term of the angular momentum (3.13) is zero. In the fast rotating system of our interest, this approximation is legitimate, since the interaction does not change the structure of each cell and the wave function is described by the LLL approximation. We note that this approximation was not used in Ref. [45], which took account of the leading term of the total energy in terms of the number of vortices N_v. From the approximation, the angular momentum becomes $L = I\Omega_v + N\hbar$. We omit the constant second term in the following.

From Eq. (3.14), we find that the term $\rho\cdot\mathbf{r}_\perp$ in Eq. (3.10) vanishes. From a similar calculation in Eq. (3.14), the term $\hbar\boldsymbol{\Omega}_v\cdot(\mathbf{R}_j\times\nabla\phi_j)_z$ in the total energy (3.10) is given by

$$\sum_j \int_j \mathrm{d}^3\mathbf{r}\; nf^2\hbar\boldsymbol{\Omega}_v\cdot(\mathbf{R}_j\times\nabla\phi_j) \simeq -\hbar\Omega_v\int \mathrm{d}^3\mathbf{r}\; nf^2. \tag{3.15}$$

The details of the calculation are given in App. A.1.2. The total energy in the rotating frame of reference $E' = E - \Omega L$ is given by

$$\begin{aligned}E' = &\frac{1}{2}I(\omega_\perp^2 + \Omega_v^2 - 2\Omega\Omega_v) + \int \mathrm{d}^3\mathbf{r}\;\left\{\frac{\hbar^2(\nabla\sqrt{n})}{2M} + \frac{M}{2}n\omega_z^2 z^2\right\} \\ &+ \sum_j \int_j \mathrm{d}^3\mathbf{r}\; n(\mathbf{r})\left[\frac{\hbar^2(\nabla f)^2}{2M} + \left(\frac{\hbar^2(\nabla\phi_j)^2}{2M} + \frac{1}{2}M\Omega_v^2\rho^2 - \hbar\Omega_v\right) + \frac{g}{2}nf^4\right].\end{aligned} \tag{3.16}$$

To separate the term in I that depends on f^2, we rewrite I as

$$I = \bar{I} + \sum_j \int_j \mathrm{d}^3\mathbf{r}\; n(f^2-1)r_\perp^2, \tag{3.17}$$

where $\bar{I} = \int \mathrm{d}^3\mathbf{r}\; Mnr_\perp^2$ is the moment of inertia. The second term of Eq. (3.17) is given by

$$\sum_j \int_j \mathrm{d}^3\mathbf{r}\; n(f^2-1)r_\perp^2 \simeq -\sum_j \int_j \mathrm{d}^3\mathbf{r}\; n(f^2-1)\rho^2. \tag{3.18}$$

The details of the calculation are given in App. A.1.3. The total moment of inertia of the system I becomes

$$I = \bar{I} - \sum_j \int_j \mathrm{d}^3\mathbf{r}\; n(f^2-1)\rho^2 = \bar{I} + \frac{\hbar N}{2\Omega_v} - \sum_j \int_j \mathrm{d}^3\mathbf{r}\; n f^2\rho^2. \tag{3.19}$$

We find

$$E' = \frac{1}{2}\left(\bar{I} + \frac{\hbar N}{2\Omega_v}\right)(\omega_\perp^2 + \Omega^2 - 2\Omega\Omega_v) + \int \mathrm{d}^3\mathbf{r}\; \left\{\frac{\hbar^2(\nabla\sqrt{n})}{2M} + \frac{M}{2}n\omega_z^2 z^2\right\} - \hbar\Omega_v N + \sum_j E_j, \tag{3.20}$$

where

$$E_j = \int_j \mathrm{d}^3\mathbf{r}\; n(\mathbf{r})\left\{\frac{\hbar^2}{2M}\left[\left(\frac{\partial f}{\partial\rho}\right)^2 + \frac{f^2}{\rho^2}\right] + \frac{M}{2}(2\Omega\Omega_v - \omega_\perp^2)f^2\rho^2 + \frac{g}{2}nf^4\right\}, \tag{3.21}$$

includes all terms that depend on f. Here we ignore the difference $\Omega - \Omega_v$. To find the structure of a vortex at each unit cell, we minimize Eq. (3.21) with respect to f with $\int_j d^2\rho(f^2-1) = 0$ and the boundary condition $f(0) = 0$ and $\frac{\partial f}{\partial\rho} = 0$ at $\rho = \ell$. In the following, we give the form of f in the LLL approximation.

We define the averages over the unit cell of the following quantities depending on the distribution of the density in the unit cell as

$$a = \frac{\ell^2}{2}\left\langle\left(\frac{\partial f}{\partial\rho}\right)^2 + \frac{f^2}{\rho^2}\right\rangle, \quad b' = \frac{1}{\ell^2}\left\langle\rho^2 f^2\right\rangle, \quad b = \left\langle f^4\right\rangle. \tag{3.22}$$

Then the structure of a vortex is removed from Eq. (3.21) and its energy is rewritten as

$$E_j = \int_j \mathrm{d}^3\mathbf{r}\; n\left\{\hbar\Omega_v a + b'\hbar\left(\Omega - \frac{\omega_\perp^2}{2\Omega_v}\right) + \frac{gnb}{2}\right\}. \tag{3.23}$$

We obtain the total energy of the vortex lattice on a scale much larger than that of the unit cell. In the mean-field LLL regime, where the system is rapidly rotating, we assume that f has the structure of a p-state of oscillator to the lowest order, which is given by

$$f(\rho) = C\frac{\rho}{\ell}e^{-\rho^2/2\ell^2}, \tag{3.24}$$

where $C = (1-2/e)^{-1/2}$ is the normalization factor. By substituting the state (3.24) into the energy in the unit cell (3.21), we find

$$E_j = \int_j \mathrm{d}^3\mathbf{r}\; n\left(2\hbar\Omega_v - \frac{M}{2}(\omega_\perp^2 + \Omega_v^2 - 2\Omega\Omega_v)f^2\rho^2 + \frac{g}{2}nf^4\right), \tag{3.25}$$

so that the total energy is given by

$$E' = \frac{1}{2}I(\omega_\perp^2 + \Omega^2 - 2\Omega\Omega_v) + \int \mathrm{d}^3\mathbf{r}\; \left(\frac{\hbar^2(\nabla\sqrt{n})}{2M} + \frac{M}{2}n\omega_z^2 z^2 + \frac{gbn^2}{2}\right) + N\hbar\Omega_v. \tag{3.26}$$

The average of ρ^2/ℓ^2 is given by

$$b' = \frac{1}{\ell^2}\frac{\int_j \mathrm{d}^2\rho\ \rho^2 f^2}{\int_j \mathrm{d}^2\rho} = \frac{2e-5}{e-2} \simeq 0.608, \tag{3.27}$$

and we find $a = 2 - b'/2$. The renormalization factor of the coupling constant in the LLL approximation is given by

$$b = \frac{\int_j \mathrm{d}^2\rho\ f^4}{\int_j \mathrm{d}^2\rho} = \frac{e^2-5}{4(e-2)^2} \simeq 1.158. \tag{3.28}$$

To obtain Ω_v, we minimize Eq. (3.26) ($\delta E'/\delta\Omega_v = 0$) with respect to Ω_v. For an angular velocity Ω, we obtain

$$\Omega_v = \Omega - N/I. \tag{3.29}$$

By substituting Eq. (3.29) into Eq. (3.26), the total energy of the system is given by

$$E' = \frac{1}{2}I(\omega_\perp^2 - \Omega^2) + N\hbar\Omega - \frac{N^2}{2I} + \int \mathrm{d}^3\mathbf{r}\ \left(\frac{\hbar^2(\nabla\sqrt{n})}{2M} + \frac{M}{2}n\omega_z^2 z^2 + \frac{gbn^2}{2}\right), \tag{3.30}$$

which is consistent with the exact result in [46].

3.2 Effective-field theory of vortex lattices

In this section, we derive the effective-field theory of vortex lattices in binary BECs in the LLL approximation. In Sec. 3.2.1, we describe the system under consideration. In Sec. 3.2.2, we derive the effective-field theory for the binary systems by extending the derivation for a scalar case. In Sec. 3.2.3, we discuss the elastic energy used for the effective-field theory. We find that the elastic energy terms which are unique to the binary system are related to the quadratic and linear dispersion relations and an important term is missing in the previous study [47]. In Sec. 3.2.4, we discuss the renormalization of the coupling constants in a binary system.

3.2.1 Description of the system

We consider a system of two-dimensional binary (pseudospin-1/2) BECs having two hyperfine spin states, which we label by $\alpha = \uparrow, \downarrow$. The two components are subjected to synthetic magnetic fields $B_\uparrow$ and $B_\downarrow$ in mutually parallel or antiparallel directions. The Lagrangian density of the system is given by

$$\mathcal{L} = \sum_{\alpha=\uparrow,\downarrow}\left[\frac{i\hbar}{2}(\psi_\alpha^\dagger\dot{\psi}_\alpha - \dot{\psi}_\alpha^\dagger\psi_\alpha) - \frac{1}{2M}|(-i\hbar\nabla - q\mathbf{A}_\alpha)\psi_\alpha|^2\right] - \sum_{\alpha,\beta=\uparrow,\downarrow}\frac{g_{\alpha\beta}}{2}|\psi_\alpha|^2|\psi_\beta|^2, \tag{3.31}$$

where $\psi_\alpha(\mathbf{r},t)$ is the bosonic field of the spin-α component and q is the fictitious charge of an atom whose mass is M. The gauge field $\mathbf{A}_\alpha(\mathbf{r})$ for the spin-α component is given by

$$\mathbf{A}_\alpha = \frac{B_\alpha}{2}\mathbf{e}_z \times \mathbf{r} = \epsilon_\alpha\frac{B}{2}(-y, x, 0), \tag{3.32}$$

where $\epsilon_\uparrow = \epsilon_\downarrow = 1$ ($\epsilon_\uparrow = -\epsilon_\downarrow = 1$) for parallel (antiparallel) fields. We assume $qB > 0$ in the following. For a two-dimensional system whose area is given by A, the number of magnetic flux quanta piercing each component, which is equivalent to the number of vortices, is given by $N_\mathrm{v} = A/(2\pi\ell^2)$, where $\ell := \sqrt{\hbar/qB}$ is the magnetic length. In this system, the numbers of spin-$\uparrow$ and $\downarrow$ atoms, $N_\uparrow$ and $N_\downarrow$, respectively, are separately conserved. We define the total filling factor as $\nu := N/N_\mathrm{v}$, where $N := N_\uparrow + N_\downarrow$ is the total number of atoms.

We assume that the two-body interaction between atoms is a contact interaction and we set $g_{\uparrow\uparrow} = g_{\downarrow\downarrow} \equiv g > 0$, $|g_{\uparrow\downarrow}| < g$. We also assume that $N_\uparrow = N_\downarrow$ in the following. From these conditions, the system in parallel fields is invariant under the interchange of the two components while the system in antiparallel fields is invariant under time reversal. In order to use the LLL approximation, the energy scale of the interaction per atom $|g_{\alpha\beta}|n$ must be much smaller than the Landau-level spacing $\hbar\omega_\mathrm{c}$, where $n := N_\uparrow/A = N_\downarrow/A$ is the average density of $\uparrow$ or $\downarrow$ atoms and $\omega_\mathrm{c} := qB/M$ is the cyclotron frequency. We assume that the synthetic magnetic fields B_α are sufficiently strong or the interactions are sufficiently weak.

3.2.2 Derivation of effective-field theory

To derive the low-energy effective-field theory, we rewrite the field as $\psi_\alpha = \mathrm{e}^{-\mathrm{i}\theta_\alpha}\sqrt{n_\alpha}$, where $n_\alpha(\mathbf{r},t)$ and $\theta_\alpha(\mathbf{r},t)$ are the density and phase variables, respectively. Using these variables, the Lagrangian density (3.31) is given by

$$\mathcal{L} = \sum_\alpha \left[\hbar n_\alpha \dot{\theta}_\alpha - \frac{n_\alpha}{2M}(\hbar\nabla\theta_\alpha + q\mathbf{A}_\alpha)^2 - \frac{\hbar^2(\nabla n_\alpha)^2}{8n_\alpha M}\right] - \sum_{\alpha,\beta}\frac{g_{\alpha\beta}}{2}n_\alpha n_\beta. \tag{3.33}$$

In the presence of vortices, the phase variables $\{\theta_\alpha(\mathbf{r},t)\}$ involve singularities. We decompose the phase θ_α into its regular and singular parts as $\theta_\alpha = \theta_{\mathrm{reg},\alpha} + \theta_{\mathrm{sing},\alpha}$. We also introduce the displacement of a vortex from the equilibrium position as $\mathbf{u}_\alpha(\mathbf{r},t) = \mathbf{r} - \mathbf{X}_\alpha(\mathbf{r},t)$, where $\mathbf{r}$ is the equilibrium position of the vortex and $\mathbf{X}_\alpha$ is its position at time t. The displacement fields $\mathbf{u}_\alpha$ can be related to the derivatives of the singular part $\theta_{\mathrm{sing},\alpha}$ of the phase as [48, 49]

$$\hbar\dot{\theta}_{\mathrm{sing},\alpha} = -\frac{qB}{2}(\mathbf{u}_\alpha \times \dot{\mathbf{u}}_\alpha)_z, \quad \hbar\nabla\theta_{\mathrm{sing},\alpha} + q\mathbf{A}_\alpha = qB_\alpha \mathbf{e}_z \times \mathbf{u}_\alpha - \frac{qB_\alpha}{2}\epsilon_{ij}u_\alpha^i \nabla u_\alpha^j, \tag{3.34}$$

where ϵ_{ij} is the antisymmetric tensor with $\epsilon_{xy} = -\epsilon_{yx} = +1$. The displacement $\mathbf{u}_\alpha(\mathbf{r},t)$ determines the elastic energy $\int \mathrm{d}^2\mathbf{r}\ \mathcal{E}_\mathrm{el}(\mathbf{u}_\alpha, \partial_i\mathbf{u}_\alpha)$, whose form is constrained by the symmetry of the ground state of vortex lattices. Details will be discussed in Sec. 3.2.3. The Lagrangian density in terms of $\{\theta_{\mathrm{reg},\alpha}, \mathbf{u}_\alpha, n_\alpha\}$ is expressed as

$$\begin{aligned}\mathcal{L} = \sum_\alpha \Bigg[&\hbar n_\alpha \dot{\theta}_{\mathrm{reg},\alpha} - \frac{qB_\alpha n_\alpha}{2}(\mathbf{u}_\alpha \times \dot{\mathbf{u}}_\alpha)_z - \frac{n_\alpha}{2M}\left(\hbar\nabla\theta_{\mathrm{reg},\alpha} + qB_\alpha \mathbf{e}_z \times \mathbf{u}_\alpha - \frac{qB_\alpha}{2}\epsilon_{ij}u_\alpha^i\nabla u_\alpha^j\right)^2 \\ &- \frac{\hbar^2(\nabla n_\alpha)^2}{8n_\alpha M}\Bigg] - \sum_{\alpha,\beta}\frac{\bar{g}_{\alpha\beta}}{2}n_\alpha n_\beta - \mathcal{E}_\mathrm{el}.\end{aligned} \tag{3.35}$$

In the following, we omit the subscript "reg" for $\theta_{\mathrm{reg},\alpha}$.

In the interaction term in Eq. (3.35), we have introduced renormalized coupling constants $\bar{g}_{\alpha\beta}$ with $\bar{g}_{\uparrow\uparrow} = \bar{g}_{\downarrow\downarrow} \equiv \bar{g}$ and $\bar{g}_{\uparrow\downarrow} = \bar{g}_{\downarrow\uparrow}$, since we have coarse-grained the model by introducing vortex displacement fields. This modification is important to discuss the vortex lattices in the LLL and compare the theory with the Bogoliubov theory in Chap. 4. We discuss details about how to obtain the renormalized coupling constants in Sec. 3.2.4.

Since $\{\mathbf{u}_\alpha\}$ have the mass term $-\mathbf{u}_\alpha^2$ in Eq. (3.35), we expect that they are integrated out safely in discussing the low-energy dynamics. The Euler-Lagrange equations for $\{\mathbf{u}_\alpha\}$ are given by

$$\mathbf{u}_\alpha - \epsilon_\alpha \ell^2 \mathbf{e}_z \times \nabla\theta_\alpha - \frac{\epsilon_\alpha}{\omega_\mathrm{c}} \mathbf{e}_z \times \dot{\mathbf{u}}_\alpha + \frac{\ell^2}{n\hbar\omega_\mathrm{c}} \left[\frac{\partial \mathcal{E}_\mathrm{el}}{\partial \mathbf{u}_\alpha} - \sum_j \partial_j \left(\frac{\partial \mathcal{E}_\mathrm{el}}{\partial (\partial_j \mathbf{u}_\alpha)} \right) \right] = 0, \tag{3.36}$$

where we have made the approximation $n_\alpha \approx n$. We can ignore the third and fourth terms on the left-hand side in the LLL approximation, since $\hbar\omega, \ell^2 \mathcal{E}_\mathrm{el} \ll \hbar\omega_\mathrm{c}$, where ω is the frequency of our interest.

Since the elastic energy depends on $\mathbf{u}_\pm := \mathbf{u}_\uparrow \pm \mathbf{u}_\downarrow$ as we will see in Sec. 3.2.3, we rewrite the Euler-Lagrange equation (3.36) as

$$\mathbf{u}_\pm = \begin{cases} \ell^2 \mathbf{e}_z \times \nabla\theta_\pm & \text{(parallel fields);} \\ \ell^2 \mathbf{e}_z \times \nabla\theta_\mp & \text{(antiparallel fields),} \end{cases} \tag{3.37}$$

where $\theta_\pm := \theta_\uparrow \pm \theta_\downarrow$. These relations indicate that in parallel fields the symmetric $\mathbf{u}_+$ (antisymmetric $\mathbf{u}_-$) is coupled to the symmetric θ_+ (antisymmetric θ_-), while in antiparallel fields they are coupled in a crossed manner. We also find the vortex is displaced in the direction perpendicular to the wave vector $\mathbf{k}$. We introduce $\hbar n_\pm = \hbar(n_\uparrow \pm n_\downarrow)/2$ as the conjugate momenta of $\theta_\pm$ since n_α are the conjugate momenta of θ_α, as can be seen from the first term of Eq. (3.35).

By eliminating the displacement fields $\mathbf{u}_\alpha$ in Eq. (3.35) by substituting Eqs. (3.36) and (3.37) in Eq. (3.35), the Lagrangian density in terms of $\{\theta_\nu, n_\nu\}$ is given as

$$\mathcal{L} = \sum_{\nu=\pm} \left[\hbar n_\nu \dot{\theta}_\nu - \frac{\hbar^2 (\nabla n_\nu)^2}{4nM} - \bar{g}_\nu n_\nu^2 \right] - \mathcal{E}_\mathrm{el}, \quad \bar{g}_\pm := \bar{g} \pm \bar{g}_{\uparrow\downarrow}, \tag{3.38}$$

where we ignore the higher-derivative terms. The Hamiltonian density is obtained as

$$\mathcal{H} = \sum_{\nu=\pm} \left[\bar{g}_\nu n_\nu^2 + \frac{\hbar^2 (\nabla n_\nu)^2}{4nM} \right] + \mathcal{E}_\mathrm{el}. \tag{3.39}$$

We require the canonical commutation relations

$$[\theta_\nu(\mathbf{r}), n_{\nu'}(\mathbf{r}')] = \mathrm{i}\delta_{\nu\nu'}\delta(\mathbf{r} - \mathbf{r}') \quad (\nu, \nu' = \pm), \tag{3.40}$$

in quantizing the theory of vortex lattices.

3.2.3 Elastic energy

Since the elastic energy is invariant under the translation of the lattices, $\mathcal{E}_{\rm el}$ is a function of $\partial_i \mathbf{u}_+$ $(i = x, y)$ and $\mathbf{u}_-$, which are invariant under a constant change in $\mathbf{u}_\alpha(\mathbf{r}, t)$, to the leading order in the derivative expansion. Therefore we can decompose it as

$$\mathcal{E}_{\rm el} = \mathcal{E}_{\rm el}^{(+)}(\partial_i \mathbf{u}_+) + \mathcal{E}_{\rm el}^{(-)}(\mathbf{u}_-) + \mathcal{E}_{\rm el}^{(+-)}(\partial_i \mathbf{u}_+, \mathbf{u}_-). \tag{3.41}$$

To express $\mathcal{E}_{\rm el}^{(+)}$, it is useful to introduce the stress tensors given by

$$w_0 := \partial_x u_+^x + \partial_y u_+^y, \quad w_1 := \partial_x u_+^x - \partial_y u_+^y, \quad w_2 := \partial_y u_+^x + \partial_x u_+^y. \tag{3.42}$$

Since the vortex density stays constant in the LLL regime, we find $w_0 = 0$. This can also be confirmed by substituting Eq. (3.37) into w_0. From a symmetry consideration which we will describe in App. A.2, the three terms in Eq. (3.41) are expressed as

$$\begin{aligned}
\mathcal{E}_{\rm el}^{(+)}(\partial_i \mathbf{u}_+) &= \frac{gn^2}{2}\left(C_1 {w_1}^2 + C_2 {w_2}^2 + C_3 w_1 w_2\right), \\
\mathcal{E}_{\rm el}^{(-)}(\mathbf{u}_-) &= \frac{gn^2}{2\ell^2}\left[D_1 \left(u_-^x\right)^2 + D_2 \left(u_-^y\right)^2 + D_3 u_-^x u_-^y\right], \\
\mathcal{E}_{\rm el}^{(+-)}(\partial_i \mathbf{u}_+, \mathbf{u}_-) &= \frac{gn^2}{2\ell} F_1 \left(w_1 u_-^y + w_2 u_-^x\right),
\end{aligned} \tag{3.43}$$

where C_i, D_i $(i = 1, 2, 3)$ and F_1 are the dimensionless elastic constants. For each of the vortex lattices in Fig. 2.2 (a)-(e), the dimensionless elastic constants $\{C_1, C_2, C_3, D_1, D_2, D_3, F_1\}$ satisfy

$$\begin{aligned}
&\text{(a) } C_1 = C_2 \equiv C > 0,\ D_1 = D_2 \equiv D > 0,\ C_3 = D_3 = F_1 = 0; \\
&\text{(b) } C_1 = C_2 \equiv C > 0, D_1 = D_2 \equiv D > 0,\ C_3 = D_3 = 0,\ F_1 \neq 0; \\
&\text{(c) } C_1, C_2, D_1, D_2 > 0,\ C_3, D_3 \neq 0,\ F_1 = 0; \\
&\text{(d) } C_1, C_2 > 0,\ D_1 = D_2 \equiv D > 0,\ C_3 = D_3 = F_1 = 0; \\
&\text{(e) } C_1, C_2 > 0,\ D_1, D_2 > 0,\ C_3 = D_3 = F_1 = 0.
\end{aligned} \tag{3.44}$$

In a scalar case, the elastic energy of a triangular vortex lattice is only given by the stress tensors due to the invariance of the elastic energy with respect to the translation of the lattice. In the following section, the linear dispersion relation is obtained by $\mathcal{E}_{\rm el}^{(-)}$ and the quadratic dispersion relation is obtained by $\mathcal{E}_{\rm el}^{(+)}$ and $\mathcal{E}_{\rm el}^{(+-)}$. The emergence of the linear dispersion relation originates from the invariance of $\mathbf{u}_-$ against the translation of lattices, which is unique to the binary system.

We note that the term $\mathcal{E}_{\rm el}^{(+-)}$ was missing in the previous study by Keçeli and Oktel [47] from the symmetrical consideration since they impose the invariance of the elastic energy under the exchange of components, which does not occur in interlaced vortex lattices (b). The F_1 term is allowed by the C_3 symmetry of interlaced vortex lattices (b). As this term couples the symmetric and antisymmetric displacement $\mathbf{u}_\pm$, the low-energy spectrum of interlaced vortex lattices with a quadratic dispersion relation changes drastically. An anisotropy of the quadratic dispersion relation $f_2(\varphi)$ depicted in Fig. 4.4 (b) has C_6 symmetry owing to the new term while the anisotropy function $f_2(\varphi)$ was constant in the previous research [47].

From the calculation of the change of the energy due to the deformation of the vortex lattices in the mean-field theory, Keçeli and Oktel [47] determined the constants $\{C_1, C_2, C_3, D_1, D_2, D_3\}$. We calculate the dimensionless elastic constants $\{C_1, C_2, C_3, D_1, D_2, D_3, F_1\}$ by fitting an analytical forms of excitation spectra to the numerical results based on the Bogoliubov theory in Chap. 4. From the one-to-one correspondence of the GP energy functionals between parallel and antiparallel fields, we find that the values of the elastic constants are the same between two cases. This correspondence will be confirmed for each of the vortex lattices in Sec. 4.2.1.

3.2.4 Renormalization of coupling constants

On the basis of the study about a vortex lattice in a scalar BEC [44], we show that the coupling constant in the LLL approximation is renormalized according to Eq. (3.28). To obtain the renormalization factor for a binary system, we first note that the value of the renormalization factor remains the same even if the integral over the unit cell is changed into the integral over the system. Since the order parameter of the spin-α component is given by $\psi_\alpha(\mathbf{r}) = \sqrt{nA}\Psi_{\mathbf{q}_\alpha,\alpha}(\mathbf{r})$, where $\Psi_{\mathbf{q}_\alpha,\alpha}(\mathbf{r})$ is the LLL magnetic Bloch state, which we will discuss in Chap. 4, we find that the density is constant and a rapidly varying part is given by $f_\alpha = \sqrt{A}\Psi_{\mathbf{q}_\alpha,\alpha}(\mathbf{r})$. Therefore the coupling constant $g_{\alpha\beta}$ is renormalized as $\bar{g}_{\alpha\beta} = \beta_{\alpha\beta} g_{\alpha\beta}$ with the renormalization factor $\beta_{\alpha\beta}$ given as

$$\beta_{\alpha\beta} = \frac{\int \mathrm{d}^2\mathbf{r}\ f_\alpha^2 f_\beta^2}{\int \mathrm{d}^2\mathbf{r}} = \int \mathrm{d}^2\mathbf{r}\ |\Psi_{\mathbf{q}_\alpha,\alpha}(\mathbf{r})|^2 |\Psi_{\mathbf{q}_\beta,\beta}(\mathbf{r})|^2, \tag{3.45}$$

where the integration runs over the system instead of a unit cell. By assuming that the renormalized coupling constants $\bar{g}_{\alpha\beta}$ satisfy $\bar{g}_{\uparrow\uparrow} = \bar{g}_{\downarrow\downarrow} \equiv \bar{g} > 0$ and $\bar{g}_{\uparrow\downarrow} = \bar{g}_{\downarrow\uparrow}$, we find that $\beta_{\alpha\beta}$ is obtained by the numerically calculation of

$$\beta_{\alpha\beta} = \frac{A}{g_{\alpha\beta}} V_{\alpha\beta}(\mathbf{q}_\alpha, \mathbf{q}_\beta, \mathbf{q}_\beta, \mathbf{q}_\alpha), \tag{3.46}$$

where $V_{\alpha\beta}$ is the interaction matrix element discussed in Chap. 4. As we see from Eq. (3.45), $\bar{g}_{\alpha\beta}$ is determined by the contribution of each interaction term to the mean-field ground-state energy.

Figure 3.1 presents the renormalization factors $\beta := \bar{g}/g$ and $\beta_{\uparrow\downarrow} := \bar{g}_{\uparrow\downarrow}/g_{\uparrow\downarrow}$ calculated for the mean-field vortex lattice structures. We find that β and $\beta_{\uparrow\downarrow}$ are independent of $g_{\uparrow\downarrow}/g$ for overlapping triangular, interlaced triangular, and square lattices since the lattice structures remain unchanged in the corresponding regions. In contrast, β and $\beta_{\uparrow\downarrow}$ do depend on $g_{\uparrow\downarrow}/g$ for the other lattices, since the inner angle θ and the aspect ratio b/a continuously vary within the regime of rhombic and rectangular lattices, respectively.

We find that the intracomponent coupling is always enhanced by the renormalization. We indeed confirm that $\beta > 1$ in all the regions in Fig. 3.1. We also find that the intercomponent repulsion $g_{\uparrow\downarrow} > 0$ (attraction $g_{\uparrow\downarrow} < 0$) is reduced (enhanced) by the renormalization owing to the displacement (overlap) of vortices between the components. In Fig. 3.1, we indeed confirm $\beta_{\uparrow\downarrow} < 1$ ($\beta_{\uparrow\downarrow} > 1$) for $g_{\uparrow\downarrow} > 0$ ($g_{\uparrow\downarrow} < 0$). Furthermore, β ($\beta_{\uparrow\downarrow}$) monotonically increases (decreases) as a function of $g_{\uparrow\downarrow}/g$ for $g_{\uparrow\downarrow} > 0$. This reflects the fact that with increasing $g_{\uparrow\downarrow}/g$, vortices in different components tend to repel more strongly with each other at the cost of increasing the intracomponent interaction energy.

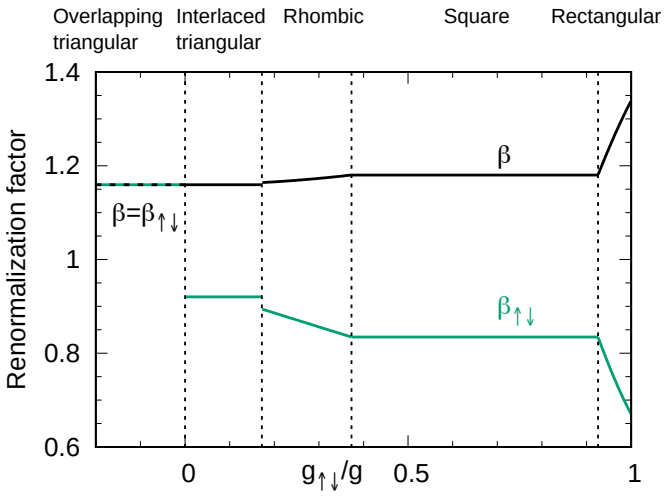

Figure 3.1: Renormalization factors $\beta := \bar{g}/g$ (black) and $\beta_{\uparrow\downarrow} := \bar{g}_{\uparrow\downarrow}/g_{\uparrow\downarrow}$ (green) for the intracomponent and intercomponent coupling constants. For the mean-field vortex lattice structure for each $g_{\uparrow\downarrow}/g$, these factors are calculated from Eq. (3.46). Vertical dashed lines indicate the transition points in the mean-field phase diagram [17]. They take the same values for parallel and antiparallel fields. We set $N_{\rm v} = 97^2$, with which a sufficient convergence to the thermodynamic limit is achieved. For overlapping triangular lattices ($-1 < g_{\uparrow\downarrow}/g < 0$), we have $\beta = \beta_{\uparrow\downarrow}$, so that the two curves are overlapping and the value is $\beta = \beta_{\uparrow\downarrow} = 1.1596$. The value in this region coincides with the renormalization factor obtained for a scalar BEC [13, 50, 51].

3.3 Diagonalization of the Hamiltonian

In this section, we diagonalize the Hamiltonian to obtain the dispersion relations analytically (Sec. 3.3.1). The quadratic and linear dispersion relations appear in all the phases. We obtain the rescaling relations between the dispersion relations for parallel and antiparallel fields, so that we relate the excitation modes in parallel and antiparallel fields although the two modes are different. We also obtain analytic forms of correlation functions and the fraction of depletion for the next discussion (Sec. 3.3.2).

3.3.1 Dispersion relations

We calculate the energy spectrum of the Hamiltonian $H = \int \mathrm{d}^2\mathbf{r}\ \mathcal{H}$, where the Hamiltonian density $\mathcal{H}$ is given by Eq. (3.39). We perform Fourier expansions

$$\theta_\nu(\mathbf{r}) = \frac{1}{\sqrt{A}} \sum_{\mathbf{k}} \theta_{\mathbf{k},\nu} \mathrm{e}^{\mathrm{i}\mathbf{k}\cdot\mathbf{r}}, \quad n_\nu(\mathbf{r}) = \frac{1}{\sqrt{A}} \sum_{\mathbf{k}} n_{\mathbf{k},\nu} \mathrm{e}^{\mathrm{i}\mathbf{k}\cdot\mathbf{r}} \quad (\nu = \pm), \tag{3.47}$$

where the Fourier components satisfy

$$[\theta_{\mathbf{k},\nu}, n_{-\mathbf{k}',\nu'}] = \mathrm{i}\delta_{\nu\nu'}\delta_{\mathbf{k}\mathbf{k}'}, \quad \theta^\dagger_{\mathbf{k},\nu} = \theta_{-\mathbf{k},\nu}, \quad n^\dagger_{\mathbf{k},\nu} = n_{-\mathbf{k},\nu} \quad (\nu, \nu' = \pm), \tag{3.48}$$

since $n(\mathbf{r})$ and $\theta(\mathbf{r})$ are real functions and satisfy the commutation relation (3.40). We note that the $\mathbf{k} = \mathbf{0}$ component of the densities $n_{\mathbf{0},\pm}$ and the atom numbers are related

to $n_{\mathbf{0},\pm} = (N_\uparrow \pm N_\downarrow)/(2\sqrt{A})$. The Hamiltonian H is given by

$$H = \frac{n}{2}\sum_{\mathbf{k}} \begin{pmatrix} \theta_{-\mathbf{k},+} & \theta_{-\mathbf{k},-} \end{pmatrix} \begin{pmatrix} \Gamma_\pm(\mathbf{k}) & \pm \mathrm{i}\Gamma(\mathbf{k}) \\ \mp \mathrm{i}\Gamma(\mathbf{k}) & \Gamma_\mp(\mathbf{k}) \end{pmatrix} \begin{pmatrix} \theta_{\mathbf{k},+} \\ \theta_{\mathbf{k},-} \end{pmatrix} + \frac{1}{2n}\sum_{\mathbf{k}}\sum_{\nu=\pm} e_{\mathbf{k},\nu} n_{-\mathbf{k},\nu} n_{\mathbf{k},\nu}, \quad (3.49)$$

where[1]

$$\begin{aligned} e_{\mathbf{k},\nu} &= 2g_\nu n + \epsilon_{\mathbf{k}}, \\ \Gamma_+(\mathbf{k}) &= gn\ell^4 \left[C_1 \left(2k_x k_y\right)^2 + C_2 \left(k_x^2 - k_y^2\right)^2 - C_3 \left(2k_x k_y\right)\left(k_x^2 - k_y^2\right) \right], \\ \Gamma_-(\mathbf{k}) &= gn\ell^2 \left(D_1 k_y^2 + D_2 k_x^2 - D_3 k_x k_y \right), \\ \Gamma(\mathbf{k}) &= \frac{1}{2} gn\ell^3 F_1 \left(3k_x^2 k_y - k_y^3 \right). \end{aligned} \quad (3.50)$$

In Eq. (3.49), the upper and lower signs correspond to the cases of parallel and antiparallel fields, respectively.[2]

The Hamiltonian (3.49) is decomposed into a part of the zero mode ($\mathbf{k} = \mathbf{0}$) and a part of the oscillator mode ($\mathbf{k} \neq \mathbf{0}$) for usefulness. The former is given by

$$H^{\mathrm{zero}} = \sum_{\nu=\pm} \bar{g}_\nu n_{\mathbf{0},\nu}^2 = \frac{\bar{g}_+}{4A} N^2 + \frac{\bar{g}_-}{4A} (N_\uparrow - N_\downarrow)^2. \quad (3.51)$$

We find that the atom numbers $N_\uparrow$ and $N_\downarrow$ specify the zero-mode energy. In our setting of balanced population $N_\uparrow = N_\downarrow$, the zero-mode state is given by the product state $|N_\uparrow = N/2\rangle\,|N_\downarrow = N/2\rangle$, which has no intercomponent entanglement as we will discuss in Chap. 5.

Next, we discuss the oscillator-mode part H^{osc} of the Hamiltonian (3.49). We perform canonical transformations in two steps to diagonalize it. The first transformation reads

$$\tilde{\theta}_{\mathbf{k},+} = r_{\mathbf{k}}^{-1}\theta_{\mathbf{k},+},\ \tilde{\theta}_{\mathbf{k},-} = r_{\mathbf{k}}\theta_{\mathbf{k},-},\ \tilde{n}_{\mathbf{k},+} = r_{\mathbf{k}} n_{\mathbf{k},+},\ \tilde{n}_{\mathbf{k},-} = r_{\mathbf{k}}^{-1} n_{\mathbf{k},-}, \quad (3.52)$$

where $r_{\mathbf{k}} := (e_{\mathbf{k},+}/e_{\mathbf{k},-})^{1/4}$. We find that H^{osc} is rewritten as

$$H^{\mathrm{osc}} = \frac{n}{2}\sum_{\mathbf{k}\neq\mathbf{0}} \begin{pmatrix} \tilde{\theta}_{-\mathbf{k},+} & \tilde{\theta}_{-\mathbf{k},-} \end{pmatrix} M(\mathbf{k}) \begin{pmatrix} \tilde{\theta}_{\mathbf{k},+} \\ \tilde{\theta}_{\mathbf{k},-} \end{pmatrix} + \frac{1}{2n}\sum_{\mathbf{k}\neq\mathbf{0}}\sum_{\nu=\pm} e_{\mathbf{k}} \tilde{n}_{-\mathbf{k},\nu} \tilde{n}_{\mathbf{k},\nu}, \quad (3.53)$$

where $e_{\mathbf{k}} := \sqrt{e_{\mathbf{k},+} e_{\mathbf{k},-}}$. The 2×2 matrix $M(\mathbf{k})$ is given by

$$M(\mathbf{k}) = \begin{pmatrix} \tilde{\Gamma}_\pm(\mathbf{k}) & \pm \mathrm{i}\Gamma(\mathbf{k}) \\ \mp \mathrm{i}\Gamma(\mathbf{k}) & \tilde{\Gamma}_\mp(\mathbf{k}) \end{pmatrix} = \frac{\tilde{\Gamma}_+(\mathbf{k}) + \tilde{\Gamma}_-(\mathbf{k})}{2} I \mp \Gamma(\mathbf{k})\sigma_y \pm \frac{\tilde{\Gamma}_+(\mathbf{k}) - \tilde{\Gamma}_-(\mathbf{k})}{2}\sigma_z, \quad (3.54)$$

where $\tilde{\Gamma}_+(\mathbf{k}) := r_{\mathbf{k}}^{\pm 2}\Gamma_+(\mathbf{k})$, $\tilde{\Gamma}_-(\mathbf{k}) := r_{\mathbf{k}}^{\mp 2}\Gamma_-(\mathbf{k})$, I is the identity matrix, and $(\sigma_x, \sigma_y, \sigma_z)$ are the Pauli matrices. The second canonical transformation is performed by using the unitary matrix $U(\mathbf{k})$ as

$$\begin{pmatrix} \tilde{\theta}_{\mathbf{k},+} \\ \tilde{\theta}_{\mathbf{k},-} \end{pmatrix} = U(\mathbf{k}) \begin{pmatrix} \bar{\theta}_{\mathbf{k},1} \\ \bar{\theta}_{\mathbf{k},2} \end{pmatrix}, \quad \begin{pmatrix} \tilde{n}_{\mathbf{k},+} \\ \tilde{n}_{\mathbf{k},-} \end{pmatrix} = U(\mathbf{k}) \begin{pmatrix} \bar{n}_{\mathbf{k},1} \\ \bar{n}_{\mathbf{k},2} \end{pmatrix}. \quad (3.55)$$

[1] The definitions of $\Gamma_\pm(\mathbf{k})$ and $\Gamma(\mathbf{k})$ are changed from Ref. [31]. We divide them by n so that the dimension is an energy.

[2] The same sign rule applies to Eqs. (3.54), (3.57), (3.62), (3.64), (3.65), (3.71), (3.73), and (3.77) below.

We note that if $U(-\mathbf{k})^t U(\mathbf{k}) = I$ for all $\mathbf{k} \neq \mathbf{0}$, the second term of Eq. (3.53) is invariant under this transformation. We choose $U(\mathbf{k})$ which diagonalizes the Hermitian matrix $M(\mathbf{k})$ as

$$U^{-1}(\mathbf{k})M(\mathbf{k})U(\mathbf{k}) = \begin{pmatrix} m_{\mathbf{k},1} & 0 \\ 0 & m_{\mathbf{k},2} \end{pmatrix}, \quad U(\mathbf{k}) = \mathrm{e}^{\mathrm{i}\chi_{\mathbf{k}}\sigma_x/2} = \begin{pmatrix} \cos(\chi_{\mathbf{k}}/2) & \mathrm{i}\sin(\chi_{\mathbf{k}}/2) \\ \mathrm{i}\sin(\chi_{\mathbf{k}}/2) & \cos(\chi_{\mathbf{k}}/2) \end{pmatrix}, \tag{3.56}$$

where

$$\begin{aligned} m_{\mathbf{k},j} &= \frac{\tilde{\Gamma}_+(\mathbf{k}) + \tilde{\Gamma}_-(\mathbf{k})}{2} + (-1)^{j-1}\Lambda(\mathbf{k}) \quad (j = 1, 2), \\ \cos\chi_{\mathbf{k}} &= \pm\frac{\tilde{\Gamma}_+(\mathbf{k}) - \tilde{\Gamma}_-(\mathbf{k})}{2\Lambda(\mathbf{k})}, \quad \sin\chi_{\mathbf{k}} = \mp\frac{\Gamma(\mathbf{k})}{\Lambda(\mathbf{k})}, \quad \Lambda(\mathbf{k}) = \left[\frac{1}{4}\left(\tilde{\Gamma}_+(\mathbf{k}) - \tilde{\Gamma}_-(\mathbf{k})\right)^2 + \Gamma(\mathbf{k})^2\right]^{1/2}. \end{aligned} \tag{3.57}$$

Since $\tilde{\Gamma}_\pm(\mathbf{k}) = \tilde{\Gamma}_\pm(-\mathbf{k})$ and $\Gamma(-\mathbf{k}) = -\Gamma(\mathbf{k})$, we find $\chi_{-\mathbf{k}} = -\chi_{\mathbf{k}}$ and thus $U(-\mathbf{k})^t = U(\mathbf{k})^\dagger = U(\mathbf{k})^{-1}$ is satisfied. Therefore the aforementioned condition $U(-\mathbf{k})^t U(\mathbf{k}) = I$ is met. In terms of the new set of canonical variables, the Hamiltonian (3.53) is rewritten as

$$H^{\mathrm{osc}} = \frac{1}{2}\sum_{\mathbf{k}\neq\mathbf{0}}\sum_{j=1,2}\left(n m_{\mathbf{k},j}\bar{\theta}_{-\mathbf{k},j}\bar{\theta}_{\mathbf{k},j} + \frac{e_{\mathbf{k}}}{n}\bar{n}_{-\mathbf{k},j}\bar{n}_{\mathbf{k},j}\right), \tag{3.58}$$

where the new variables $\bar{\theta}_{\mathbf{k},j}$ and $\bar{n}_{\mathbf{k},j}$ satisfy $[\bar{\theta}_{\mathbf{k},j}, \bar{n}_{-\mathbf{k}',j'}] = \mathrm{i}\delta_{jj'}\delta_{\mathbf{k}\mathbf{k}'}$ ($\mathbf{k}, \mathbf{k}' \neq \mathbf{0}$; $j, j' = 1, 2$) since the canonical transformations in Eq. (3.52) and (3.55) leave the commutation relations unchanged. Finally, introducing the annihilation and creation operators

$$\gamma_{\mathbf{k},j} = \frac{1}{\sqrt{2}}\left(\sqrt{n}\zeta_{\mathbf{k},j}\bar{\theta}_{\mathbf{k},j} + \frac{\mathrm{i}\bar{n}_{\mathbf{k},j}}{\sqrt{n}\zeta_{\mathbf{k},j}}\right), \ \gamma^\dagger_{\mathbf{k},j} = \frac{1}{\sqrt{2}}\left(\sqrt{n}\zeta_{\mathbf{k},j}\bar{\theta}_{-\mathbf{k},j} - \frac{\mathrm{i}\bar{n}_{-\mathbf{k},j}}{\sqrt{n}\zeta_{\mathbf{k},j}}\right) \ (\mathbf{k} \neq \mathbf{0};\ j = 1, 2), \tag{3.59}$$

with $\zeta_{\mathbf{k},j} := (m_{\mathbf{k},j}/e_{\mathbf{k}})^{1/4}$, the Hamiltonian is diagonalized (3.58) as

$$H^{\mathrm{osc}} = \sum_{\mathbf{k}\neq\mathbf{0}}\sum_{j=1,2} E_j(\mathbf{k})\left(\gamma^\dagger_{\mathbf{k},j}\gamma_{\mathbf{k},j} + \frac{1}{2}\right), \quad E_j(\mathbf{k}) = \sqrt{m_{\mathbf{k},j}e_{\mathbf{k}}}. \tag{3.60}$$

The ground state $|0^{\mathrm{osc}}\rangle$ of this Hamiltonian is specified by the condition $\gamma_{\mathbf{k},\pm}|0^{\mathrm{osc}}\rangle = 0$ for all $\mathbf{k} \neq \mathbf{0}$.

In order to obtain the single-particle spectrum $E_j(\mathbf{k})$ ($j = 1, 2$) in the long-wavelength limit $k\ell \ll 1$, we keep the leading term. As $\Gamma_-(\mathbf{k}) \gg \Gamma(\mathbf{k}) \gg \Gamma_+(\mathbf{k})$ in this limit, we approximate $m_{\mathbf{k},j}$ in Eq. (3.57) as

$$\begin{aligned} m_{\mathbf{k},j} &\approx \frac{\tilde{\Gamma}_+(\mathbf{k}) + \tilde{\Gamma}_-(\mathbf{k})}{2} + (-1)^{j-1}\frac{\tilde{\Gamma}_-(\mathbf{k})}{2}\left[1 - \frac{\tilde{\Gamma}_+(\mathbf{k})}{\tilde{\Gamma}_-(\mathbf{k})} + \frac{2\Gamma(\mathbf{k})^2}{\tilde{\Gamma}_-(\mathbf{k})^2}\right] \\ &\approx \begin{cases} \tilde{\Gamma}_-(\mathbf{k}) & (j = 1); \\ \tilde{\Gamma}_+(\mathbf{k}) - \Gamma(\mathbf{k})^2/\tilde{\Gamma}_-(\mathbf{k}) & (j = 2). \end{cases} \end{aligned} \tag{3.61}$$

By parametrizing the wave vector in the polar coordinate as $(k_x, k_y) = k(\cos\varphi, \sin\varphi)$ where k and φ are the radial coordinate and the azimuth angle, respectively, $m_{\mathbf{k},j}$ are

expressed as

$$m_{\mathbf{k},1} \approx \left(\frac{\bar{g}_{\mp}}{\bar{g}_{\pm}}\right)^{1/2} gnD(\varphi)(k\ell)^2, \quad m_{\mathbf{k},2} \approx \left(\frac{\bar{g}_{\pm}}{\bar{g}_{\mp}}\right)^{1/2} gnC(\varphi)(k\ell)^4, \tag{3.62}$$

where

$$\begin{aligned} C(\varphi) &= C_1 \sin^2(2\varphi) + C_2 \cos^2(2\varphi) - C_3 \sin(2\varphi)\cos(2\varphi) - C_4 \sin^2(3\varphi), \\ D(\varphi) &= D_1 \sin^2(\varphi) + D_2 \cos^2(\varphi) - D_3 \sin(\varphi)\cos(\varphi), \end{aligned} \tag{3.63}$$

with $C_4 := F_1^2/4D_1$. We thus obtain the low-energy dispersion relations as

$$E_j(\mathbf{k}) \approx \sqrt{2(\bar{g}_+\bar{g}_-)^{1/2} n m_{\mathbf{k},j}} \approx \sqrt{2} gn (k\ell)^j f_j(\varphi) \quad (j = 1, 2), \tag{3.64}$$

where the dependence on the azimuth angle φ is given by the dimensionless functions

$$f_1(\varphi) = \sqrt{\bar{g}_{\mp} D(\varphi)/g}, \quad f_2(\varphi) = \sqrt{\bar{g}_{\pm} C(\varphi)/g}. \tag{3.65}$$

The anisotropy of the linear and quadratic dispersion relations of the low-energy modes depends on the lattice structure as the elastic constants are subjected to the constraints (3.44). Furthermore, we find rescaling relations between the low-energy dispersion relations for parallel (P) and antiparallel (AP) fields as

$$E_1^{\mathrm{P}}(\mathbf{k})/\sqrt{\bar{g}_-} = E_1^{\mathrm{AP}}(\mathbf{k})/\sqrt{\bar{g}_+}, \quad E_2^{\mathrm{P}}(\mathbf{k})/\sqrt{\bar{g}_+} = E_2^{\mathrm{AP}}(\mathbf{k})/\sqrt{\bar{g}_-}. \tag{3.66}$$

More specifically, the rescaling relations for the two types of fields are rewritten by using the angular part of the dispersion relations $f_j(\varphi)$ $(j = 1, 2)$ as

$$f_1^{\mathrm{P}}(\varphi)\sqrt{\frac{g}{\bar{g}_-}} = f_1^{\mathrm{AP}}(\varphi)\sqrt{\frac{g}{\bar{g}_+}} = \sqrt{D(\varphi)}, \quad f_2^{\mathrm{P}}(\varphi)\sqrt{\frac{g}{\bar{g}_+}} = f_2^{\mathrm{AP}}(\varphi)\sqrt{\frac{g}{\bar{g}_-}} = \sqrt{C(\varphi)}. \tag{3.67}$$

In Chap. 4, we confirm these relations by numerically obtaining the energy spectra by the Bogoliubov theory for all the five vortex-lattice structures in Fig. 2.2 (a)-(e).[3]

In Sec. 2.3.3, we review that the ground states for parallel and antiparallel fields are equivalent in a mean-field regime, while the excited states are not. From the rescaling relations, we relate the excited states for parallel and antiparallel fields at low energies.

Since $\mathbf{u}_+(\mathbf{u}_-)$ is coupled to $\theta_+(\theta_-)$ in parallel fields due to the equation of motion in Eq. (3.37) while they are coupled in a crossed manner in the antiparallel fields, the linear and quadratic dispersion relations are related to the symmetric n_+ and the antisymmetric n_-, respectively, in parallel fields while they are related in an opposite manner in antiparallel fields. Therefore, the oscillation modes corresponding to the quadratic and linear dispersion relations are the in- and anti- (anti- and in-) phase oscillations, respectively, in parallel (antiparallel) fields. Since the quadratic dispersion relation has energy smaller than the linear one, we expect that the oscillation mode corresponding to the quadratic dispersion relation appears at low energies in experiment.

[3] The important difference between Eq. (3.66) and similar rescaling relations in Ref. [31] is that we use the renormalized coupling constants $\bar{g}_{\pm}$ in Eq. (3.39). The dispersion relations for overlapping vortex lattices have accidentally satisfied the rescaling relations without the renormalization in Ref. [31] due to $\beta = \beta_{\uparrow\downarrow}$.

3.3.2 Correlation functions and quantum depletion

Finally, we calculate some correlators of the spin-↑ component in the oscillator part for the following chapters. By using Eqs. (3.52), (3.55), and (3.59), we express the phase and the density of the spin-↑ component in terms of the bogolon operators as

$$\begin{aligned}\theta_{\mathbf{k},\uparrow} &= \frac{1}{2}(\theta_{\mathbf{k},+}+\theta_{\mathbf{k},-}) = \frac{1}{2}\sum_{j=1,2} R_{\mathbf{k},j}\bar{\theta}_{\mathbf{k},j} = \frac{1}{2\sqrt{2n}}\sum_{j=1,2} R_{\mathbf{k},j}\zeta_{\mathbf{k},j}^{-1}\left(\gamma_{\mathbf{k},j}+\gamma_{-\mathbf{k},j}^{\dagger}\right),\\ n_{\mathbf{k},\uparrow} &= n_{\mathbf{k},+}+n_{\mathbf{k},-} = \sum_{j=1,2} R_{\mathbf{k},3-j}\bar{n}_{\mathbf{k},j} = \frac{1}{\mathrm{i}}\sqrt{\frac{n}{2}}\sum_{j=1,2} R_{\mathbf{k},3-j}\zeta_{\mathbf{k},j}\left(\gamma_{\mathbf{k},j}-\gamma_{-\mathbf{k},j}^{\dagger}\right),\end{aligned} \tag{3.68}$$

where we introduce

$$R_{\mathbf{k},1} = r_{\mathbf{k}}\cos\frac{\chi_{\mathbf{k}}}{2}+\mathrm{i}r_{\mathbf{k}}^{-1}\sin\frac{\chi_{\mathbf{k}}}{2},\quad R_{\mathbf{k},2} = r_{\mathbf{k}}^{-1}\cos\frac{\chi_{\mathbf{k}}}{2}+\mathrm{i}r_{\mathbf{k}}\sin\frac{\chi_{\mathbf{k}}}{2}, \tag{3.69}$$

which satisfy $R_{-\mathbf{k},j} = R_{\mathbf{k},j}^{*}$ $(j=1,2)$. Using Eq. (3.68), the correlators with respect to the phase and the density are given by

$$\begin{aligned}\langle 0^{\mathrm{osc}}|\theta_{-\mathbf{k},\uparrow}\theta_{\mathbf{k},\uparrow}|0^{\mathrm{osc}}\rangle &= \frac{1}{8n}\sum_{j=1,2}|R_{\mathbf{k},j}|^2\zeta_{\mathbf{k},j}^{-2} = \frac{1}{8n\zeta_{\mathbf{k},1}\zeta_{\mathbf{k},2}}\left(|R_{\mathbf{k},1}|^2\frac{\zeta_{\mathbf{k},2}}{\zeta_{\mathbf{k},1}}+|R_{\mathbf{k},2}|^2\frac{\zeta_{\mathbf{k},1}}{\zeta_{\mathbf{k},2}}\right),\\ \langle 0^{\mathrm{osc}}|n_{-\mathbf{k},\uparrow}n_{\mathbf{k},\uparrow}|0^{\mathrm{osc}}\rangle &= \frac{n}{2}\sum_{j=1,2}|R_{\mathbf{k},3-j}|^2\zeta_{\mathbf{k},j}^{2} = \frac{n\zeta_{\mathbf{k},1}\zeta_{\mathbf{k},2}}{2}\left(|R_{\mathbf{k},1}|^2\frac{\zeta_{\mathbf{k},2}}{\zeta_{\mathbf{k},1}}+|R_{\mathbf{k},2}|^2\frac{\zeta_{\mathbf{k},1}}{\zeta_{\mathbf{k},2}}\right).\end{aligned} \tag{3.70}$$

In the long-wavelength limit $k\ell \ll 1$ where $\Gamma_{-}(\mathbf{k}) \gg \Gamma(\mathbf{k}) \gg \Gamma_{+}(\mathbf{k})$, we find

$$\begin{aligned}&\zeta_{\mathbf{k},1} \approx \left[\frac{gD(\varphi)}{2\bar{g}_{\pm}}\right]^{1/4}\sqrt{k\ell},\quad \zeta_{\mathbf{k},2} \approx \left[\frac{gC(\varphi)}{2\bar{g}_{\mp}}\right]^{1/4}k\ell,\quad \cos\chi_{\mathbf{k}} \approx \mp 1,\\ &|R_{\mathbf{k},1}|^2 = r_{\mathbf{k}}^2\frac{1+\cos\chi_{\mathbf{k}}}{2}+r_{\mathbf{k}}^{-2}\frac{1-\cos\chi_{\mathbf{k}}}{2} \approx r_{\mathbf{0}}^{\mp 2} = \sqrt{\frac{\bar{g}_{\mp}}{\bar{g}_{\pm}}},\\ &|R_{\mathbf{k},2}|^2 = r_{\mathbf{k}}^{-2}\frac{1+\cos\chi_{\mathbf{k}}}{2}+r_{\mathbf{k}}^{2}\frac{1-\cos\chi_{\mathbf{k}}}{2} \approx r_{\mathbf{0}}^{\pm 2} = \sqrt{\frac{\bar{g}_{\pm}}{\bar{g}_{\mp}}}.\end{aligned} \tag{3.71}$$

In this limit, the correlators are rewritten as

$$\langle\theta_{-\mathbf{k},\uparrow}\theta_{\mathbf{k},\uparrow}\rangle \approx \frac{1}{nF(\varphi)k^2\ell^2},\quad \langle n_{-\mathbf{k},\uparrow}n_{\mathbf{k},\uparrow}\rangle \approx \frac{nk\ell}{G(\varphi)}\quad (\mathbf{k}\neq\mathbf{0}), \tag{3.72}$$

where

$$F(\varphi) = 4\sqrt{\frac{2gC(\varphi)}{\bar{g}_{\pm}}},\ G(\varphi) = 2\sqrt{\frac{2\bar{g}_{\mp}}{gD(\varphi)}}, \tag{3.73}$$

express the dependences on the azimuth angle φ.

The one-particle density matrix characterizes the BEC [52–54]. In our coarse-grained description, we introduce the modified bosonic field $\tilde{\psi}_{\uparrow} = e^{-i\theta_{\uparrow}}\sqrt{n_{\uparrow}}$. Since $\theta_{\uparrow}(\mathbf{r})$ is the

regular part of the phase and $n_\uparrow(\mathbf{r})$ is the coarse-grained density, we expect that $\tilde{\psi}(\mathbf{r})$ varies slowly over space. The modified one-particle density matrix is given by

$$\langle \tilde{\psi}_\uparrow(\mathbf{r})^\dagger \tilde{\psi}_\uparrow(\mathbf{0})\rangle = \left\langle \sqrt{n_\uparrow(\mathbf{r})} \mathrm{e}^{i(\theta_\uparrow(\mathbf{r})-\theta_\uparrow(\mathbf{0}))} \sqrt{n_\uparrow(\mathbf{0})} \right\rangle. \tag{3.74}$$

We find that Eq. (3.74) describes the slowly varying component of the original one-particle density matrix. The behavior of the density matrix is determined dominantly by the phase fluctuation. Here we consider overlapping triangular lattices in Fig. 2.2 (a) where $F(\varphi)$ is constant. Then by using Eq. (3.72), the phase correlation function in real space is obtained as

$$\left\langle [\theta_\uparrow(\mathbf{r}) - \theta_\uparrow(\mathbf{0})]^2 \right\rangle = \frac{2}{A} \sum_{\mathbf{k}\neq\mathbf{0}} \mathrm{e}^{-\alpha k} \left[1 - \cos\left(\mathbf{k}\cdot\mathbf{r}\right)\right] \left\langle \theta_{-\mathbf{k},\uparrow}\theta_{\mathbf{k},\uparrow}\right\rangle \approx \frac{1}{\pi n F \ell^2} \ln\frac{r}{2\alpha} \quad (r \gg \alpha), \tag{3.75}$$

where the convergence factor $\mathrm{e}^{-\alpha k}$ is introduced to regularize the infinite sum. The details of the derivation will be discussed in App. A.3. Then the modified one-particle density matrix is obtained as

$$\langle \tilde{\psi}_\uparrow(\mathbf{r})^\dagger \tilde{\psi}_\uparrow(\mathbf{0})\rangle \approx n \exp\left[-\frac{1}{2}\left\langle [\theta_\uparrow(\mathbf{r}) - \theta_\uparrow(\mathbf{0})]^2 \right\rangle\right] \approx n \left(\frac{r}{2\alpha}\right)^{-\frac{1}{2\pi n F \ell^2}}. \tag{3.76}$$

We find a quasi-long-range order from the one-particle density matrix.

The density n_0 of the condensate is estimated by the one-particle density matrix (3.76) at the large separation $r = \sqrt{A}/2$ for a finite system of area A. The density of the depletion n' is given by $n' = n - n_0$. Assuming $n' \ll n$ as required for the Bogoliubov theory and the present effective theory, the fraction of depletion is estimated as

$$\frac{n'}{n} \approx \frac{1}{2}\left\langle [\theta_\uparrow(\mathbf{r}) - \theta_\uparrow(\mathbf{0})]^2 \right\rangle \Big|_{r=\sqrt{A}/2} \approx \frac{1}{2\pi n F \ell^2} \ln\frac{\sqrt{A}}{4\alpha} = \frac{1}{2\nu}\left(\frac{\bar{g}_\pm}{2gC}\right)^{1/2} \ln\frac{\sqrt{A}}{4\alpha}, \tag{3.77}$$

where we introduce the filling factor

$$\nu = \frac{N}{N_\mathrm{v}} = \frac{2nA}{A/(2\pi\ell^2)} = 4\pi n \ell^2. \tag{3.78}$$

From Eq. (3.77), we find that the quantum depletion is larger for parallel (antiparallel) fields when the intercomponent interaction is repulsive (attractive). By substituting $A = 2\pi\ell^2 N_\mathrm{v}$ into Eq. (3.77), we find that $\nu n'/n$ is proportional to $\ln N_\mathrm{v}$. We confirm these properties of the quantum depletion by the Bogoliubov theory in Chap. 4.

Chapter 4

Bogoliubov theory of vortex lattices in binary BECs

In this chapter, we find shifts of the transition points of the ground-state phase diagram of vortex lattices in binary BECs due to the the quantum correction of the ground-state energy, so that the phase diagrams with the quantum correction for parallel and antiparallel fields are different, while the two diagrams in the mean-field theory without the quantum correction are equivalent, by formulating the Bogoliubov theory of binary BECs in the LLL approximation by extending the derivation for a scalar case [50, 55, 56]. Since shifts of the transition points and the quantum depletion for parallel fields are larger than those for antiparallel fields, we indicate that the modification of the phase diagram is enhanced as the quantum fluctuation increases. In Sec. 4.1, we obtain the Bogoliubov Hamiltonian using the LLL magnetic Bloch states as a basis set of states, and derive expressions of the Lee-Huang-Yang correction and the quantum depletion. In Sec. 4.2, we present numerical results on ground-state and excitation properties. From the energy spectra, we confirm the quadratic and linear dispersion relations and the rescaling relations. Then we find the phase diagram with the quantum corrections and the ground-state energy with respect to the interaction ratio $g_{\uparrow\downarrow}/g$. Finally we present the quantum depletion to make comparison with the corrected phase diagram.

4.1 Bogoliubov Hamiltonian

In this section, we formulate the Bogoliubov theory of the vortex lattices in binary BECs. In Sec. 4.1.1, the LLL magnetic Bloch state in which zero points appear periodically is introduced to develop the theory of vortex lattices. In Sec. 4.1.2, the Bogoliubov theory using the magnetic Bloch states as a basis set of states is given. In Sec. 4.1.3, we consider the diagonalization of the Bogoliubov Hamiltonian via the Bogoliubov transformation, so that we obtain the excitation spectra, the quantum depletion and the Lee-Huang-Yang correction.

4.1.1 Lowest-Landau-level magnetic Bloch state

To discuss the Bogoliubov theory of the vortex lattice, we choose the basis which is consistent with the periodicity of the lattice. In the LLL approximation, we use the LLL

magnetic Bloch states [56–59] as a basis set of states. Let $\mathbf{a}_1$ and $\mathbf{a}_2$ be the primitive vectors of a vortex lattice and let $\mathbf{b}_1$ and $\mathbf{b}_2$ be the reciprocal primitive vectors. The primitive vectors satisfy $(\mathbf{a}_1 \times \mathbf{a}_2)_z = 2\pi\ell^2 = A/N_\mathrm{v}$, which implies that a single vortex appears in each unit cell of the lattice. The reciprocal vectors are written as $\mathbf{b}_1 = -\mathbf{e}_z \times \mathbf{a}_2/\ell^2$ and $\mathbf{b}_2 = \mathbf{e}_z \times \mathbf{a}_1/\ell^2$, which satisfy $\mathbf{a}_i \cdot \mathbf{b}_j = 2\pi\delta_{ij}$. The first Brillouin zones for the five types of vortex-lattice structures in Fig. 2.2 are depicted in Fig. 4.1 (a)-(e) and the primitive vectors are presented in Fig. 4.1 (f). Using the pseudomomentum $\mathbf{K}_\alpha = \mathbf{p} - q\mathbf{A}_\alpha + qB_\alpha \mathbf{e}_z \times \mathbf{r} = (K_{\alpha,x}, K_{\alpha,y})$ for a spin-α component, which satisfies the commutation relation $[K_{\alpha,x}, K_{\alpha,y}] = -\mathrm{i}\epsilon_\alpha \hbar^2/\ell^2$, we introduce the magnetic translation operator as $T_\alpha(\mathbf{s}) = \mathrm{e}^{-\mathrm{i}\mathbf{K}_\alpha \cdot \mathbf{s}/\hbar}$ [60]. By translating the most localized symmetric LLL wave function $c_0(\mathbf{r}) = \mathrm{e}^{-\mathbf{r}^2/4\ell^2}/\sqrt{2\pi\ell^2}$ in the $\mathbf{a}_1$ and $\mathbf{a}_2$ directions by multiplying two translation operators, we construct a set of LLL wave functions as

$$c_{\mathbf{m}\alpha}(\mathbf{r}) = T_\alpha(m_1\mathbf{a}_1)T_\alpha(m_2\mathbf{a}_2)c_0(\mathbf{r}) = \frac{(-1)^{m_1 m_2}}{\sqrt{2\pi\ell^2}} \exp\left[-\frac{1}{4\ell^2}(\mathbf{r}-\mathbf{r}_\mathbf{m})^2 - \frac{\mathrm{i}\epsilon_\alpha}{2\ell^2}(\mathbf{r}\times\mathbf{r}_\mathbf{m})_z\right], \tag{4.1}$$

where $\mathbf{r}_\mathbf{m} = m_1\mathbf{a}_1 + m_2\mathbf{a}_2$, with $\mathbf{m} = (m_1, m_2) \in \mathbb{Z}^2$. Here $T_\alpha(m_1\mathbf{a}_1)$ and $T_\alpha(m_2\mathbf{a}_2)$ commute with each other since a single magnetic flux quantum pierces each unit cell. By superposing $c_{\mathbf{m}\alpha}(\mathbf{r})$ for N_v possible translations $\mathbf{m}$ on a torus, we can construct the LLL magnetic Bloch state as[1]

$$\Psi_{\mathbf{k}\alpha}(\mathbf{r}) = \frac{1}{\sqrt{N_\mathrm{v}\zeta(\mathbf{k})}} \sum_\mathbf{m} c_{\mathbf{m}\alpha}(\mathbf{r}) \mathrm{e}^{i\mathbf{k}\cdot\mathbf{r}_\mathbf{m}}, \tag{4.2}$$

with the normalization factor

$$\zeta(\mathbf{k}) = \sum_\mathbf{m} (-1)^{m_1 m_2} \mathrm{e}^{-\mathbf{r}_\mathbf{m}^2/4\ell^2 - \mathrm{i}\mathbf{k}\cdot\mathbf{r}_\mathbf{m}}. \tag{4.3}$$

The LLL magnetic Bloch state $\Psi_{\mathbf{k}\alpha}(\mathbf{r})$ is an eigenstate of $T_\alpha(\mathbf{a}_j)$ with an eigenvalue $e^{-i\mathbf{k}\cdot\mathbf{a}_j}$ (as expected for a "Bloch state"). Therefore, by taking N_v discrete wave vectors $\mathbf{k}$ consistent with the boundary conditions of the system, $\Psi_{\mathbf{k}\alpha}(\mathbf{r})$ forms a complete orthogonal basis of the LLL manifold. Secondly, $\Psi_{\mathbf{k}\alpha}(\mathbf{r})$ has a periodic pattern of zeros at [58]

$$\mathbf{r} = \mathbf{r}_\mathbf{n} + \frac{1}{2}(\mathbf{a}_1 + \mathbf{a}_2) - \epsilon_\alpha \ell^2 \mathbf{e}_z \times \mathbf{k}, \quad \mathbf{n} = (n_1, n_2) \in \mathbb{Z}^2. \tag{4.4}$$

Therefore, $\Psi_{\mathbf{k}\alpha}(\mathbf{r})$ represents a vortex lattice with primitive vectors $\mathbf{a}_1$ and $\mathbf{a}_2$ for any $\mathbf{k}$, and the locations of vortices (zeros) can be shifted by varying $\mathbf{k}$. We can prove this by rewriting Eq. (4.2) as

$$\begin{aligned}\sqrt{N_\mathrm{v}\zeta(\mathbf{k})}\Psi_{\mathbf{k}\alpha}(\mathbf{r}) &= \sum_\mathbf{m} c^*_{\mathbf{m}\alpha}(\mathbf{r}) \exp\left[i\left(-\frac{\epsilon_\alpha}{\ell^2}\mathbf{e}_z \times \mathbf{r} + \mathbf{k}\right)\cdot\mathbf{r}_\mathbf{m}\right] \\ &= \sum_\mathbf{m} c^*_{\mathbf{m}\alpha}(\mathbf{r}) \exp\left\{-\frac{i\epsilon_\alpha}{\ell^2}\left[\mathbf{e}_z \times \left(\mathbf{r} + \epsilon_\alpha \ell^2 \mathbf{e}_z \times \mathbf{k}\right)\right]\cdot\mathbf{r}_\mathbf{m}\right\}\end{aligned} \tag{4.5}$$

[1] In numerical calculations to be presented later, we set $\mathbf{k} = \frac{n_1}{N_{\mathrm{v}1}}\mathbf{b}_1 + \frac{n_2}{N_{\mathrm{v}2}}\mathbf{b}_2$ with $n_j \in \{0, 1, \ldots, N_{\mathrm{v}j} - 1\}$ and $N_{\mathrm{v}1}N_{\mathrm{v}2} = N_\mathrm{v}$.

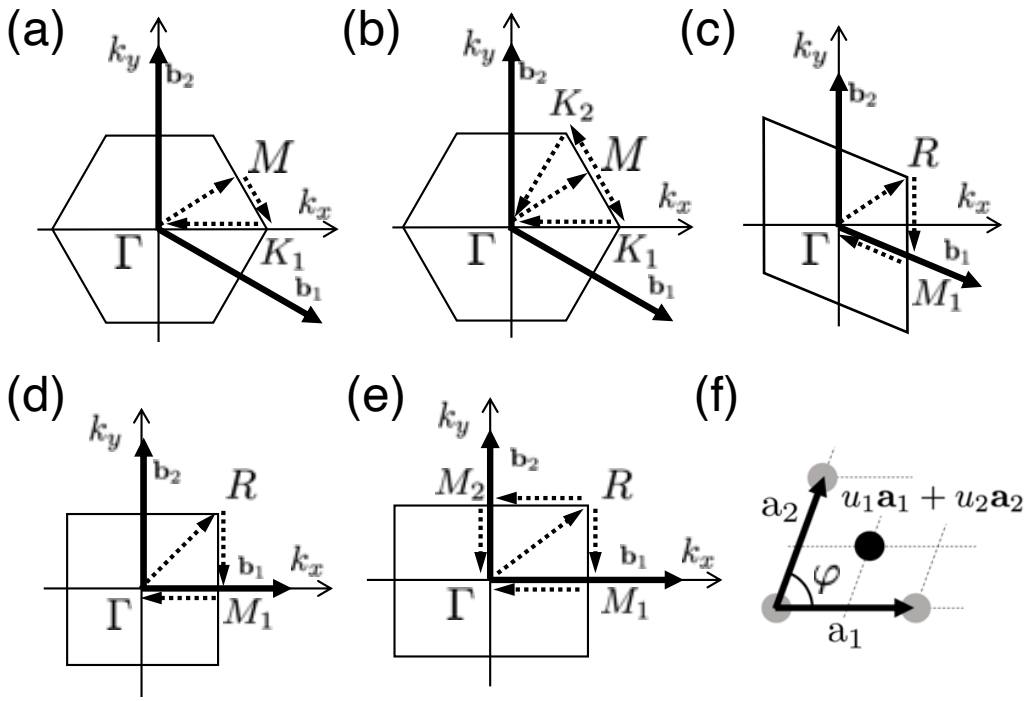

Figure 4.1: First Brillouin zones for (a) overlapping triangular, (b) interlaced triangular, (c) rhombic, (d) square, (e) rectangular lattices which are depicted in Fig. 2.2. Letters indicate high-symmetry points. Energy spectra and entanglement spectra are calculated along the paths indicated by dotted arrows. In (f), the primitive vectors $\mathbf{a}_1 = (a, 0)$ and $\mathbf{a}_2 = b(\cos\varphi, \sin\varphi)$ and the displacement $u_1\mathbf{a}_1 + u_2\mathbf{a}_2$ of the vortex of one component from the other are depicted. The inner angle φ and the aspect ratio b/a change continuously as a function of $g_{\uparrow\downarrow}/g$, for rhombic and rectangular lattices, respectively; these correspond to η and $|\tau|$ in Fig. 2.3.

and comparing it with the complex conjugate of the Perelomov overcompleteness equation $\sum_{\mathbf{m}}(-1)^{m_1+m_2}c_{\mathbf{m}\alpha}(\mathbf{r}) = 0$ [61].

The vortex lattice for each component in binary BECs is given by the LLL magnetic Bloch state $\Psi_{\mathbf{q}_\alpha,\alpha}(\mathbf{r})$, where the wave vectors $\mathbf{q}_\alpha$ ($\alpha = \uparrow, \downarrow$) are chosen in consistency with the displacement $u_1\mathbf{a}_1 + u_2\mathbf{a}_2$ between the components [see Fig. 4.1(f)]. We choose its value as

$$\begin{aligned}\mathbf{q}_\uparrow &= +\frac{\epsilon_\uparrow}{2\ell^2}\mathbf{e}_z \times (u_1\mathbf{a}_1 + u_2\mathbf{a}_2) = \frac{\epsilon_\uparrow}{2}(-u_2\mathbf{b}_1 + u_1\mathbf{b}_2),\\ \mathbf{q}_\downarrow &= -\frac{\epsilon_\downarrow}{2\ell^2}\mathbf{e}_z \times (u_1\mathbf{a}_1 + u_2\mathbf{a}_2) = \frac{\epsilon_\downarrow}{2}(+u_2\mathbf{b}_1 - u_1\mathbf{b}_2).\end{aligned} \tag{4.6}$$

With this choice, the vortices for the spin-$\uparrow$ and spin-$\downarrow$ components are shifted by $(u_1\mathbf{a}_1 + u_2\mathbf{a}_2)/2$ and $-(u_1\mathbf{a}_1 + u_2\mathbf{a}_2)/2$ [relative to the $\mathbf{k} = \mathbf{0}$ case of Eq. (4.4)], respectively, realizing the mutual separation by $u_1\mathbf{a}_1+u_2\mathbf{a}_2$. Instead of displacing the spin-$\uparrow$ component by $u_1\mathbf{a}_1+u_2\mathbf{a}_2$, we displace the vortices as explained above in order to avoid the divergence of the denominator and the numerator of the LLL magnetic Bloch state (4.2) at the high-symmetry point in the first Brillouin zone.

4.1.2 Bogoliubov approximation

In the LLL approximation, the kinetic term of the Hamiltonian can be omitted, because the single-particle energy is the constant term $\hbar\omega_c$. We focus on the interaction term given by

$$H_{\text{int}} = \sum_{\alpha,\beta}\frac{g_{\alpha\beta}}{2}\int \mathrm{d}^2\mathbf{r}\ \hat{\psi}^\dagger_\alpha(\mathbf{r})\hat{\psi}^\dagger_\beta(\mathbf{r})\hat{\psi}_\beta(\mathbf{r})\hat{\psi}_\alpha(\mathbf{r}), \tag{4.7}$$

where $\hat{\psi}_\alpha(\mathbf{r})$ is a bosonic field operator of the spin-α component and the properties of the coupling constants $g_{\alpha\beta}$ of the contact interactions satisfy $g_{\uparrow\uparrow} = g_{\downarrow\downarrow} \equiv g > 0$, $|g_{\uparrow\downarrow}| < g$ as explained in Sec. 3.2.1. Using the magnetic Bloch states (4.2), we can expand the field operator as $\hat{\psi}_\alpha(\mathbf{r}) = \sum_{\mathbf{k}}\Psi_{\mathbf{k}\alpha}(\mathbf{r})b_{\mathbf{k}\alpha}$, where $b_{\mathbf{k}\alpha}$ is a bosonic annihilation operator satisfying $[b_{\mathbf{k}\alpha}, b^\dagger_{\mathbf{k}'\alpha'}] = \delta_{\mathbf{k}\mathbf{k}'}\delta_{\alpha\alpha'}$, and $\mathbf{k}$ runs over the discrete momenta in the first Brillouin zone. Substituting this expansion into Eq. (4.7), we obtain

$$H_{\text{int}} = \frac{1}{2}\sum_{\alpha,\beta}\sum_{\mathbf{k}_1,\mathbf{k}_2,\mathbf{k}_3,\mathbf{k}_4} V_{\alpha\beta}(\mathbf{k}_1,\mathbf{k}_2,\mathbf{k}_3,\mathbf{k}_4)b^\dagger_{\mathbf{k}_1\alpha}b^\dagger_{\mathbf{k}_2\beta}b_{\mathbf{k}_3\beta}b_{\mathbf{k}_4\alpha}, \tag{4.8}$$

where

$$V_{\alpha\beta}(\mathbf{k}_1,\mathbf{k}_2,\mathbf{k}_3,\mathbf{k}_4) = g_{\alpha\beta}\int \mathrm{d}^2\mathbf{r}\ \Psi^*_{\mathbf{k}_1\alpha}(\mathbf{r})\Psi^*_{\mathbf{k}_2\beta}(\mathbf{r})\Psi_{\mathbf{k}_3\beta}(\mathbf{r})\Psi_{\mathbf{k}_4\alpha}(\mathbf{r}). \tag{4.9}$$

The interaction matrix element $V_{\alpha\beta}(\mathbf{k}_1,\mathbf{k}_2,\mathbf{k}_3,\mathbf{k}_4)$ is calculated to be

$$V_{\alpha\beta}(\mathbf{k}_1,\mathbf{k}_2,\mathbf{k}_3,\mathbf{k}_4) = \delta^{\text{P}}_{\mathbf{k}_1+\mathbf{k}_2,\mathbf{k}_3+\mathbf{k}_4}\frac{g_{\alpha\beta}}{2A}\frac{S_{\alpha\beta}(\mathbf{k}_1,\mathbf{k}_2,\mathbf{k}_3)}{\sqrt{\zeta(\mathbf{k}_1)\zeta(\mathbf{k}_2)\zeta(\mathbf{k}_3)\zeta(\mathbf{k}_4)}}, \tag{4.10}$$

as described in App. B. Here, $\delta^{\text{P}}_{\mathbf{k}\mathbf{k}'} := \sum_{\mathbf{G}}\delta_{\mathbf{k},\mathbf{k}'+\mathbf{G}}$ is the periodic Kronecker's delta, where $\mathbf{G}$ runs over the reciprocal lattice vectors. For parallel fields, the function $S_{\alpha\beta}(\mathbf{k}_1,\mathbf{k}_2,\mathbf{k}_3)$,

which is independent of α or β, is given by

$$S(\mathbf{k}_1,\mathbf{k}_2,\mathbf{k}_3) = \sum_{\mathbf{p}\in\{0,1\}^2} (-1)^{p_1 p_2} e^{-\mathbf{r}_\mathbf{p}^2/4\ell^2 + i\mathbf{k}_3\cdot\mathbf{r}_\mathbf{p}} \tilde{\zeta}\left(\mathbf{k}_1+\mathbf{k}_2-2\mathbf{k}_3+(\mathbf{r}_\mathbf{p}\times\mathbf{e}_z - i\mathbf{r}_\mathbf{p})/2\ell^2\right) \times \zeta\left(\mathbf{k}_1+(\mathbf{r}_\mathbf{p}\times\mathbf{e}_z+i\mathbf{r}_\mathbf{p})/4\ell^2\right)\zeta\left(\mathbf{k}_2+(\mathbf{r}_\mathbf{p}\times\mathbf{e}_z+i\mathbf{r}_\mathbf{p})/4\ell^2\right), \tag{4.11}$$

where

$$\tilde{\zeta}(\mathbf{k}) := \sum_{\mathbf{m}} e^{-\mathbf{r}_\mathbf{m}^2/2\ell^2 - i\mathbf{k}\cdot\mathbf{r}_\mathbf{m}}. \tag{4.12}$$

For antiparallel fields, $S_{\alpha\beta}(\mathbf{k}_1,\mathbf{k}_2,\mathbf{k}_3)$, which depends on α and β, is given in terms of $S(\mathbf{k}_1,\mathbf{k}_2,\mathbf{k}_3)$ in Eq. (4.11) [31] by

$$\begin{aligned} &S_{\uparrow\uparrow}(\mathbf{k}_1,\mathbf{k}_2,\mathbf{k}_3) = S(\mathbf{k}_1,\mathbf{k}_2,\mathbf{k}_3), \quad S_{\downarrow\downarrow}(\mathbf{k}_1,\mathbf{k}_2,\mathbf{k}_3) = S(-\mathbf{k}_1,-\mathbf{k}_2,-\mathbf{k}_3)^*, \\ &S_{\uparrow\downarrow}(\mathbf{k}_1,\mathbf{k}_2,\mathbf{k}_3) = S(\mathbf{k}_1,-\mathbf{k}_3,-\mathbf{k}_2), \quad S_{\downarrow\uparrow}(\mathbf{k}_1,\mathbf{k}_2,\mathbf{k}_3) = S(-\mathbf{k}_1,\mathbf{k}_3,\mathbf{k}_2)^*. \end{aligned} \tag{4.13}$$

The condensate is only weakly depleted at high filling factors. This is true in typical experiment of ultracold atomic gases, in which the number of flux N_v is of the order of 100. In this case, we can apply the Bogoliubov approximation [50, 52, 55, 56]. When the condensation occurs at the wave vector $\mathbf{q}_\alpha$ in the spin-α component as in Eq. (4.6), we introduce

$$\tilde{b}_{\mathbf{k}\alpha} := b_{\mathbf{q}_\alpha+\mathbf{k},\alpha}, \quad \tilde{V}_{\alpha\beta}(\mathbf{k}_1,\mathbf{k}_2,\mathbf{k}_3,\mathbf{k}_4) := V_{\alpha\beta}(\mathbf{q}_\alpha+\mathbf{k}_1,\mathbf{q}_\beta+\mathbf{k}_2,\mathbf{q}_\beta+\mathbf{k}_3,\mathbf{q}_\alpha+\mathbf{k}_4). \tag{4.14}$$

By setting

$$\tilde{b}_{\mathbf{0}\alpha} \simeq \tilde{b}_{\mathbf{0}\alpha}^\dagger \simeq \sqrt{N_\alpha - \sum_{\mathbf{k}\neq\mathbf{0}} \tilde{b}_{\mathbf{k}\alpha}^\dagger \tilde{b}_{\mathbf{k}\alpha}}, \tag{4.15}$$

and retaining terms up to the second order in $\tilde{b}_{\mathbf{k}\alpha}$ and $\tilde{b}_{\mathbf{k}\alpha}^\dagger$ ($\mathbf{k}\neq 0$), we obtain the Bogoliubov Hamiltonian

$$\begin{aligned} H_\mathrm{int} =& \frac{1}{2}\sum_{\alpha,\beta} N_\alpha N_\beta \tilde{V}_{\alpha\beta}(\mathbf{0},\mathbf{0},\mathbf{0},\mathbf{0}) - \frac{1}{2}\sum_{\mathbf{k}\neq\mathbf{0}}\sum_{\alpha}\left[h_\alpha(\mathbf{k})+\omega_{\alpha\alpha}(\mathbf{k})\right] \\ &+ \frac{1}{2}\sum_{\mathbf{k}\neq\mathbf{0}} \left(\tilde{b}_{\mathbf{k}\uparrow}^\dagger, \tilde{b}_{\mathbf{k}\downarrow}^\dagger, \tilde{b}_{-\mathbf{k},\uparrow}, \tilde{b}_{-\mathbf{k},\downarrow}\right) \mathcal{M}(\mathbf{k}) \begin{pmatrix} \tilde{b}_{\mathbf{k}\uparrow} \\ \tilde{b}_{\mathbf{k}\downarrow} \\ \tilde{b}_{-\mathbf{k},\uparrow}^\dagger \\ \tilde{b}_{-\mathbf{k},\downarrow}^\dagger \end{pmatrix}. \end{aligned} \tag{4.16}$$

Here, the matrix $\mathcal{M}(\mathbf{k})$ is given by

$$\mathcal{M}(\mathbf{k}) = \begin{pmatrix} h_\uparrow(\mathbf{k})+\omega_{\uparrow\uparrow}(\mathbf{k}) & \omega_{\uparrow\downarrow}(\mathbf{k}) & \lambda_{\uparrow\uparrow}(\mathbf{k}) & \lambda_{\uparrow\downarrow}(\mathbf{k}) \\ \omega_{\downarrow\uparrow}(\mathbf{k}) & h_\downarrow(\mathbf{k})+\omega_{\downarrow\downarrow}(\mathbf{k}) & \lambda_{\downarrow\uparrow}(\mathbf{k}) & \lambda_{\downarrow\downarrow}(\mathbf{k}) \\ \lambda_{\uparrow\uparrow}^*(\mathbf{k}) & \lambda_{\downarrow\uparrow}^*(\mathbf{k}) & h_\uparrow(-\mathbf{k})+\omega_{\uparrow\uparrow}(-\mathbf{k}) & \omega_{\downarrow\uparrow}(-\mathbf{k}) \\ \lambda_{\uparrow\downarrow}^*(\mathbf{k}) & \lambda_{\downarrow\downarrow}^*(\mathbf{k}) & \omega_{\uparrow\downarrow}(-\mathbf{k}) & h_\downarrow(-\mathbf{k})+\omega_{\downarrow\downarrow}(-\mathbf{k}) \end{pmatrix}, \tag{4.17}$$

where

$$\begin{aligned} &h_\alpha(\mathbf{k}) := \sum_\beta N_\beta \left[\tilde{V}_{\alpha\beta}(\mathbf{k},\mathbf{0},\mathbf{0},\mathbf{k}) - \tilde{V}_{\alpha\beta}(\mathbf{0},\mathbf{0},\mathbf{0},\mathbf{0})\right], \\ &\omega_{\alpha\beta}(\mathbf{k}) := \sqrt{N_\alpha N_\beta}\tilde{V}_{\alpha\beta}(\mathbf{k},\mathbf{0},\mathbf{k},\mathbf{0}), \quad \lambda_{\alpha\beta}(\mathbf{k}) := \sqrt{N_\alpha N_\beta}\tilde{V}_{\alpha\beta}(\mathbf{k},-\mathbf{k},\mathbf{0},\mathbf{0}). \end{aligned} \tag{4.18}$$

4.1.3 Diagonalization of the Bogoliubov Hamiltonian

We diagonalize the Bogoliubov Hamiltonian (4.16) by performing the Bogoliubov transformation

$$\begin{pmatrix} \tilde{b}_{\mathbf{k}\uparrow} \\ \tilde{b}_{\mathbf{k}\downarrow} \\ \tilde{b}^\dagger_{-\mathbf{k},\uparrow} \\ \tilde{b}^\dagger_{-\mathbf{k},\downarrow} \end{pmatrix} = W(\mathbf{k}) \begin{pmatrix} \gamma_{\mathbf{k},1} \\ \gamma_{\mathbf{k},2} \\ \gamma^\dagger_{-\mathbf{k},1} \\ \gamma^\dagger_{-\mathbf{k},2} \end{pmatrix}, \qquad W(\mathbf{k}) = \begin{pmatrix} \mathcal{U}(\mathbf{k}) & \mathcal{V}^*(-\mathbf{k}) \\ \mathcal{V}(\mathbf{k}) & \mathcal{U}^*(-\mathbf{k}) \end{pmatrix}, \tag{4.19}$$

where $W(\mathbf{k})$ is a paraunitary matrix which satisfies

$$W^\dagger(\mathbf{k})\tau_3 W(\mathbf{k}) = W(\mathbf{k})\tau_3 W^\dagger(\mathbf{k}) = \tau_3 := \mathrm{diag}(1,1,-1,-1), \tag{4.20}$$

so that the bosonic commutation relation is invariant. By choosing the matrix $W(\mathbf{k})$ satisfying

$$W^\dagger(\mathbf{k})\mathcal{M}(\mathbf{k})W(\mathbf{k}) = \mathrm{diag}(E_1(\mathbf{k}), E_2(\mathbf{k}), E_1(-\mathbf{k}), E_2(-\mathbf{k})), \tag{4.21}$$

the Bogoliubov Hamiltonian is diagonalized as

$$\begin{aligned} H_{\mathrm{int}} =& \frac{1}{2}\sum_{\alpha,\beta} N_\alpha N_\beta \tilde{V}_{\alpha\beta}(\mathbf{0},\mathbf{0},\mathbf{0},\mathbf{0}) - \frac{1}{2}\sum_{\mathbf{k}\neq\mathbf{0}}\sum_{\alpha}\left[h_\alpha(\mathbf{k}) + \omega_{\alpha\alpha}(\mathbf{k})\right] \\ &+ \sum_{\mathbf{k}\neq\mathbf{0}}\sum_{j=1,2} E_i(\mathbf{k})\left(\gamma^\dagger_{\mathbf{k}j}\gamma_{\mathbf{k}j} + \frac{1}{2}\right). \end{aligned} \tag{4.22}$$

By multiplying Eq. (4.21) from the left by $W(\mathbf{k})\tau_3$ and using Eq. (4.20), we find

$$\tau_3\mathcal{M}(\mathbf{k})W(\mathbf{k}) = W(\mathbf{k})\mathrm{diag}(E_1(\mathbf{k}), E_2(\mathbf{k}), -E_1(-\mathbf{k}), -E_2(-\mathbf{k})). \tag{4.23}$$

We calculate the excitation energies $E_j(\mathbf{k})$ $(j=1,2)$ by obtaining the right eigenvectors of $\tau_3\mathcal{M}(\mathbf{k})$ numerically.

The ground state of Eq. (4.22) is given by the bogolon vacuum $|0\rangle$, which is determined from the condition $\gamma_{\mathbf{k}j}|0\rangle = 0$ for all $\mathbf{k}\neq\mathbf{0}$ and $j=1,2$. The ground-state energy E_{GS} scaled by the interaction energy scale gn^2A is given by

$$\begin{aligned} \frac{E_{\mathrm{GS}}}{gn^2A} =& \frac{1}{2}\sum_{\alpha,\beta}\frac{A}{g}\tilde{V}_{\alpha\beta}(\mathbf{0},\mathbf{0},\mathbf{0},\mathbf{0}) + \frac{1}{gn\nu N_{\mathrm{v}}}\sum_{\mathbf{k}\neq\mathbf{0}}\left\{\sum_j E_j(\mathbf{k}) - \sum_\alpha\left[h_\alpha(\mathbf{k}) + \omega_{\alpha\alpha}(\mathbf{k})\right]\right\} \\ =& \frac{1}{2}\sum_{\alpha,\beta}\frac{A}{g}\tilde{V}_{\alpha\beta}(\mathbf{0},\mathbf{0},\mathbf{0},\mathbf{0}) + \frac{1}{2\pi gn\nu}\int_{\mathrm{BZ}}\mathrm{d}^2\mathbf{k}\ell^2\left\{\sum_j E_j(\mathbf{k}) - \sum_\alpha\left[h_\alpha(\mathbf{k}) + \omega_{\alpha\alpha}(\mathbf{k})\right]\right\}. \end{aligned} \tag{4.24}$$

Here, in the second line, we take the thermodynamic limit $N_{\mathrm{v}}\to\infty$ so that the sum may be replaced by the integral over the Brillouin zone as $\frac{1}{N_{\mathrm{v}}}\sum_{\mathbf{k}\neq\mathbf{0}} \to \frac{1}{|\mathbf{b}_1\times\mathbf{b}_2|}\int\mathrm{d}^2\mathbf{k} = \frac{1}{2\pi}\int_{\mathrm{BZ}}\mathrm{d}^2\mathbf{k}\ell^2$. The first term on the right-hand side of Eq. (4.24) gives the mean-field ground-state energy of vortex lattices which has been analyzed by Mueller and Ho [17]. The renormalization factors for the intracomponent and intercomponent interactions (3.46) are obtained from this term due to the similar calculation. The other terms in

Eq. (4.24) give a quantum correction (known as the Lee-Huang-Yang correction), which is inversely proportional to the filling factor ν. In Sec. 4.2.4, we numerically evaluate the first line of Eq. (4.24) to discuss how the quantum correction affects the ground-state phase diagram and shifts the transition points.

Using Eq. (4.19), we calculate correlators in the ground state as

$$\langle 0|\tilde{b}^\dagger_{\mathbf{k},\alpha}\tilde{b}_{\mathbf{k},\alpha}|0\rangle = \sum_j |\mathcal{V}_{\alpha,j}(-\mathbf{k})|^2, \quad \langle 0|\tilde{b}_{-\mathbf{k},\alpha}\tilde{b}^\dagger_{-\mathbf{k},\alpha}|0\rangle = \sum_j |\mathcal{U}_{\alpha,j}(-\mathbf{k})|^2, \tag{4.25a}$$

$$\langle 0|\tilde{b}_{-\mathbf{k},\alpha}\tilde{b}_{\mathbf{k},\alpha}|0\rangle = \sum_j \mathcal{U}_{\alpha,j}(-\mathbf{k})\mathcal{V}^*_{\alpha,j}(-\mathbf{k}), \quad \langle 0|\tilde{b}^\dagger_{\mathbf{k},\alpha}\tilde{b}^\dagger_{-\mathbf{k},\alpha}|0\rangle = \sum_j \mathcal{U}^*_{\alpha,j}(-\mathbf{k})\mathcal{V}_{\alpha,j}(-\mathbf{k}). \tag{4.25b}$$

Here, we have nonzero "anomalous" correlators in Eq. (4.25b) since the particle numbers $N_\uparrow$ and $N_\downarrow$ are not conserved in the Bogoliubov Hamiltonian (4.16). From Eq. (4.25a), we obtain the fraction of depletion n'/n, which is equal for the two components, as

$$\frac{n'}{n} = \frac{1}{N_\alpha}\sum_{\mathbf{k}\neq\mathbf{0}}\langle 0|\tilde{b}^\dagger_{\mathbf{k},\alpha}\tilde{b}_{\mathbf{k},\alpha}|0\rangle = \frac{2}{\nu N_\mathrm{v}}\sum_{\mathbf{k}\neq\mathbf{0}}\sum_{j=1,2}|\mathcal{V}_{\alpha,j}(-\mathbf{k})|^2 \quad (\alpha=\uparrow,\downarrow). \tag{4.26}$$

As discussed in Chap. 3, we expect that the fraction of depletion diverges logarithmically as a function of N_v since $|\mathcal{V}_{\alpha,2}(-\mathbf{k})|^2$ in Eq. (4.26) diverges for $\mathbf{k}\to\mathbf{0}$. We confirm this behavior numerically in the following section. In contrast, all the quantities in the summand of Eq. (4.24) are finite over the entire Brillouin zone and Eq. (4.24) is convergent even in the limit $N_\mathrm{v}\to\infty$. However, the Bogoliubov theory should be applied in the condition of weak depletion $n'/n \ll 1$. We note that since the order of N_v is at most 100 in typical experiments of ultracold atomic gases [16], the condition of weak depletion is validated.

4.2 Numerical calculation

In this section, we present the numerical results based on the Bogoliubov theory described above. In Sec. 4.2.1, we show the excitation spectra and analyze their anisotropy. We argue that the linear and quadratic dispersion relations are expected to be related with the symmetries which are spontaneously broken. The experiments which observe the excitation modes are discussed. Then, we numerically confirm their anisotropy and the rescaling relations obtained by the effective-field theory in Chap. 3. In Sec. 4.2.2, we obtain the elastic constants by fitting the excitation spectra to the analytic expressions, so that all the parameters introduced in the effective-field theory are determined. In Sec. 4.2.3, we calculate the fraction of depletion in Eq. (4.26) and confirm its logarithmical divergence with an increase in the number of quantum fluxes N_v. In Sec. 4.2.4, we present shifts of the transition points by minimizing the ground-state energy that includes the quantum correction. We discuss the difference between the phase diagrams for parallel and antiparallel fields, which is induced by the quantum fluctuation, and its uniqueness in the binary system. We also relate the large shifts of the transition points with an increase in the quantum depletion.

4.2.1 Excitation spectrum

We obtain the excitation spectrum $E_j(\mathbf{k})$ $(j = 1, 2)$ by numerically calculating the right eigenvectors of the 4×4 matrix $\tau_3 \mathcal{M}(\mathbf{k})$ in Eq. (4.23) for given $\mathbf{k}$. We note that the component of the matrix involves an infinite sum with respect to two integer variables. Since the summand in Eqs. (4.3) and (4.12) decays exponentially with respect to integers m_1, m_2, we numerically obtain its value in high accuracy even we exclude the summands with large integers.

In Fig. 4.2, we present the excitation spectra for all the lattice structures (a)-(e) shown in Fig. 2.2 for both parallel and antiparallel fields. From the figure, we find that the spectra at low energies are consistent with the linear and quadratic dispersion relations obtained analytically in the effective-field theory. In the case of the scalar case, the energy spectrum has a quadratic dispersion relation at low energies and its excited states are called the Tkacehnko mode [50, 55, 56, 62, 63].

In non-relativistic systems, the dispersion relations can be either linear or quadratic and the corresponding Nambu-Goldstone modes with linear and quadratic dispersion relations are classified as type-I and type-II, respectively. Recently, the criterion which gives the number of two types of Nambu-Goldstone modes has been found [48,64,65]. From the criterion, we find that the type-II Nambu-Goldstone modes appear when the generators of broken symmetries are noncommutable such as spin operators in the Heisenberg model. These theories are formulated for the internal symmetries, so that the Nambu-Goldstone modes which appear when the spacetime symmetry are spontaneously broken, such as a quantized vortex or a domain wall, cannot be discussed. However, a similar criterion is expected to hold in the case of the spacetime symmetry breaking [66]. In the case of the vortex lattices, the generators are pseudomomenta which are noncommutable. Since the oscillations in the x and y direction are coupled, a quadratic dispersion relation emerges. Although the generators of broken symmetries for the vortex lattices in binary BECs have not been identified yet, we infer that the emergence of a pair of linear (type-I) and quadratic (type-II) dispersion relations can be clarified by a similar procedure.

The excited states of a vortex lattice for a scalar BEC were first observed by JILA group [67]. By blasting the atoms at the center of BEC with the blasting laser, the vortex lattice is made to oscillate. Since the average angular momentum per particle increases due to the reduction of the numbers of the atoms with a small angular momentum by blasting, the strength of the synthetic magnetic field increases. Also a dip in the density created by the blasting laser creates an inward flow to fill the dip. By the Coriolis force acting on the gas, the vortices are dragged from their equilibrium position. In the case of vortex lattices in binary BECs, the oscillation of square lattices for parallel fields is observed in the JILA experiments [19]. By extending the effective-field theory and the Bogoliubov theory for a uniform system to a trapped system, the excitation modes for parallel and antiparallel fields, which may be observed in experiment, can be illustrated and two modes can be compared while only the dynamics of vortex lattices for parallel fields has been discussed [68]. We may observe the in-phase oscillation in the parallel fields and the anti-phase oscillation in the antiparallel fields as discussed in Sec. 3.3.1. By observing the oscillation of the vortex lattices depending on the direction of magnetic fields, we will find an interesting character of the oscillation, which is unique to the binary system.

We note that the emergence of line and point nodes at high energies is related to a fractional translation symmetry as discussed in Ref. [31]. Although we do not explain it in detail in this thesis, we find that the Bogoloubov matrix $\mathcal{M}(\mathbf{k})$ at some of these points can be divided into two independent blocks. When the two components are decoupled at the particular points, we find the divergence of the ES (Fig. 5.2) indicating the disentanglement of two components.

In Fig. 4.3, we display excitation spectra for the five lattice structures rescaled according to the rescaling relations in Eq. (3.66). We can confirm that the rescaling relations hold at sufficiently low energies around the Γ point. At such low energies, we find that the spectrum can be fit well by linear and quadratic dispersion relations given by

$$E_j(\mathbf{k}) = \sqrt{2}gn(k\ell)^j f_j(\varphi) \quad (j = 1, 2), \tag{4.27}$$

where the wave vector is parametrized as $\mathbf{k} = k(\cos\varphi, \sin\varphi)$ and $\{f_j(\varphi)\}$ are dimensionless functions that express the anisotropy of the spectra as in Eq. (3.64). In Fig. 4.4, we depict the functions $\{f_j(\varphi)\}$ obtained numerically for the same cases as in Fig. 4.3, where the superscripts P and AP indicate parallel and antiparallel fields, respectively. From the rescaling relation (3.67), we obtain the functions $\sqrt{C(\varphi)}$ and $\sqrt{D(\varphi)}$ whose square are related to the elastic constants as in Eq. (3.63). We find that the anisotropy of the energy spectra is consistent with the symmetry of the vortex lattices since the numerical results of $\sqrt{C(\varphi)}$ and $\sqrt{D(\varphi)}$ are consistent with the analytic forms obtained by the effective-field theory. In particular, the function $\sqrt{C(\varphi)}$ for interlaced triangular lattices is consistent with the effective-field theory as we introduce the elastic constant F_1 in Sec. 3.2.3. We infer that the elastic constant F_1 can be observed in an experiment by determining the excitation spectra for interlaced triangular lattices from the oscillation of the lattices. If interlaced triangular lattices are prepared by controlling the coupling constants, the lattices can be oscillated as in the JILA experiment [19].

We also find that the functions $\sqrt{C(\varphi)}$ and $\sqrt{D(\varphi)}$ obtained from the excitation spectra for parallel and antiparallel fields agree perfectly up to numerical precision. Since the rescaling relations are confirmed numerically at low energies, we verify that the excited states for parallel and antiparallel fields are indeed related to each other. In my master thesis and Ref. [31], the problem that the rescaling relations hold only for overlapping triangular lattices has remained unsolved. We identify the origin of the problem as due to the fact that we used the bare coupling constants $g_{\alpha\beta}$ for the rescaling relations. Using the renormalized coupling constants introduced in Chap. 3, we demonstrate the rescaling relations (3.66) for all the five structures (a)-(e) shown in Fig. 2.2 and we obtain the elastic constants consistently for parallel and antiparallel fields as discussed in the next section.

4.2.2 Elastic constants

In the previous section, we numerically determined $\sqrt{C(\varphi)}$ and $\sqrt{D(\varphi)}$. We can determine the dimensionless elastic constants $\{C_i\}$ and $\{D_i\}$ by comparing the analytical expressions in Eq. (3.63) with the numerical results. Figure 4.5 shows the determined elastic constants as a function of $g_{\uparrow\downarrow}/g$. Since we use the renormalized coupling constants, we find that the elastic constants obtained for parallel and antiparallel fields are equal in contrast to Ref. [31], where only the elastic constants for overlapping triangular lattices

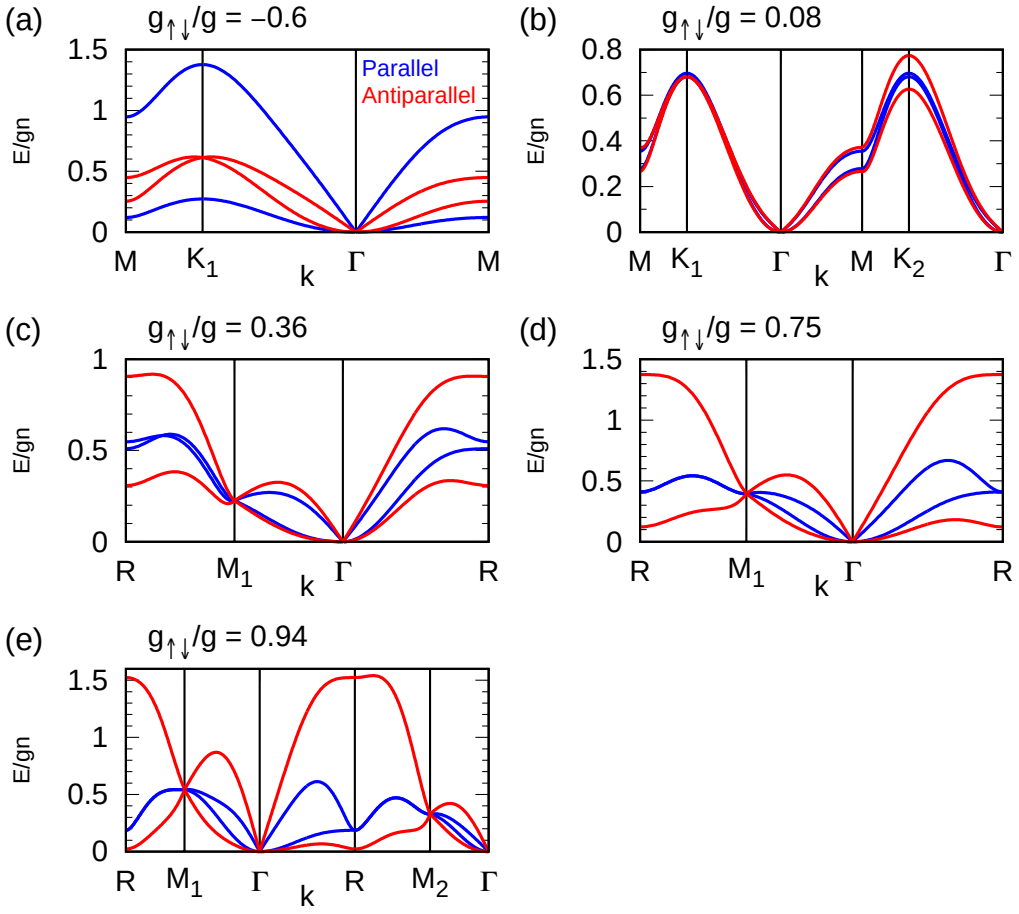

Figure 4.2: Bogoliubov excitation spectra $\{E_j(\mathbf{k})\}$ scaled by gn for (a) overlapping triangular, (b) interlaced triangular, (c) rhombic, (d) square, (e) rectangular lattices, whose structures are shown in Fig. 2.2 (a)-(e). For each value of $g_{\uparrow\downarrow}/g$, we show both results of parallel (blue) and antiparallel (red) magnetic fields. The energy spectra are calculated along the paths indicated by dotted arrows shown in the first Brillouin zone for each structure in Fig. 4.1.

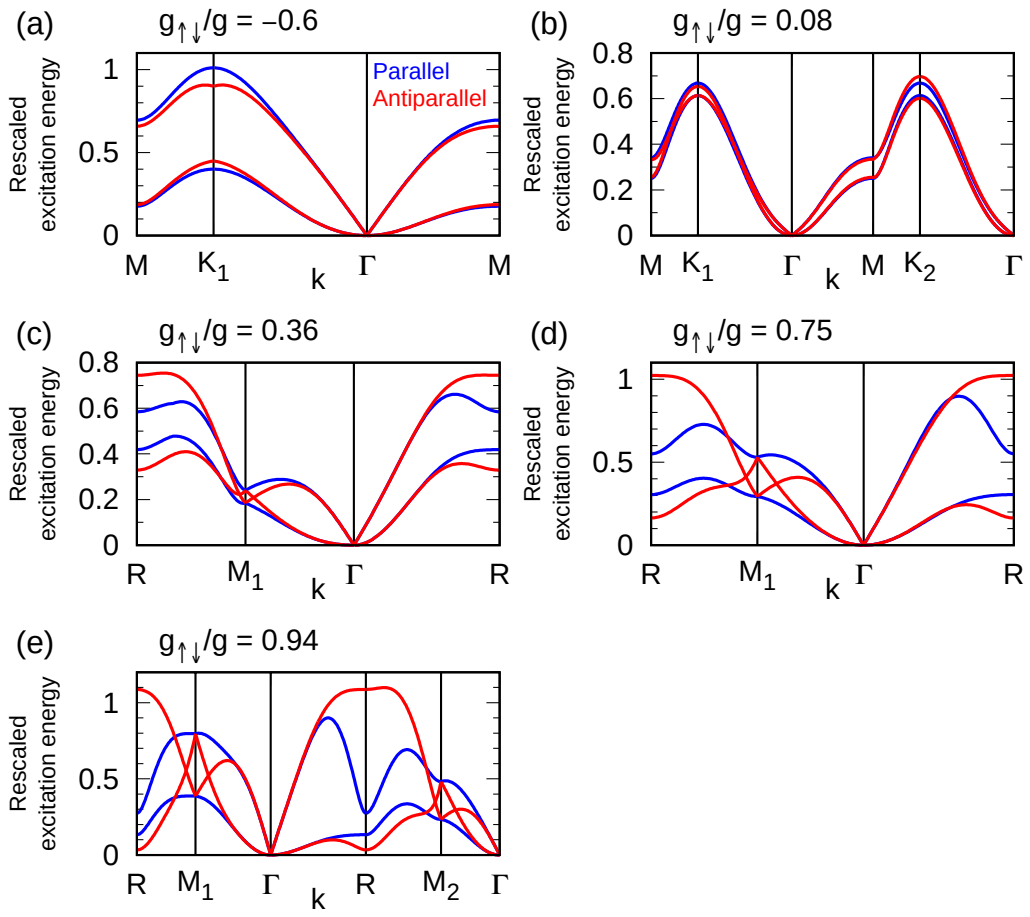

Figure 4.3: Rescaled Bogoliubov excitation spectra for the five cases (a)-(e) shown in Fig. 4.2 along the paths indicated by dotted arrows shown in Fig. 4.1. Blue curves show $E_1^{\rm P}(\mathbf{k})/(\sqrt{g\bar{g}_-}n)$ and $E_2^{\rm P}(\mathbf{k})/(\sqrt{g\bar{g}_+}n)$ for parallel (P) fields while red curves show $E_1^{\rm AP}(\mathbf{k})/(\sqrt{g\bar{g}_+}n)$ and $E_2^{\rm AP}(\mathbf{k})/(\sqrt{g\bar{g}_-}n)$ for antiparallel (AP) fields. We can confirm that the rescaling relations in Eq. (3.66) hold at sufficiently low energies around the Γ point.

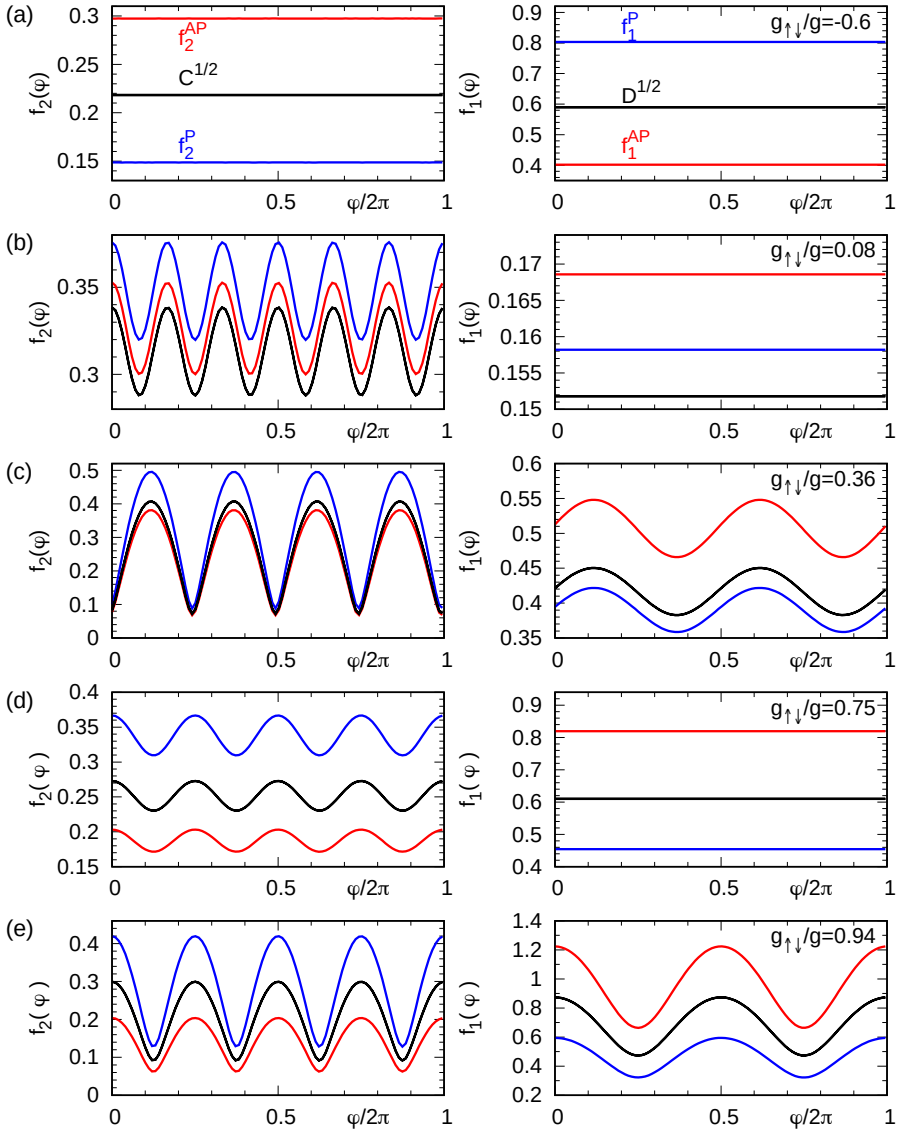

Figure 4.4: Dimensionless functions $f_2^{\mathrm{P/AP}}(\varphi)$ (left) and $f_1^{\mathrm{P/AP}}(\varphi)$ (right) for parallel (P; blue) and antiparallel (AP; red) fields for the same cases as in Fig. 4.2(a)-(e). The anisotropy of the low-energy spectra given in Eq. (4.27) is calculated from the Bogoliubov excitation spectra $\{E_j(\mathbf{k})\}$ along a circular path $\mathbf{k} = k(\cos\varphi, \sin\varphi)$ with $k = 0.001a/\ell^2$ and $\varphi \in [0, 2\pi)$. After proper rescaling given in Eq. (3.67), the curves for parallel and antiparallel fields coincide up to high numerical precision. In the left panels, the rescaled functions $f_2^{\mathrm{P}}(\varphi)\sqrt{g/\bar{g}_+}$ and $f_2^{\mathrm{AP}}(\varphi)\sqrt{g/\bar{g}_-}$ give the common function $\sqrt{C(\varphi)}$, and in the right panels, the rescaled functions $f_1^{\mathrm{P}}(\varphi)\sqrt{g/\bar{g}_-}$ and $f_1^{\mathrm{AP}}(\varphi)\sqrt{g/\bar{g}_+}$ give the common function $\sqrt{D(\varphi)}$. $\sqrt{C(\varphi)}$ and $\sqrt{D(\varphi)}$ are both depicted by black curves. We note that the obtained functions $\sqrt{C(\varphi)}$ and $\sqrt{D(\varphi)}$ are consistent with the analytic forms given in Eq. (3.63).

are equal. The values of the elastic constants are also corrected because of the renormalization of the coupling constants. We note that the dependence of elastic constants on $g_{\uparrow\downarrow}/g$ has also been analyzed in Ref. [47]; the results in the reference are similar to ours except for interlaced triangular lattices where we have identified the missing term. By obtaining the elastic constants, all parameters which appear in the effective-field theory are determined. Therefore any quantity which is numerically calculated with the Bogoliubov theory can be compared with its analytic form obtained by the effective-field theory.

4.2.3 Quantum depletion

In the left panel of Fig. 4.6, we plot the quantum depletion obtained from Eq. (4.26) for all the vortex structures in the mean-field regime. We find that the quantum depletion for parallel (antiparallel) fields is larger than that for antiparallel (parallel) fields with repulsive (attractive) $g_{\uparrow\downarrow}$. We will see similar behavior in EE in Chap. 5. At the transition point between interlaced triangular lattices and rhombic lattices, the quantum depletion changes discontinuously owing to the discontinuous change of the lattice structure. Meanwhile, the quantum depletion diverges at both the transition points between rhombic, square and rectangular lattices; this is likely to be related to the rapid changes in the inner angle and the aspect ratio as shown in Fig. 2.3.

The field-theoretical result in Eq. (3.77) shows that the quantum depletion logarithmically diverges with an increase in the number of flux quanta $N_{\rm v}$. In the right panel of Fig. 4.6, we show the quantum depletion as a function of $N_{\rm v}$ for a representative point in the square-lattices phase. Due to a repulsive intercomponent interaction in square lattices, the quantum depletion for parallel fields is larger than that for antiparallel fields as we expect from Eq. (3.77). Since the quantum depletion indeed shows a logarithmic increase, we find that the quantum fluctuation is enhanced as the system size is enlarged and the quantum fluctuation will diverge in the thermodynamic limit.

4.2.4 Lee-Huang-Yang correction

We analyze the effect of quantum fluctuations on the ground-state phase diagrams for parallel and antiparallel fields. Mueller and Ho [17] found that five types of vortex-lattice structures which depend on the interaction ratio $g_{\uparrow\downarrow}/g$ appear within the mean-field theory as shown in Fig. 2.3. We consider how the transition points vary due to the Lee-Huang-Yang correction in Eq. (4.24). By assuming that the same types of structures as the mean-field case appear, we calculate the correction to the ground-state energy due to zero-point fluctuations in Eq. (4.24), which is proportional to ν^{-1}.

In Fig. 4.7, we present the mean-field ground-state energy as well as those with quantum corrections for parallel and antiparallel fields, where the filling factor is $\nu = 20$. We minimize the ground-state energy in Eq. (4.24) with respect to the inner angle θ for rhombic lattices and the aspect ratio b/a for rectangular lattices. As seen in Fig. 4.7 (a), the transition points between rhombic, square and rectangular lattices shift to the left due to the quantum corrections. We find that the transition points shift more significantly for parallel fields. In contrast, the transition point $g_{\uparrow\downarrow}/g = 0$ between the overlapping and interlaced triangular lattices remains unchanged against quantum corrections. The transition point does not shift to minimize (maximize) the contact area for

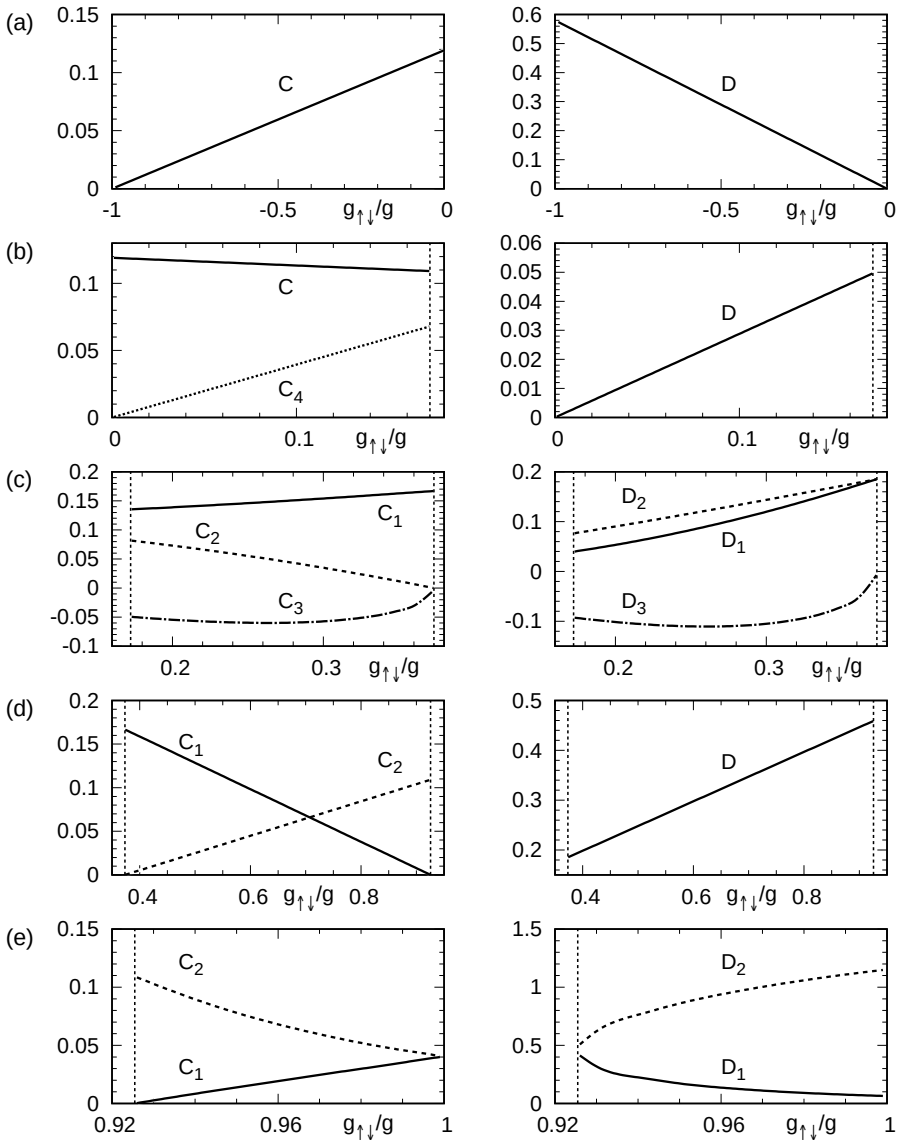

Figure 4.5: Dimensionless elastic constants C_i $(i = 1, 2, 3, 4)$ (left) and D_i $(i = 1, 2, 3)$ (right) for the lattice structures (a)-(e) shown in Fig. 2.2: (a) overlapping triangular, (b) interlaced triangular, (c) rhombic, (d) square, and (e) rectangular lattices. These constants are obtained by fitting the numerically obtained functions $\sqrt{C(\varphi)}$ and $\sqrt{D(\varphi)}$, which are common for parallel and antiparallel fields as shown in Fig. 4.4, to the analytic expressions of the dispersion relations given in Eq. (3.64). See Eq. (3.44) for the symmetry constraints on the constants. Vertical dashed lines indicate the transition points in the mean-field ground state.

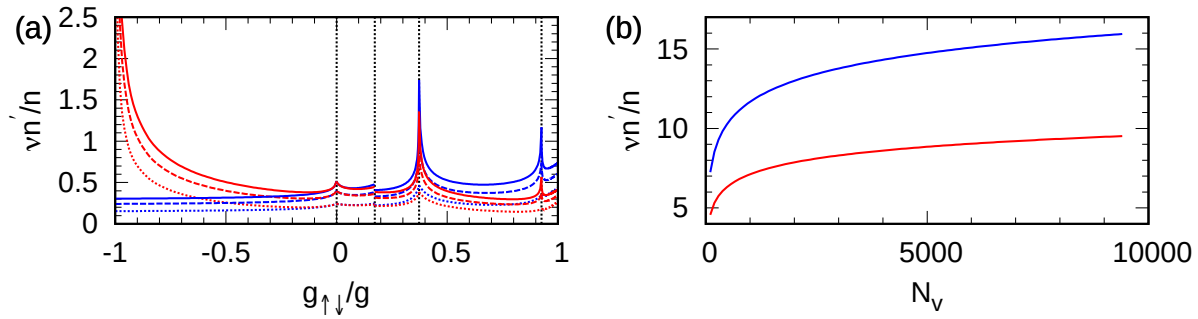

Figure 4.6: (a) Fraction of depletion n'/n (scaled by ν^{-1}) as a function of $g_{\uparrow\downarrow}/g$ for parallel (blue) and antiparallel (red) fields for $N_{\rm v} = 5^2$ (dotted), 11^2 (dashed) and 19^2 (solid). Vertical dashed lines indicate the transition points. We find $\nu n'/n$ is larger for parallel (antiparallel) fields when the intercomponent interaction $g_{\uparrow\downarrow}$ is repulsive (attractive). (b) $\nu n'/n$ versus $N_{\rm v}$ for $g_{\uparrow\downarrow}/g = 0.75$. A fit to the form $\nu n'/n = \gamma_1 \ln N_{\rm v} + \gamma_2$ (solid line) gives $(\gamma_1, \gamma_2) = (1.91026, -1.52925)$ for parallel fields and $(\gamma_1, \gamma_2) = (1.08532, -0.397055)$ for antiparallel fields.

repulsive (attractive) intercomponent interactions. While the shift of the transition point between the interlaced triangular and rhombic lattices is not clearly seen in Fig. 4.7 (a), we find that the shift indeed occurs in the zoomed plot in Fig. 4.7 (b). The transition point moves to the right (left) for parallel (antiparallel) fields. We find that the energy (scaled by gn^2A) for rhombic lattices has a nonzero imaginary part of the order of 10^{-6} in the regime $0.318 < g_{\uparrow\downarrow}/g < 0.3733$ for parallel fields and $0.337 < g_{\uparrow\downarrow}/g < 0.3733$ for antiparallel fields (not shown) while the order of the real part is 1. We note that the imaginary part only appears in the rhombic lattices and does not appear in minimizing the energy for rectangular lattices.

We present the inner angle θ of the rhombic lattices in Fig. 4.8 (a) and the aspect ratio b/a of the rectangular lattices in Fig. 4.8 (b). They are obtained through the one-parameter minimization of the ground-state energy (4.24). The corrected transition point between rhombic and square lattices is determined when the inner angle becomes 90° and the transition point between square and rectangular lattices is determined when the aspect ratio becomes larger than 1.

In Sec. 2.3.3, we reviewed the equivalence of the ground-state phase diagrams for parallel and antiparallel fields in the mean-field theory while the phase diagrams for parallel and antiparallel fields are different in the quantum Hall regime, where the mean-field theory breaks down. Since the ground-state phase diagrams with the quantum correction are different from those in the mean-field theory, we find that the quantum correction affects the ground-state phase diagram. Furthermore, we see that the ground-state phase diagrams for parallel and antiparallel fields are different from each other due to the quantum correction. This result indicates that the quantum fluctuation causes the difference between the cases of parallel and antiparallel fields. Since the parallel and antiparallel fields are unique to the binary system, the difference does not appear in the scalar system. We also note the relation between shifts of the transition points and the values of the quantum depletion since both the shifts and the quantum depletion for parallel fields are significantly larger than those for antiparallel fields when the intercomponent

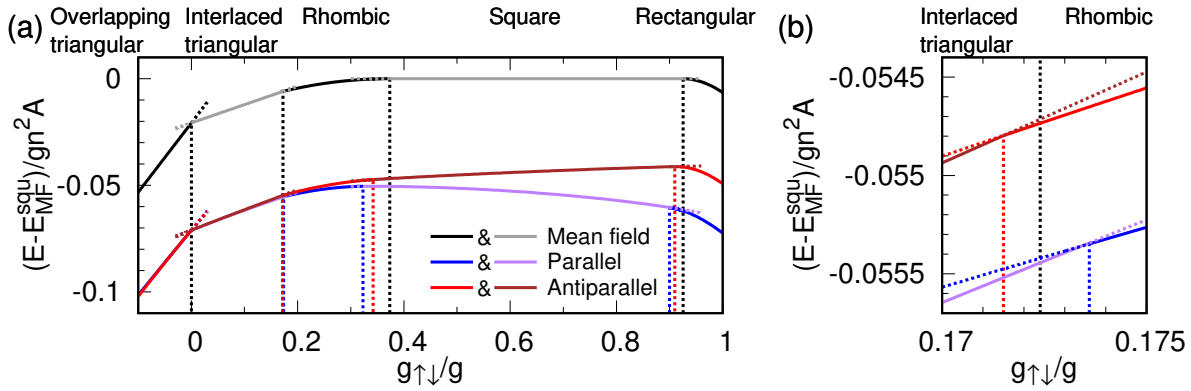

Figure 4.7: (a) Ground-state energy as a function of the interaction ratio $g_{\uparrow\downarrow}/g$. The mean-field energy (black and grey) is changed sufficiently by the quantum correction, as shown for both parallel (blue and purple) and antiparallel (red and brown) fields for $\nu = 20$. The mean-field energy for the square lattices, $E_{\mathrm{MF}}^{\mathrm{squ}}/gn^2A = 1.18034{+}0.834627g_{\uparrow\downarrow}/g$, is subtracted to emphasize the changes due to quantum fluctuations. Alternating colors for each case correspond to different phases, and vertical dashed lines indicate the transition points. In particular, the transition points between rhombic-, square- and rectangular lattices shift appreciably owing to the quantum corrections. In contrast, the transition point at $g_{\uparrow\downarrow}/g = 0$ between the overlapping and interlaced triangular lattices remain unchanged by the quantum corrections. (b) Enlarged figure of (a) around the transition point between the interlaced triangular and rhombic lattices, which also shows small shifts due to the quantum corrections.

interaction is repulsive. The result implies that the ground-state phase diagram is modified significantly when the quantum fluctuation increases. Since the quantum depletion increases logarithmically with respect to the system size, the transition points will shift significantly as the area of the system is extended.

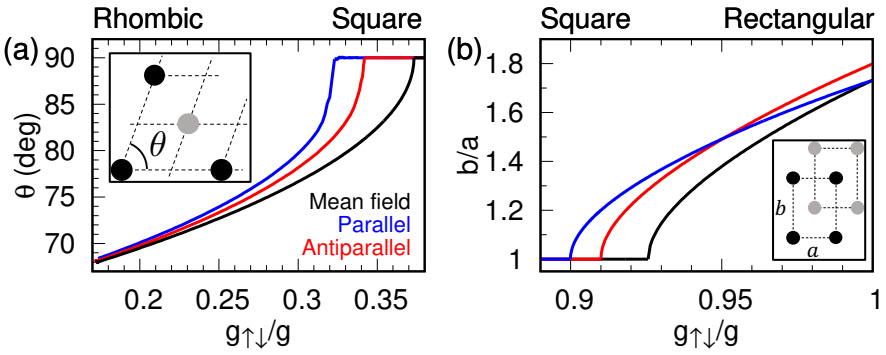

Figure 4.8: (a) Inner angle θ of the rhombic lattices and (b) the aspect ratio b/a of the rectangular lattices, plotted against the interaction ratio $g_{\uparrow\downarrow}/g$. The mean-field results (black) [17] are significantly altered by the Lee-Huang-Yang corrections, as shown both for parallel (blue) and antiparallel (red) fields. Insets show the definitions of θ and b/a.

Chapter 5

Intercomponent entanglement entropy and entanglement spectrum

In this chapter, we discuss the EE and the ES between two components in binary BECs under synthetic magnetic fields. We find that the behavior of the intercomponent EE is reflected in the ground-state phase diagram with the quantum corrections since both need the excitation spectra in calculation, so that we give the restriction to the ground states in the intermediate regime between the mean-field regime and the quantum Hall regime. From the ES, we find excitation modes which contribute to the intercomponent entanglement and discuss the emergence of the long-range interaction in the entanglement Hamiltonian from the correlation functions. Finally, we discuss that the logarithmic contribution of the intercomponent EE may be related with the continuous symmetry breaking. In Sec. 5.1, we review the EE and the ES in condensed-matter systems. In Sec. 5.2, we obtain analytical expressions of the EE and ES using the effective-field theory of vortex lattices. In Sec. 5.3, we numerically calculate the EE and ES using the Bogoliubov theory and compare them with analytical forms. Then we discuss the correspondence between the intercomponent EE and the ground-state phase diagrams. We also discuss the intercomponent ES and the subleading term of the EE.

5.1 Review of entanglement in condensed-matter system

In this section, we review the entanglement in condensed-matter systems. In Sec. 5.1.1, we review the EE in systems with the continuous symmetry breaking and topological systems. We consider both the leading term of the EE and its subleading term which logarithmically increases with respect to the boundary size. In Sec. 5.1.2, we define the ES and review the ES of topological systems and ladder systems.

5.1.1 Entanglement entropy

There has been a lot of interest in the entanglement of condensed-matter systems. The entanglement of a many-body state $|\Psi\rangle$ is usually characterized by the EE. By dividing the system into subsystem A and its complement $\bar{A}$, the reduced density matrix for the

subsystem is given by $\rho_A = \mathrm{Tr}_{\bar{A}}|\Psi\rangle\langle\Psi|$. Then the EE (von Neuman entropy) of the subregion A is given by

$$S_A = -\mathrm{Tr}_A[\rho_A \ln \rho_A]. \tag{5.1}$$

In many cases, the system is divided in real space. In our work, we instead divide the binary system in terms of components to discuss the intercomponent entanglement.

The EE of a d-dimensional condensed-matter system presenting a spontaneous symmetry breaking of a continuous symmetry at absolute zero in the thermodynamic limit has been investigated. Metlitski and Grover [26] have obtained an analytic form of EE based on a quantum rotor and a non-linear sigma model as

$$S_A = CL^{d-1} + \frac{n_G}{2} \ln\left(\frac{\rho_s}{v} L^{d-1}\right) + \gamma^{\mathrm{ord}} + \cdots, \tag{5.2}$$

where C is a non-universal constant and L is the length scale of the system. In the second term, n_G is the number of Nambu-Goldstone modes, ρ_s is the stiffness, v is the spin wave velocity and γ^{ord} is a universal geometric constant. It is known that in a variety of quantum many-body systems, the leading contribution of EE in the ground state scales with the boundary size of the subsystem as in the first term of Eq. (5.2). This is known as the area law. However, the area law is violated in one-dimensional critical systems, where the EE exhibits a logarithmic scaling [69].

Corrections to the area law give important pieces of information about the system. In systems with the continuous symmetry breaking, an additive correction which logarithmically diverges with respect to the boundary size appears as in the second term of Eq. (5.2). This term appears from the spin wave excitations (Nambu-Goldstone modes) and the "tower of state" due to the symmetry restoration in a finite volume. For binary BECs, the logarithmic term has been obtained for the intercomponent EE and its coefficient is related to the Nambu-Goldstone mode and the "tower of state" [30]. In the third term of Eq. (5.2), a universal constant term appears. Reference [26] has shown that the third term depends on the geometry of the subsystem. In contrast, in topological systems, this constant subleading term of EE characterizes the topological order of the system. The term is called a topological EE. For instance, the topological EE for the toric code is $\gamma = \ln 2$.

From the ground-state phase diagrams in Figs. 2.5 and 2.6, we naturally expect that the intercomponent EE for parallel (antiparallel) fields is larger for a repulsive (attractive) intercomponent interaction even in the regime of vortex lattices. It is also an interesting question to ask whether the logarithmic additional term appears in the scaling of the EE.

5.1.2 Entanglement spectrum

The detail of the entanglement is further investigated by the ES. When the reduced density matrix of the subsystem is written as

$$\rho_A = \exp(-H_{\mathrm{e}}), \tag{5.3}$$

the ES is calculated as the energy spectrum of the entanglement Hamiltonian H_{e}. For topological systems, in particular, a remarkable correspondence between the ES and the energy spectrum of the edge state for quantum Hall states has been found by Li and

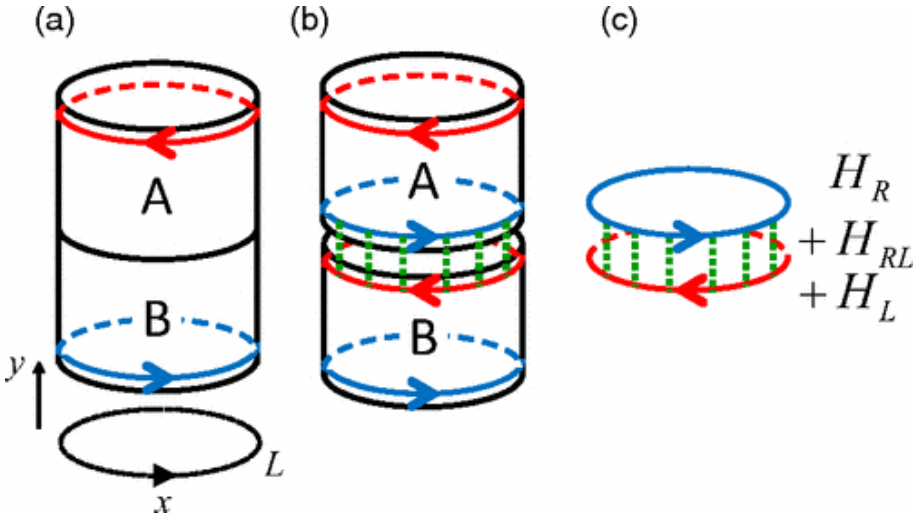

Figure 5.1: "Cut and glue" approach. (a) The system on the cylinder of circumference L is divided into two halves. The ES between subsystems A and B is investigated. (b) At the boundary of two subsystems, gapless modes described by two chiral TLLs with Hamiltonians H_R and H_L appear. They are glued along the edges by turning on the interaction between A and B with the interaction Hamiltonian H_{RL}. (c) The entanglement of the quantum Hall state is reduced to the entanglement between two chiral TLLs. Reproduced from Fig. 1 of Ref. [29]. Copyright © 2013 by the American Physical Society.

Haldane [70]. In a two-dimensional fractional quantum Hall state on a cylinder, the linear energy spectrum of the edge state has been shown to correspond to the ES at the low-energy regime, where the subsystem is given by the upper half of the entire system. By the "cut and glue" approach, the correspondence has been analytically proved by coupling two chiral TLLs [28].

However, when two non-chiral TLLs which are not the edge state of a topological system are coupled, the ES is not always linear. When the energy spectrum of the two coupled non-chiral TLLs is partially gapless (i.e. one of the symmetric and antisymmetric channels is gapless) or fully gapless, the ES has square-root or gapped dispersion relations, respectively [29]. These interesting features of the ES are related to the long-range interaction proportional to the logarithm of the chord distance on a unit circle in the entanglement Hamiltonian .

In a related work for homogeneous binary BECs (without synthetic gauge fields) [30], we have found that the intercomponent ES featuring a square-root dispersion relation appears when two components are coupled by a Rabi coupling. We have found that a long-range interaction appears in the entanglement Hamiltonian for one-, two- and three-dimensional systems, similarly to the case of coupled TLLs in one spatial dimension. In the following sections, we calculate the intercomponent ES of vortex lattices and investigate the long-range interaction in the entanglement Hamiltonian.

5.2 Effective-field theory

In this section, we discuss the intercomponent entanglement of binary BECs under synthetic gauge fields by using the effective-field theory. In Sec. 5.2.1, we obtain an analytic expression of the ES of our system. We find that a new long-range interaction term appears in the entanglement Hamiltonian. In Sec. 5.2.2, we calculate an analytic form of the intercomponent EE.

5.2.1 Entanglement Hamiltonian and entanglement spectrum

We calculate the reduced density matrix $\rho_\uparrow$ for the spin-$\uparrow$ component, which is defined by tracing out the degrees of freedom in the spin-$\downarrow$ component from the ground state $|0^{\rm zero}\rangle \otimes |0^{\rm osc}\rangle$ of the total system. Since the zero and oscillator modes are decoupled, the reduced density matrix is given as $\rho_\uparrow = \rho_\uparrow^{\rm zero} \otimes \rho_\uparrow^{\rm osc}$. As the zero-mode ground state $|N_\uparrow = N/2\rangle\,|N_\downarrow = N/2\rangle$ is a product state, there is no intercomponent entanglement in the zero-mode part and the reduced density matrix in this part is written as $\rho_\uparrow^{\rm zero} = |N_\uparrow = N/2\rangle\langle N_\uparrow = N/2|$. We only consider the oscillator-mode part $\rho_\uparrow^{\rm osc}$ in the following.

For the oscillator-mode part of the reduced density matrix $\rho_\uparrow^{\rm osc}$, we introduce the following Gaussian ansatz [26, 29, 30, 71–73]:

$$\rho_\uparrow^{\rm osc} = \frac{1}{Z_{\rm e}^{\rm osc}} {\rm e}^{-H_{\rm e}^{\rm osc}},\ Z_{\rm e}^{\rm osc} = {\rm Tr}\, {\rm e}^{-H_{\rm e}^{\rm osc}},\ H_{\rm e}^{\rm osc} = \frac{1}{2}\sum_{\mathbf{k}\neq\mathbf{0}} \left(n F_{\mathbf{k}} \theta_{-\mathbf{k},\uparrow}\theta_{\mathbf{k},\uparrow} + \frac{G_{\mathbf{k}}}{n} n_{-\mathbf{k},\uparrow} n_{\mathbf{k},\uparrow} \right), \quad (5.4)$$

where $F_{\mathbf{k}}$ and $G_{\mathbf{k}}$ are positive dimensionless coefficients which are to be determined later. We assume $F_{\mathbf{k}} = F_{-\mathbf{k}}$ and $G_{\mathbf{k}} = G_{-\mathbf{k}}$ without loss of generality. By introducing annihilation and creation operators as

$$\begin{aligned} \eta_{\mathbf{k}} =& \frac{1}{\sqrt{2}} \left[\sqrt{n} \left(\frac{F_{\mathbf{k}}}{G_{\mathbf{k}}} \right)^{1/4} \theta_{\mathbf{k},\uparrow} + \frac{\mathrm{i}}{\sqrt{n}} \left(\frac{G_{\mathbf{k}}}{F_{\mathbf{k}}} \right)^{1/4} n_{\mathbf{k},\uparrow} \right], \\ \eta_{\mathbf{k}}^\dagger =& \frac{1}{\sqrt{2}} \left[\sqrt{n} \left(\frac{F_{\mathbf{k}}}{G_{\mathbf{k}}} \right)^{1/4} \theta_{-\mathbf{k},\uparrow} - \frac{\mathrm{i}}{\sqrt{n}} \left(\frac{G_{\mathbf{k}}}{F_{\mathbf{k}}} \right)^{1/4} n_{-\mathbf{k},\uparrow} \right] \quad (\mathbf{k} \neq \mathbf{0}), \end{aligned} \quad (5.5)$$

the entanglement Hamiltonian $H_{\rm e}^{\rm osc}$ in Eq. (5.4) is diagonalized as

$$H_{\rm e}^{\rm osc} = \sum_{\mathbf{k}\neq\mathbf{0}} \xi_{\mathbf{k}} \left(\eta_{\mathbf{k}}^\dagger \eta_{\mathbf{k}} + \frac{1}{2} \right), \quad (5.6)$$

where $\xi_{\mathbf{k}} = \sqrt{F_{\mathbf{k}} G_{\mathbf{k}}}$ is the single-particle ES.

Using the relations in Eq. (5.5) and the Bose distribution function

$${\rm Tr} \left(\eta_{\mathbf{k}}^\dagger \eta_{\mathbf{k}} \rho_\uparrow^{\rm osc} \right) = \frac{1}{{\rm e}^{\xi_{\mathbf{k}}} - 1} \equiv f_{\rm B}(\xi_{\mathbf{k}}), \quad (5.7)$$

we obtain the phase and density correlations as

$$\begin{aligned}
\mathrm{Tr}\left(\theta_{-\mathbf{k},\uparrow}\theta_{\mathbf{k},\uparrow}\rho_{\uparrow}^{\mathrm{osc}}\right) &= \frac{1}{2n}\left(\frac{G_{\mathbf{k}}}{F_{\mathbf{k}}}\right)^{1/2}\mathrm{Tr}\left[\left(\eta_{\mathbf{k}}^{\dagger}+\eta_{-\mathbf{k}}\right)\left(\eta_{\mathbf{k}}+\eta_{-\mathbf{k}}^{\dagger}\right)\rho_{\uparrow}^{\mathrm{osc}}\right] \\
&= \frac{1}{n}\left(\frac{G_{\mathbf{k}}}{F_{\mathbf{k}}}\right)^{1/2}\left[f_{\mathrm{B}}(\xi_{\mathbf{k}})+\frac{1}{2}\right], \\
\mathrm{Tr}\left(n_{-\mathbf{k},\uparrow}n_{\mathbf{k},\uparrow}\rho_{\uparrow}^{\mathrm{osc}}\right) &= \frac{n}{2}\left(\frac{F_{\mathbf{k}}}{G_{\mathbf{k}}}\right)^{1/2}\mathrm{Tr}\left[\left(\eta_{\mathbf{k}}^{\dagger}-\eta_{-\mathbf{k}}\right)\left(\eta_{\mathbf{k}}-\eta_{-\mathbf{k}}^{\dagger}\right)\rho_{\uparrow}^{\mathrm{osc}}\right] \\
&= n\left(\frac{F_{\mathbf{k}}}{G_{\mathbf{k}}}\right)^{1/2}\left[f_{\mathrm{B}}(\xi_{\mathbf{k}})+\frac{1}{2}\right].
\end{aligned} \tag{5.8}$$

We require that they are equivalent to the correlators for the oscillator ground state $|0^{\mathrm{osc}}\rangle$ calculated in Eq. (3.70). We then find

$$\begin{aligned}
f_{\mathrm{B}}(\xi_{\mathbf{k}})+\frac{1}{2} &= \sqrt{\langle 0^{\mathrm{osc}}|\theta_{-\mathbf{k},\uparrow}\theta_{\mathbf{k},\uparrow}|0^{\mathrm{osc}}\rangle\langle 0^{\mathrm{osc}}|n_{-\mathbf{k},\uparrow}n_{\mathbf{k},\uparrow}|0^{\mathrm{osc}}\rangle} = \frac{1}{4}\left(|R_{\mathbf{k},1}|^2\frac{\zeta_{\mathbf{k},2}}{\zeta_{\mathbf{k},1}}+|R_{\mathbf{k},2}|^2\frac{\zeta_{\mathbf{k},1}}{\zeta_{\mathbf{k},2}}\right), \\
\sqrt{\frac{F_{\mathbf{k}}}{G_{\mathbf{k}}}} &= \frac{1}{n}\sqrt{\frac{\langle 0^{\mathrm{osc}}|n_{-\mathbf{k},\uparrow}n_{\mathbf{k},\uparrow}|0^{\mathrm{osc}}\rangle}{\langle 0^{\mathrm{osc}}|\theta_{-\mathbf{k},\uparrow}\theta_{\mathbf{k},\uparrow}|0^{\mathrm{osc}}\rangle}} = 2\zeta_{\mathbf{k},1}\zeta_{\mathbf{k},2}.
\end{aligned} \tag{5.9}$$

From Eq. (3.71) in the long-wavelength limit $k\ell \ll 1$, we find that $f_{\mathrm{B}}(\xi_{\mathbf{k}})$ and $\sqrt{F_{\mathbf{k}}/G_{\mathbf{k}}}$ in Eq. (5.9) are given as

$$f_{\mathrm{B}}(\xi_{\mathbf{k}}) \approx \frac{1}{4}\left[\frac{\bar{g}_{\pm}D(\varphi)}{\bar{g}_{\mp}C(\varphi)}\right]^{1/4}(k\ell)^{-1/2}, \quad \sqrt{\frac{F_{\mathbf{k}}}{G_{\mathbf{k}}}} \approx \left[\frac{4g^2C(\varphi)D(\varphi)}{\bar{g}_{+}\bar{g}_{-}}\right]^{1/4}(k\ell)^{3/2}. \tag{5.10}$$

where the upper and lower signs correspond to the cases of parallel and antiparallel fields, respectively.[1] We obtain the long-wavelength expressions of the single-particle ES $\xi_{\mathbf{k}}$ and the coefficients $F_{\mathbf{k}}$ and $G_{\mathbf{k}}$ as

$$\begin{aligned}
\xi_{\mathbf{k}} &= \ln\left[1+\frac{1}{f_{\mathrm{B}}(\xi_{\mathbf{k}})}\right] \approx \frac{1}{f_{\mathrm{B}}(\xi_{\mathbf{k}})} \approx c(\varphi)\sqrt{k\ell}, \\
F_{\mathbf{k}} &= \xi_{\mathbf{k}}\sqrt{\frac{F_{\mathbf{k}}}{G_{\mathbf{k}}}} \approx F(\varphi)(k\ell)^2, \quad G_{\mathbf{k}} = \xi_{\mathbf{k}}\sqrt{\frac{G_{\mathbf{k}}}{F_{\mathbf{k}}}} \approx \frac{G(\varphi)}{k\ell},
\end{aligned} \tag{5.11}$$

where the dependences on the angle φ for the ES and the entanglement Hamiltonian are expressed in terms of the dimensionless functions

$$c(\varphi) = 4\left[\frac{\bar{g}_{\mp}C(\varphi)}{\bar{g}_{\pm}D(\varphi)}\right]^{1/4}, \quad F(\varphi) = 4\sqrt{\frac{2gC(\varphi)}{\bar{g}_{\pm}}}, \quad G(\varphi) = 2\sqrt{\frac{2\bar{g}_{\mp}}{gD(\varphi)}}. \tag{5.12}$$

From Eq. (5.11), we find that the ES shows an anomalous square-root dispersion relation with anisotropy depending on the lattice structure. Similarly to the rescaling relations

[1] The same sign rule applies to Eqs. (5.12) and (5.30) below.

of the excitation spectra in Eq. (3.66), the single-particle ESs $\xi_{\mathbf{k}}$ for parallel (P) and antiparallel (AP) fields are related to each other by the rescaling relation given as

$$\left(\frac{\bar{g}_+}{\bar{g}_-}\right)^{1/4} \xi_{\mathbf{k}}^{\mathrm{P}} = \left(\frac{\bar{g}_-}{\bar{g}_+}\right)^{1/4} \xi_{\mathbf{k}}^{\mathrm{AP}}. \tag{5.13}$$

Moreover, the dimensionless functions $c(\varphi)$ for the two types of fields are related to each other as

$$\left(\frac{\bar{g}_+}{\bar{g}_-}\right)^{1/4} c^{\mathrm{P}}(\varphi) = \left(\frac{\bar{g}_-}{\bar{g}_+}\right)^{1/4} c^{\mathrm{AP}}(\varphi) = 4\left[\frac{C(\varphi)}{D(\varphi)}\right]^{1/4}. \tag{5.14}$$

We obtain the entanglement Hamiltonian by substituting $F_{\mathbf{k}}$ and $G_{\mathbf{k}}$ in Eq. (5.11) in the long-wavelength limit into $H_{\mathrm{e}}^{\mathrm{osc}}$ in Eq. (5.4). By using the fields $\theta_\uparrow(\mathbf{r})$ and $n_\uparrow(\mathbf{r})$ in real space, it is expressed as

$$H_{\mathrm{e}} = \int \mathrm{d}^2\mathbf{r} \int \mathrm{d}^2\mathbf{r}' \left[\frac{n\ell^2}{2} U_F(\mathbf{r}-\mathbf{r}') \nabla\theta_\uparrow(\mathbf{r}) \cdot \nabla\theta_\uparrow(\mathbf{r}') + \frac{1}{2n} U_G(\mathbf{r}-\mathbf{r}') n_\uparrow(\mathbf{r}) n_\uparrow(\mathbf{r}')\right], \tag{5.15}$$

where we introduce the interaction potentials as

$$U_F(\mathbf{r}-\mathbf{r}') = \frac{1}{A}\sum_{\mathbf{k}} F(\varphi) \mathrm{e}^{\mathrm{i}\mathbf{k}\cdot(\mathbf{r}-\mathbf{r}')}, \quad U_G(\mathbf{r}-\mathbf{r}') = \lim_{\alpha\to 0^+} \frac{1}{A}\sum_{\mathbf{k}\neq\mathbf{0}} \frac{G(\varphi)}{k\ell} \mathrm{e}^{-\alpha k + \mathrm{i}\mathbf{k}\cdot(\mathbf{r}-\mathbf{r}')}. \tag{5.16}$$

To regularize the infinite sum for $U_G(\mathbf{r}-\mathbf{r}')$, we use the convergence factor $\mathrm{e}^{-\alpha k}$. For simplicity, we consider the case of overlapping triangular lattices, in which we obtain constant $C(\varphi)$ and $D(\varphi)$ due to the elastic constants for overlapping triangular lattices in Eq. (3.44) (a). In this case, $F(\varphi)$ and $G(\varphi)$ are constant, and thus the potentials in Eq. (5.16) are given by

$$U_F(\mathbf{r}-\mathbf{r}') = F\delta(\mathbf{r}-\mathbf{r}'), \quad U_G(\mathbf{r}-\mathbf{r}') = \frac{G}{2\pi\ell|\mathbf{r}-\mathbf{r}'|}. \tag{5.17}$$

The detail of the calculation of $U_G(\mathbf{r}-\mathbf{r}')$ is given in App. C. We note that $\theta_\uparrow(\mathbf{r})$ is the regular part of the superfluid phase of the spin-↑ component, so that its gradient in Eq. (5.15) is related to the regular part of the superfluid velocity $\mathbf{v}_{\mathrm{s},\uparrow}(\mathbf{r}) = -\frac{\hbar}{M}\nabla\theta_\uparrow(\mathbf{r})$. From Eqs. (5.15) and (5.17), we find that the entanglement Hamiltonian has a short-range interaction in terms of the superfluid velocity $\mathbf{v}_{s,\uparrow}(\mathbf{r})$ and a long-range one in terms of the density $n_\uparrow(\mathbf{r})$. If the density interaction were instead short-ranged, the ES would show a phonon mode with a linear dispersion relation. Therefore, the anomalous square-root dispersion relation in Eq. (5.11) is related to the presence of a long-range interaction in H_{e}.

5.2.2 Entanglement entropy

Since the zero-mode part of the ground state is a product state, we only consider the oscillation part of the EE. From the single-particle ES $\xi_{\mathbf{k}}$ in Eq. (5.11), the intercomponent EE S_{e} is calculated. We consider the canonical ensemble obtained from $H_{\mathrm{e}}^{\mathrm{osc}}$ with a fictitious temperature T. We then find the Bose distribution $\langle \eta_{\mathbf{k}}^\dagger \eta_{\mathbf{k}} \rangle = \left(e^{\xi_{\mathbf{k}}/T} - 1\right)^{-1} =$

$f_{\rm B}(\xi_{\mathbf{k}}/T)$ obeyed by the number operator $\eta^\dagger_{\mathbf{k}}\eta_{\mathbf{k}}$ in Eq. (5.7). By calculating the internal energy, we obtain the EE $S_{\rm e}^{\rm osc}$ as the thermal entropy at $T=1$. For simplicity, we assume that $\xi_{\mathbf{k}}$ is isotropic, i.e., $c(\varphi)$ is constant, as in the case of overlapping triangular lattices; however, we expect that the result holds qualitatively for all the lattice structures.

The internal energy $E_{\rm e}^{\rm osc}(T)$ at a fictitious temperature T is calculated as

$$E_{\rm e}^{\rm osc}(T)=\sum_{\mathbf{k}\neq\mathbf{0}}\xi_{\mathbf{k}}f_{\rm B}(\xi_{\mathbf{k}}/T)=\sum_{\mathbf{k}}\xi_{\mathbf{k}}f_{\rm B}(\xi_{\mathbf{k}}/T)-\xi_0 f_{\rm B}(\xi_0/T)=e(T)A-\xi_0 f_{\rm B}(\xi_0/T)\,, \tag{5.18}$$

where

$$e(T)=\int\frac{{\rm d}^2\mathbf{k}}{(2\pi)^2}\frac{\xi_{\mathbf{k}}}{{\rm e}^{\xi_{\mathbf{k}}/T}-1}=\frac{S_2}{(2\pi)^2}\int_0^\infty k{\rm d}k\frac{c\sqrt{k\ell}}{{\rm e}^{c\sqrt{k\ell}/T}-1}=\frac{T^5}{\pi(c\sqrt{\ell})^4}\int_0^\infty{\rm d}x\frac{x^4}{{\rm e}^x-1}, \tag{5.19}$$

where $S_2=2\pi$ is the circumference of a unit circle and we introduce a new variable x by $\sqrt{k}=Tx/c\sqrt{\ell}$. Since $\Gamma(s){\rm Li}_s(z)=\int_0^\infty{\rm d}x\frac{x^{s-1}}{{\rm e}^x/z-1}$, where $\Gamma(x)$ and ${\rm Li}_s(z)$ are the Gamma function and the Polylogarithm, respectively, we find

$$e(T)=\frac{\Gamma(5)\zeta(5)T^5}{\pi(c\sqrt{\ell})^4}, \tag{5.20}$$

where $\zeta(s)={\rm Li}_s(1)$ is the Riemann zeta function. By assuming $\xi_{\mathbf{k}}\ll 1$, we find

$$\xi_{\mathbf{k}}f_{\rm B}(\xi_{\mathbf{k}}/T)=\frac{\xi_{\mathbf{k}}}{\xi_{\mathbf{k}}/T+(\xi_{\mathbf{k}}/T)^2/2+\cdots}. \tag{5.21}$$

Since $\xi_{\mathbf{k}}=0$ for $\mathbf{k}=0$, we find $\xi_0 f_{\rm B}(\xi_0/T)=T$ for the second term of Eq. (5.18). The internal energy is given as

$$E_{\rm e}^{\rm osc}(T)=\frac{\Gamma(5)\zeta(5)AT^5}{\pi(c\sqrt{\ell})^4}-T. \tag{5.22}$$

The EE is obtained by

$$S_{\rm e}^{\rm osc}=\int_0^1\frac{{\rm d}T}{T}\left(\frac{\partial E_{\rm e}^{\rm osc}}{\partial T}\right)_V. \tag{5.23}$$

From the second term of Eq. (5.22), the EE for the oscillator part diverges. Since the approximation of changing the $\mathbf{k}$ sum into integration in Eq. (5.19) may be invalidated at low T, where the discrete nature of $\mathbf{k}$ becomes important, we can interpret the above divergence as a consequence of using such an invalid expression at low T. Above a certain temperature we can still use an integral over T for the thermal entropy $S_{\rm e}^{\rm osc}(T)$ and we find a contribution $-\ln T$. Since the entire energy spectrum is proportional to $c\sqrt{\ell/L}$, this contribution should appear in the form $-\ln(T\sqrt{L}/c\sqrt{\ell})$.

This logarithmic term is also obtained in a different way. The EE $S_{\rm e}^{\rm osc}$ is expressed as

$$S_{\rm e}^{\rm osc}=\sum_{\mathbf{k}\neq\mathbf{0}}\left[\frac{\xi_{\mathbf{k}}}{{\rm e}^{\xi_{\mathbf{k}}}-1}-\ln\left(1-{\rm e}^{-\xi_{\mathbf{k}}}\right)\right], \tag{5.24}$$

by using a discrete sum. We find that the summand of Eq. (5.24) is the entropy of a harmonic oscillator with the energy-level spacing $\xi_{\mathbf{k}}$ for $T = 1$. For the wave vector $\mathbf{k} = (k_1, k_2)$, we require that each element k_i run over $k_i = 2\pi n_i/L$ with $n_i \in \{-\Lambda, -\Lambda + 1, \ldots, \Lambda - 1\}$. Here, we introduce an ultraviolet cutoff by Λ which is proportional to L, so that Eq. (5.24) is a finite sum. The EE in Eq. (5.24) can be rewritten as

$$S_{\mathrm{e}}^{\mathrm{osc}} = \sum_{\mathbf{k}\neq\mathbf{0}} \left[\frac{\xi_{\mathbf{k}}}{\mathrm{e}^{\xi_{\mathbf{k}}} - 1} - \ln \frac{1 - \mathrm{e}^{-\xi_{\mathbf{k}}}}{\xi_{\mathbf{k}}} \right] - \sum_{\mathbf{k}\neq\mathbf{0}} \ln \xi_{\mathbf{k}}. \tag{5.25}$$

We find that the summand in the first sum converges in the limit $\mathbf{k} \to \mathbf{0}$. From the Euler-Maclaurin formula at the order of the trapezoid formula, the first sum of Eq. (5.25) is rewritten as

$$A \int_{-\lambda}^{\lambda} \frac{\mathrm{d}^2\mathbf{k}}{(2\pi)^2} \left[\frac{\xi_{\mathbf{k}}}{\mathrm{e}^{\xi_{\mathbf{k}}} - 1} - \ln \frac{1 - \mathrm{e}^{-\xi_{\mathbf{k}}}}{\xi_{\mathbf{k}}} \right] - 1, \tag{5.26}$$

where $\lambda := 2\pi\Lambda/L$. In the second sum of Eq. (5.25), the summand diverges for $\mathbf{k} \to \mathbf{0}$. This part is rewritten as

$$-\sum_{\mathbf{k}\neq\mathbf{0}} \ln \xi_{\mathbf{k}} = -\left[\left(\frac{\lambda L}{\pi} \right)^2 - 1 \right] \ln c\sqrt{\ell} - \frac{1}{4} \sum_{\mathbf{k}\neq\mathbf{0}} \ln \mathbf{k}^2. \tag{5.27}$$

We focus on the second term $\sum_{\mathbf{k}\neq\mathbf{0}} \ln \mathbf{k}^2$. By introducing $\delta = 2\pi/L$ and applying the Euler-Maclaurin formula (see Ref. [74] for a related calculation), we obtain

$$\begin{aligned}
&\sum_{\mathbf{k}\neq\mathbf{0}} \ln(\mathbf{k}^2) = \sum_{k_2\neq 0} \sum_{k_1} \ln(k_1^2 + k_2^2) + \sum_{k_1\neq 0} \ln k_1^2 \\
&= \frac{L}{2\pi} \sum_{k_2\neq 0} \int_{-\lambda}^{\lambda} \mathrm{d}k_1 \ \ln(k_1^2 + k_2^2) + \frac{L}{\pi} \int_{\delta}^{\lambda} \mathrm{d}k_1 \ \ln k_1^2 + \ln \delta^2 \\
&= \frac{L}{2\pi} \sum_{k_2\neq 0} \left[2\lambda \ln(\lambda^2 + k_2^2) + 4|k_2| \arctan \frac{\lambda}{|k_2|} - 4\lambda \right] + \frac{2L}{\pi} (\lambda \ln \lambda - \lambda - \delta \ln \delta + \delta) + \ln \delta^2 \\
&= \frac{L^2}{(2\pi)^2} \int_{-\lambda}^{\lambda} \mathrm{d}k_2 \left[2\lambda \ln(\lambda^2 + k_2^2) + 4|k_2| \arctan \frac{\lambda}{|k_2|} - 4\lambda \right] - 2 \ln \delta + 4.
\end{aligned} \tag{5.28}$$

By combining these results, we obtain

$$S_{\mathrm{e}} = \frac{\sigma A}{c^4 \ell^2} - \frac{1}{2} \ln \frac{\sqrt{A}}{2\pi c^2 \ell} + O(1) = \frac{2\pi\sigma N_{\mathrm{v}}}{c^4} - \frac{1}{4} \ln \frac{N_{\mathrm{v}}}{2\pi c^4} + O(1). \tag{5.29}$$

The first term gives the leading contribution proportional to the area $A = L^2$, where σ is a non-universal coefficient depending on the choice of the high-momentum cutoff. Besides, a subleading logarithimic term with the universal coefficient $-1/4$ appears when the EE is written as a function of N_{v} which is proportional to the area A. This term is obtained by carefully examining small-k contributions, and thus it originates from the Nambu-Goldstone modes. In the thermodynamic limit, the intercomponent EE per flux is given as

$$\lim_{N_{\mathrm{v}}\to\infty} \frac{S_{\mathrm{e}}}{N_{\mathrm{v}}} = \frac{2\pi\sigma}{c^4} = \frac{\pi\sigma \bar{g}_{\pm} D}{128 \bar{g}_{\mp} C}. \tag{5.30}$$

From the factor $\bar{g}_{\pm}/\bar{g}_{\mp}$ in Eq. (5.30), we find that the intercomponent EE is larger for the case of parallel (antiparallel) fields if the intercomponent interaction is repulsive (attractive). We note that this behavior of the EE for a particular interaction ratio $g_{\uparrow\downarrow}/g$ originates from the equation of motion in Eq. (3.37) from which the rescaling relations originate. This behavior qualitatively agrees with numerical results in the quantum Hall regime [23, 24] and the Bogoliubov theory as shown in the following. From Eq. (5.30), we find a large intercomponent EE when the elastic constant C is small and D is large. Since the energy difference between linear and quadratic dispersion relations becomes larger as $g_{\uparrow\downarrow}/g$ gets closer to -1, the constant C becomes smaller and D becomes bigger (Fig. 4.5). Therefore, the EE is determined by the excitation spectra. Furthermore, the ES becomes smaller from Eq. (5.11), so that two components are highly entangled in the excited states. We find that the excited states contribute to the increase of the intercomponent EE. For example, while the two same quadratic dispersion relations appear and the intercomponent EE is zero in the case of $g_{\uparrow\downarrow}/g = 0$, where two vortex lattices are independent, when an intercomponent interaction which correlates two components is turned on, the linear and quadratic dispersion relations appear and the intercomponent EE becomes nonzero. A pair of linear and quadratic dispersion relations indicates the intercomponent entanglement in the excited states, which determines the EE of the ground state.

5.3 Bogoliubov theory

In this section, we numerically obtain the EE and ES from the Bogoliubov theory. In Sec. 5.3.1, we describe the formulation to obtain the intercomponent EE and ES in the binary system. In Sec. 5.3.2, we present the numerical results and compare them with the results of the effective-field theory. Then, we discuss the restriction of the ground state due to the intercomponent EE and the excited states which contribute to the intercomponent entanglement by the ES. We also discuss the long-range interaction in the entanglement Hamiltonian which may emerge in the subsystem and the logarithmic contribution to the EE, which is related to the Nambu-Goldstone modes.

5.3.1 Entanglement in binary BECs

For the reduced density matrix $\rho_{\uparrow}$ for the spin-$\uparrow$ component, we introduce the following Gaussian ansatz [29, 71–73]:

$$\rho_{\uparrow} = \frac{1}{Z_{\mathrm{e}}} \mathrm{e}^{-H_{\mathrm{e}}}, \quad H_{\mathrm{e}} = \frac{1}{2} \sum_{\mathbf{k} \neq \mathbf{0}} \left(\tilde{b}^{\dagger}_{\mathbf{k},\uparrow}, \tilde{b}_{-\mathbf{k},\uparrow} \right) M_{\mathrm{e}}(\mathbf{k}) \begin{pmatrix} \tilde{b}_{\mathbf{k},\uparrow} \\ \tilde{b}^{\dagger}_{-\mathbf{k},\uparrow} \end{pmatrix}, \quad Z_{\mathrm{e}} = \mathrm{Tr}\ \mathrm{e}^{-H_{\mathrm{e}}}, \tag{5.31}$$

with

$$M_{\mathrm{e}}(\mathbf{k}) = \begin{pmatrix} h_{\mathbf{k}} & -\lambda_{\mathbf{k}} \\ -\lambda^{*}_{-\mathbf{k}} & h_{-\mathbf{k}} \end{pmatrix}, \ \lambda_{\mathbf{k}} = \lambda_{-\mathbf{k}}. \tag{5.32}$$

By performing a Bogoliubov transformation

$$\begin{pmatrix} \tilde{b}_{\mathbf{k}\uparrow} \\ \tilde{b}^{\dagger}_{-\mathbf{k},\uparrow} \end{pmatrix} = W_{\mathrm{e}}(\mathbf{k}) \begin{pmatrix} \eta_{\mathbf{k}} \\ \eta^{\dagger}_{-\mathbf{k}} \end{pmatrix}, \quad W_{\mathrm{e}}(\mathbf{k}) = \begin{pmatrix} \cosh\theta_{\mathbf{k}} & \mathrm{e}^{-\mathrm{i}\phi_{\mathbf{k}}} \sinh\theta_{\mathbf{k}} \\ \mathrm{e}^{\mathrm{i}\phi_{\mathbf{k}}} \sinh\theta_{\mathbf{k}} & \cosh\theta_{\mathbf{k}} \end{pmatrix}, \tag{5.33}$$

with

$$\cosh 2\theta_{\mathbf{k}} = \frac{h_{\mathbf{k}} + h_{-\mathbf{k}}}{2\tilde{h}_{\mathbf{k}}}, \quad \mathrm{e}^{-i\phi_{\mathbf{k}}} \sinh 2\theta_{\mathbf{k}} = \frac{\lambda_{\mathbf{k}}}{\tilde{h}_{\mathbf{k}}}, \quad \tilde{h}_{\mathbf{k}} = \sqrt{\frac{1}{4}\left(h_{\mathbf{k}} + h_{-\mathbf{k}}\right)^2 - |\lambda_{\mathbf{k}}|^2}, \tag{5.34}$$

the entanglement Hamiltonian H_{e} in Eq. (5.31) is diagonalized as

$$H_{\mathrm{e}} = \frac{1}{2}\sum_{\mathbf{k}\neq\mathbf{0}} \left(\xi_{\mathbf{k}}\eta_{\mathbf{k}}^\dagger\eta_{\mathbf{k}} + \xi_{-\mathbf{k}}\eta_{-\mathbf{k}}\eta_{-\mathbf{k}}^\dagger\right) = \sum_{\mathbf{k}\neq\mathbf{0}} \xi_{\mathbf{k}}\left(\eta_{\mathbf{k}}^\dagger\eta_{\mathbf{k}} + \frac{1}{2}\right), \tag{5.35}$$

where

$$\xi_{\mathbf{k}} = \tilde{h}_{\mathbf{k}} + \frac{h_{\mathbf{k}} - h_{-\mathbf{k}}}{2}, \tag{5.36}$$

is the single-particle ES.

Using the relation (5.33) and the Bose distribution function $f_{\mathrm{B}}(\xi_{\mathbf{k}})$, which satisfies

$$\mathrm{Tr}\left(\eta_{\mathbf{k}}^\dagger\eta_{\mathbf{k}}\rho_\uparrow\right) = \frac{1}{\mathrm{e}^{\xi_{\mathbf{k}}} - 1} \equiv f_{\mathrm{B}}(\xi_{\mathbf{k}}), \quad \mathrm{Tr}\left(\eta_{-\mathbf{k}}\eta_{-\mathbf{k}}^\dagger\rho_\uparrow\right) = 1 + f_{\mathrm{B}}(\xi_{-\mathbf{k}}) = -f_{\mathrm{B}}(-\xi_{-\mathbf{k}}), \tag{5.37}$$

we find that correlators are given as

$$\mathrm{Tr}\left(\tilde{b}_{\mathbf{k},\uparrow}^\dagger\tilde{b}_{\mathbf{k},\uparrow}\rho_\uparrow\right) = f_{\mathrm{B}}(\xi_{\mathbf{k}})\cosh^2\theta_{\mathbf{k}} - f_{\mathrm{B}}(-\xi_{-\mathbf{k}})\sinh^2\theta_{\mathbf{k}}, \tag{5.38a}$$

$$\mathrm{Tr}\left(\tilde{b}_{-\mathbf{k},\uparrow}\tilde{b}_{-\mathbf{k},\uparrow}^\dagger\rho_\uparrow\right) = -f_{\mathrm{B}}(-\xi_{-\mathbf{k}})\cosh^2\theta_{\mathbf{k}} + f_{\mathrm{B}}(\xi_{\mathbf{k}})\sinh^2\theta_{\mathbf{k}}, \tag{5.38b}$$

$$\begin{aligned} 2\mathrm{Tr}\left(\tilde{b}_{-\mathbf{k},\uparrow}\tilde{b}_{\mathbf{k},\uparrow}\rho_\uparrow\right) &= 2\left[f_{\mathrm{B}}(\xi_{\mathbf{k}}) - f_{\mathrm{B}}(-\xi_{-\mathbf{k}})\right]\mathrm{e}^{-i\phi_{\mathbf{k}}}\cosh\theta_{\mathbf{k}}\sinh\theta_{\mathbf{k}} \\ &= \left[f_{\mathrm{B}}(\xi_{\mathbf{k}}) - f_{\mathrm{B}}(-\xi_{-\mathbf{k}})\right]\mathrm{e}^{-i\phi_{\mathbf{k}}}\sinh\left(2\theta_{\mathbf{k}}\right). \end{aligned} \tag{5.38c}$$

We require that these are equal to the correlators with respect to the Bogoliubov ground state in Eq. (4.25). We express $f_{\mathrm{B}}(\xi_{\mathbf{k}})$ in terms of the correlators (4.25). By taking the sum and the difference of Eqs. (5.38a) and (5.38b), we respectively have

$$\langle\tilde{b}_{\mathbf{k}\uparrow}^\dagger\tilde{b}_{\mathbf{k}\uparrow}\rangle + \langle\tilde{b}_{-\mathbf{k},\uparrow}\tilde{b}_{-\mathbf{k},\uparrow}^\dagger\rangle = \left[f_{\mathrm{B}}(\xi_{\mathbf{k}}) - f_{\mathrm{B}}(-\xi_{-\mathbf{k}})\right]\cosh\left(2\theta_{\mathbf{k}}\right), \tag{5.39a}$$

$$\langle\tilde{b}_{\mathbf{k}\uparrow}^\dagger\tilde{b}_{\mathbf{k}\uparrow}\rangle - \langle\tilde{b}_{-\mathbf{k},\uparrow}\tilde{b}_{-\mathbf{k},\uparrow}^\dagger\rangle = f_{\mathrm{B}}(\xi_{\mathbf{k}}) + f_{\mathrm{B}}(-\xi_{-\mathbf{k}}), \tag{5.39b}$$

where we take the shorthand notation $\langle\cdot\rangle := \langle 0|\cdot|0\rangle$. Next, using Eqs. (5.38c) and (5.39a), we find

$$f_{\mathrm{B}}(\xi_{\mathbf{k}}) - f_{\mathrm{B}}(-\xi_{-\mathbf{k}}) = \sqrt{\left(\langle\tilde{b}_{\mathbf{k}\uparrow}^\dagger\tilde{b}_{\mathbf{k}\uparrow}\rangle + \langle\tilde{b}_{-\mathbf{k},\uparrow}\tilde{b}_{-\mathbf{k},\uparrow}^\dagger\rangle\right)^2 - 4\left|\langle\tilde{b}_{-\mathbf{k},\uparrow}\tilde{b}_{\mathbf{k}\uparrow}\rangle\right|^2}. \tag{5.40}$$

Finally, by using Eqs. (5.39b) and (5.40), we obtain

$$f_{\mathrm{B}}(\xi_{\mathbf{k}}) = \frac{1}{2}\left(\langle\tilde{b}_{\mathbf{k}\uparrow}^\dagger\tilde{b}_{\mathbf{k}\uparrow}\rangle - \langle\tilde{b}_{-\mathbf{k},\uparrow}\tilde{b}_{-\mathbf{k},\uparrow}^\dagger\rangle\right) + \sqrt{\frac{1}{4}\left(\langle\tilde{b}_{\mathbf{k}\uparrow}^\dagger\tilde{b}_{\mathbf{k}\uparrow}\rangle + \langle\tilde{b}_{-\mathbf{k},\uparrow}\tilde{b}_{-\mathbf{k},\uparrow}^\dagger\rangle\right)^2 - \left|\langle\tilde{b}_{-\mathbf{k},\uparrow}\tilde{b}_{\mathbf{k}\uparrow}\rangle\right|^2}. \tag{5.41}$$

The single-particle ES is numerically obtained from Eq. (5.41) by calculating

$$\xi_{\mathbf{k}} = \ln\left[1 + f_B(\xi_{\mathbf{k}})^{-1}\right]. \tag{5.42}$$

To obtain the intercomponent EE, we calculate

$$S_{\mathrm{e}} = \sum_{\mathbf{k}\neq\mathbf{0}} \{-f_{\mathrm{B}}(\xi_{\mathbf{k}}) \ln f_{\mathrm{B}}(\xi_{\mathbf{k}}) + [1 + f_{\mathrm{B}}(\xi_{\mathbf{k}})] \ln [1 + f_{\mathrm{B}}(\xi_{\mathbf{k}})]\} , \tag{5.43}$$

by using the obtained $\xi_{\mathbf{k}}$. As discussed in the previous section using the effective-field theory, S_{e} is expected to show a volume-law behavior followed by a subleading logarithmic term. The EE per quantum flux in the thermodynamic limit is expressed in the integral form

$$\lim_{N_{\mathrm{v}}\to\infty} \frac{S_{\mathrm{e}}}{N_{\mathrm{v}}} = \frac{1}{2\pi} \int_{\mathrm{BZ}} \mathrm{d}^2\mathbf{k}\ell^2 \{-f_{\mathrm{B}}(\xi_{\mathbf{k}}) \ln f_{\mathrm{B}}(\xi_{\mathbf{k}}) + [1 + f_{\mathrm{B}}(\xi_{\mathbf{k}})] \ln [1 + f_{\mathrm{B}}(\xi_{\mathbf{k}})]\} . \tag{5.44}$$

We note that the correlators (4.25) are independent of ν once the lattice structure is fixed. Therefore, the EE per quantum flux in Eq. (5.44) is also independent of ν in a similar manner. In the next section, we study the EE per quantum flux by assuming the structure in the mean-field ground state. When the lattice structure changes by the quantum correction, the EE per quantum flux will also change accordingly.

5.3.2 Numerical results

Based on the formulation in Sec. 5.3.1, we present numerical results on the intercomponent ES and EE in the Bogoliubov ground state. The left panels of Fig. 5.2 display the single-particle ES $\xi_{\mathbf{k}}$ for all the five lattice structures in parallel and antiparallel fields. The value of $g_{\uparrow\downarrow}/g$ for each lattice is similar to Fig. 4.2. Around the Γ point, we find the square-root dispersion relation for all the five lattice structures. At a low-energy regime, it can be well fitted by

$$\xi_{\mathbf{k}} = c(\varphi)\sqrt{k\ell}, \tag{5.45}$$

for $\mathbf{k} = k(\cos\varphi, \sin\varphi)$, where $c(\varphi)$ is a dimensionless function that expresses the anisotropy. The right panels of Fig. 5.2 show the function $c(\varphi)$ determined from the data of $\xi_{\mathbf{k}}$ along a circular path around the Γ point. By rescaling the $c(\varphi)$ for parallel and antiparallel fields according to the rescaling relation (5.14), we find that curves for parallel and antiparallel fields coincide perfectly up to numerical precision. The rescaled values of $c(\varphi)$'s are depicted by the black curves.

In the left panels of Fig. 5.2, we also find that $\xi_{\mathbf{k}}$ diverges at some high-symmetry points or along lines in the Brillouin zone. For the square (d) and rectangular (e) lattices in antiparallel fields, in particular, divergence occurs along the edges of the Brillouin zone, so that $\xi_{\mathbf{k}}$ is not shown along the paths $R \to M_1$ and $R \to M_2$. It has been found [31] that at the M_1 and M_2 points for rhombic, square and rectangular lattices in both parallel and antiparallel fields, the Bogoliubov Hamiltonian matrix $\mathcal{M}(\mathbf{k})$ has a structure in which the spin-$\uparrow$ and $\downarrow$ components are decoupled (see Appendix D in Ref. [31]). Since the two components are decoupled at these points, the ES diverges.

In Fig. 5.3 (a), the intercomponent EEs per vortex as a function of the interaction ratio $g_{\uparrow\downarrow}/g$ for parallel (blue) and antiparallel (red) fields are presented. From Fig. 5.3 (a), we find that the EE tends to be larger for repulsive (attractive) $g_{\uparrow\downarrow}$ in the case of parallel (antiparallel) fields. In exact-diagonalization analyses for $\nu = \mathcal{O}(1)$, the product state of two quantum Hall states has been shown to be robust for intercomponent attraction

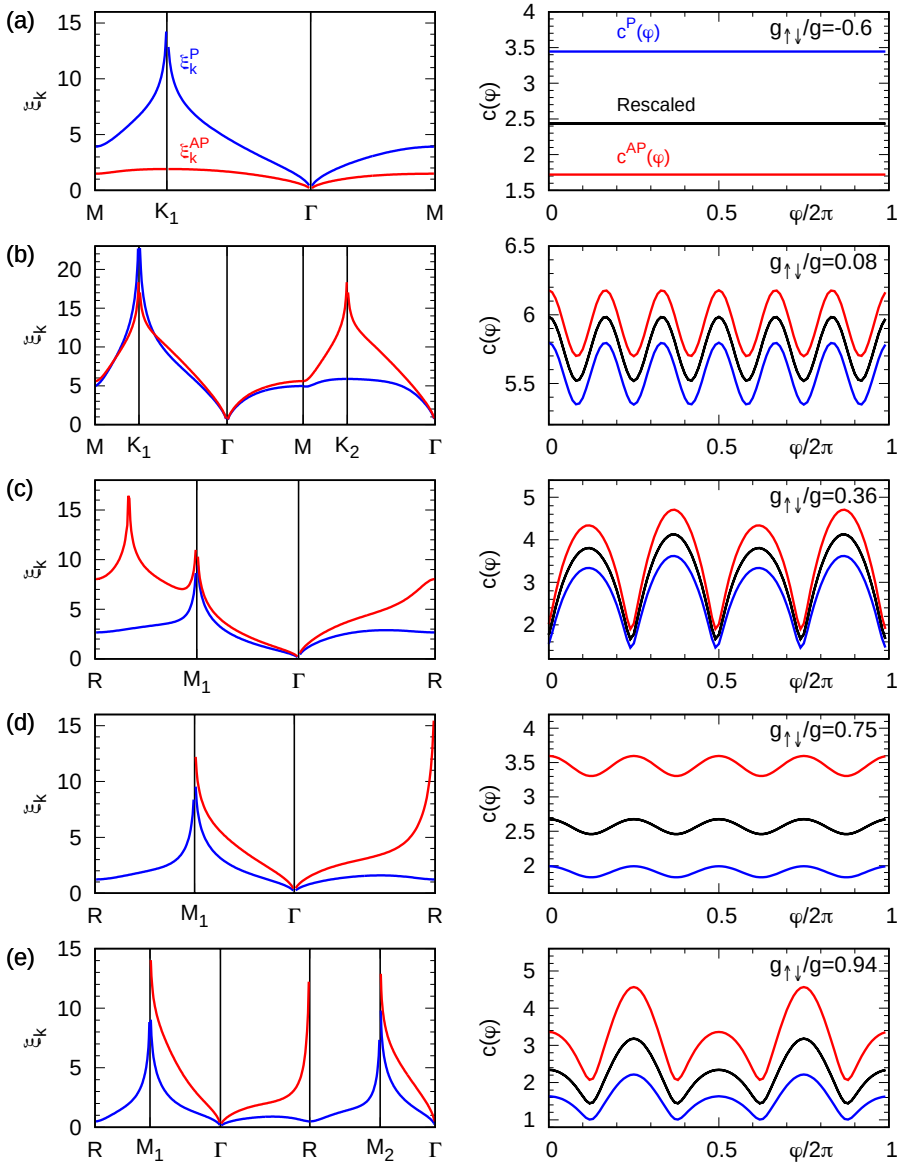

Figure 5.2: Left panels: single-particle ESs $\xi_{\mathbf{k}}^{\mathrm{P/AP}}$ in parallel (P; blue) and antiparallel (AP; red) fields for the same cases as in Fig. 4.3 (a)-(e). Calculations are done along the paths indicated by dotted arrows shown in Fig. 4.1. The spectra $\xi_{\mathbf{k}}$ show divergences at some high-symmetry points or along lines in the first Brillouin zone. In (d) and (e), in particular, the divergence occurs along the edges of the Brillouin zone for antiparallel fields and thus the value of $\xi_{\mathbf{k}}$ is not shown there. Right panels: dimensionless functions $c^{\mathrm{P/AP}}(\varphi)$ that express the anisotropy of the ES around the Γ point as in Eq. (5.45). These are calculated from $\xi_{\mathbf{k}}^{\mathrm{P/AP}}$ along a circular path $\mathbf{k} = k(\cos\varphi, \sin\varphi)$ with $k = 0.001a/\ell^2$ and $\varphi \in [0, 2\pi)$. With proper rescaling, the curves for parallel and antiparallel fields coincide perfectly up to numerical precision, confirming the rescaling relation in Eq. (5.14). Namely, $(\bar{g}_+/\bar{g}_-)^{1/4} c^{\mathrm{P}}(\varphi)$ and $(\bar{g}_-/\bar{g}_+)^{1/4} c^{\mathrm{AP}}(\varphi)$ share the same curves as shown in black.

(repulsion) and the spin-singlet state is robust for intercomponent repulsion (attraction) in the case of parallel (antiparallel) fields [23,24]. Since we expect that the intercomponent EE for the product state vanishes and the EE for the spin-singlet states is large, the interesting behavior of the EE in Fig. 5.3 (a) for the vortex-lattice regime is qualitatively consistent with the results for the quantum Hall regime with $\nu = \mathcal{O}(1)$.

In Fig. 5.3 (b), we find that the leading term of the EE is proportional to the number of fluxes and its subleading term scales logarithmically for square lattices. As expected from the effective-field theory, we find that the coefficient of the subleading term (α_2 in Fig. 5.3) is almost equal to 1/4. In Fig. 5.3 (c), we confirm a logarithmical decrease of its subleading term by subtracting the leading term from the EE. We expect that the deviation from 1/4 can be understood as being due to the correction to the Euler-Maclaurin formula.

When we obtain the ground state where the order of the filling factor ν is 10, we consider the ground-state energy by taking the quantum correction into account by using the excitation spectra. Therefore the behavior of the intercomponent EE calculated by the excitation spectra whose ground state is given from the mean-field theory will be reflected to the ground state corrected by the quantum fluctuation although the EE vanishes in the mean-field theory. Since the intercomponent EE will restrict the ground state for each interaction ratio $g_{\uparrow\downarrow}/g$ by taking the quantum correction into account, it will partially clarify the feature of the ground-state phase diagram. For example, it will predict the regime where the ground state similar to the product state appears. Furthermore, the qualitative consistency between the behavior of the EE for the vortex-lattice regime and that for the quantum Hall regime strongly supports an expectation that the intercomponent EE expresses the feature of the ground-state phase diagram for the intermediate regime between the mean-field regime and the quantum Hall regime, which has not been investigated without any approximation.

The EE is also obtained as the thermal entropy of the entanglement Hamiltonian at temperature $T = 1$ as in Eq. (5.23). The excited modes with the small ES largely contribute to the EE. Actually, the ES for antiparallel (parallel) fields is smaller than the other with an attractive (repulsive) interaction (Fig. 5.2) and this feature of the ES is consistent with the interesting behavior of the intercomponent EE. In particular, the ESs far from the Γ points in the cases of parallel and antiparallel fields are significantly different, so that the excited modes in this regime contribute to the behavior of the EE. Since the decoupling of two components at some high symmetry points (Fig. 5.2) appears due to the fractional translation symmetry [31], we can relate the different fractional translation symmetries for parallel and antiparallel fields with the behavior of the EE. We also find the emergence of the long-range interaction between densities in the entanglement Hamiltonian from the effective-field theory. In binary BECs with a Rabi coupling, a long-range interaction between currents emerges and both a long-range interaction between densities and that between currents appear when a Rabi coupling is turned off [30]. Such a difference appears since the correlation functions in the long-wavelength limit are different among two cases in binary BECs and the case of the vortex lattices, which are related to the leading order of the dispersion relations of the whole system. For instance, the correlation functions for a phase and a density for binary BECs with the Rabi coupling are proportional to k^{-1} and a constant, respectively, in the long-wavelength limit due to a pair of the linear and gapped dispersion relations. Meanwhile, the correlation

functions for a phase and a density for the vortex lattices are proportional to k^{-2} and k^{-1}, respectively, from Eq. (3.72), due to a pair of the linear and quadratic dispersion relations, although both two cases have the ES with a square-root dispersion relation. Furthermore, the long-range interaction is expected to emerge in the subsystem at absolute zero and we expect the creation of a highly controllable system with a long-range interaction by using the ultracold atoms.

Finally, we discuss the subleading term of the EE. In the case of binary BECs, the logarithmic contribution of the intercomponent EE with respect to the system size originates from both the Nambu-Goldstone modes and the zero mode due to the continuous symmetry breaking [30]. From the effective-field theory, we find that the term also originates from the Nambu-Goldstone modes, so that the term is also related to the continuous symmetry breaking for the vortex lattices in the binary system. In the case of the d-dimensional nonlinear sigma model, the coefficient of the logarithmic contribution is determined by the number of symmetries broken in the system [26]. Although, the continuous symmetry which is spontaneously broken in the present system is hard to identify as we discussed in Sec. 4.2.1, we infer that its coefficient is related to the type and the number of the symmetry which is spontaneously broken. Our case is also intriguing since the excited spectra have a pair of quadratic and linear dispersion relations, so that the spectra contain both type I and type II while the previous studies discussed only the type I case.

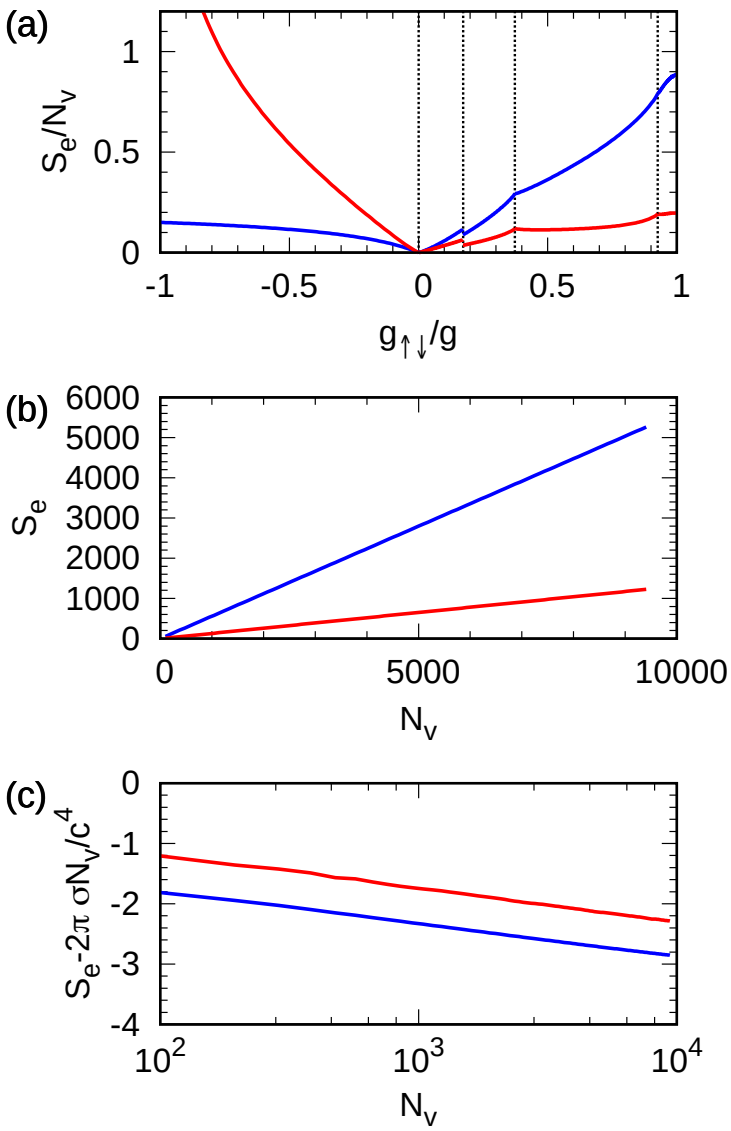

Figure 5.3: (a) Intercomponent EE per flux, S_e/N_v, as a function of $g_{\uparrow\downarrow}/g$ for parallel (blue) and antiparallel (red) fields for $N_v = 97^2$. Vertical dashed lines indicate the transition points. In consistency with the field-theoretical result in Sec. 5.2.2 [see, in particular, Eq. (5.29) therein], S_e/N_v is found to be larger for parallel (antiparallel) fields when the intercomponent interaction $g_{\uparrow\downarrow}$ is repulsive (attractive). (b) Intercomponent EE S_e versus N_v for $g_{\uparrow\downarrow}/g = 0.75$. A fit to the form $S_e = \alpha_1 N_v - \alpha_2 \ln N_v + \alpha_3$ (solid line) gives $(\alpha_1, \alpha_2, \alpha_3) = (0.559702, 0.235899, -0.701552)$ for parallel fields and $(\alpha_1, \alpha_2, \alpha_3) = (0.130402, 0.243383, -0.0583632)$ for antiparallel fields. (c) $S_e - \alpha_1 N_v$ versus N_v for $g_{\uparrow\downarrow}/g = 0.75$. The logarithmic contribution of the intercomponent EE and its coefficient can be confirmed.

Chapter 6

Summary and Outlook

In this thesis, we have studied the ground-state, collective modes, and the intercomponent entanglement of vortex lattices in binary BECs.

In Chap. 2, we have reviewed the ground state of binary BECs and the techniques of creating synthetic gauge fields. From the theoretical and experimental studies of binary BECs without synthetic gauge fields, we have discussed that two components are mixed or separated by changing the coupling constants for the intra- and intercomponent interactions. We have discussed the emergence of parallel synthetic magnetic fields in the rotating neutral-charged atomic gases in the mean-field theory. After introducing the LLL approximation, in which the ground-state wave function is expanded in terms of the basis states in the LLL [13], we have presented the ground-state phase diagram of vortex lattices with various configurations under the LLL approximation, whose structures depend on the ratio of the intercomponent interaction to the intracomponent one [17, 18]. Then we have reviewed the creation of antiparallel synthetic magnetic fields by utilizing the interaction between atoms and lasers. We have discussed a synthetic gauge field in a minimal model, which uses the spatial dependence of a coupling between two levels and a phase of a laser. We have reviewed an experiment of an ultracold atomic system in which antiparallel fields are observed [20]. Based on the equivalence of the GP energy functional for parallel and antiparallel fields, we have explained that the phase diagram of vortex lattices for antiparallel fields is the same as that for parallel fields in the GP mean-field regime [23]. Meanwhile, in the quantum Hall regime, where the mean-field theory breaks down due to strong magnetic fields, the ground-state phase diagrams of binary bosonic systems under parallel and antiparallel magnetic fields have been obtained by exact diagonalization [23,24]. These phase diagrams are presented in the plane spanned by the ratio of the coupling constants and the filling factor. Although the phase diagrams are significantly different between the two cases, we have pointed out that the ground states for parallel fields with a replusive (attractive) intercomponent interaction are similar to those for antiparallel fields with an attractive (replusive) intercomponent interaction.

In Chap. 3, we have developed an effective-field theory of vortex lattices in binary BECs. After reviewing the vortex lattice for a scalar BEC in the mean-field theory, we have discussed the renormalization of the coupling constant, which depends on a fine structure of each vortex. In deriving the effective-field theory of vortex lattices for binary BECs, we have identified a missing term in the elastic energy from a symmetry consideration of each vortex lattice, which has drastically changed the quadratic dispersion relation

for interlaced triangular lattices. We have also considered renormalization of the coupling constants under the LLL approximation by generalizing the renormalization procedure for the scalar case to a binary system. By diagonalizing the effective Hamiltonian, we have analytically obtained the dispersion relations for parallel and antiparallel fields and the rescaling relations between them. From the rescaling relations, we have clarified that the different excited states for parallel and antiparallel fields are indeed related to each other. The oscillation modes for the quadratic and linear dispersion relations have been related to in- and anti-phase oscillations, respectively, in parallel fields and in the opposite manner in antiparallel fields. We have demonstrated a quasi-long-range order of the system by using the one-particle density matrix. We have found a logarithmic increase of the fraction of depletion with respect to the number of fluxes, which implies vanishing of the condensate fraction in the thermodynamic limit.

In Chap. 4, we have presented the Bogoliubov theory of vortex lattices in binary BECs under the LLL approximation by utilizing the LLL magnetic Bloch state as a complete orthonormal basis of the LLL manifold. By employing the Bogoliubov approximation and diagonalizing the Bogoliubov Hamiltonian, we have obtained the excitation spectra, the density of depletion and the quantum correction to the ground-state energy. We have numerically obtained these values and compared them with their analytic forms obtained by the effective-field theory in the preceding chapter. We have found that the excitation spectra with quadratic and linear dispersion relations appear and that they satisfy the rescaling relations at low energies. We have revealed that the problem in the previous research [31], where the relations hold only for overlapping triangular lattices, can be solved by renormalization of the coupling constants of the interactions. We have also confirmed the consistency of the anisotropy of the energy spectra around the Γ point with the effective-field theory. In particular, the importance of the missing term has been clarified from the energy spectra for interlaced triangular lattices. By using the renormalized coupling constants, we have obtained the elastic constants, whose values are corrected in comparison with the results in Ref. [31], so that we have determined all parameters introduced in the effective-field theory. For all the phases on the basis of the ground-state phase diagram in the mean-field theory, we have obtained the quantum depletion, which for parallel (antiparallel) fields is found to be larger than the other in the case of a repulsive (attractive) intercomponent interaction. We have also demonstrated that it scales logarithmically with respect to the number of quantum fluxes as expected from its analytical expression. From the minimization of the ground-state energy with the quantum correction for the five types of structures of vortex lattices which appear in the mean-field theory, the transition points shift appreciably and the inner angle for rhombic lattices and the aspect ratio for rectangular lattices in terms of the ratio of the coupling constants are altered due to the quantum correction. We have found that the quantum fluctuation changes the ground-state phase diagram appreciably and causes the difference between the phase diagrams for parallel and antiparallel fields. Such a difference is unique to the binary system, since parallel and antiparallel fields do not appear in a scalar BEC. Then we have found that shifts of transition points increase as the quantum fluctuation is enhanced, since shifts of the transition points and the quantum depletion for parallel fields are larger than those for antiparallel fields when an intercomponent interaction is repulsive.

In Chap. 5, we have studied the intercomponent ES and EE for vortex lattices in binary

BECs. First, we have reviewed the ES and EE in condensed-matter systems. We have discussed that the subleading term of the EE of a d-dimensional system with a continuous symmetry breaking scales logarithmically with respect to L^{d-1}, where L is the length scale of the system [25, 26]. The intercomponent ES for two coupled non-chiral TLLs or binary BECs has been found to show a square-root dispersion relation, which is related to the emergence of a long-range interaction in the entanglement Hamiltonian [29, 30]. By means of the effective-field theory, we have analytically obtained the intercomponent ES for vortex lattices, which shows a square-root dispersion relation for both parallel and antiparallel fields. We have also obtained the rescaling relation between ESs for parallel and antiparallel fields. We have shown for overlapping triangular lattices that in relation to the anomalous square-root dispersion relation of the ES, the long-range interaction emerges in the entanglement Hamiltonian. We have also derived the intercomponent EE whose subleading term logarithmically scales with respect to the number of quantum fluxes. Based on the Bogoliubov theory, we have numerically obtained the intercomponent ES and EE for all the phases. We have shown that the ES exhibits a square-root dispersion relation and confirmed the consistency of its anisotropy with the effective-field theory. We have also confirmed the rescaling relation between the ESs for parallel and antiparallel fields. In the quantum Hall regime studied previously [23,24], the product states, in which two components are disentangled, appear for a repulsive (attractive) intercomponent interaction and the spin-singlet quantum Hall states, in which two components are highly entangled, appear for an attractive (repulsive) intercomponent interaction in parallel (antiparallel) fields. We have found that the behavior of the intercomponent EE for vortex lattices in parallel and antiparallel fields are qualitatively consistent with that for the quantum Hall regime, which is described above. We have restricted the ground-state phase diagram with the quantum correction by the EE since both the corrected ground-state energy and the EE are obtained by the excitation spectra, so that the EE reflects the corrected ground states. For example, we can identify the regime where the ground states similar to the product states appear. We presume that this behavior of the EE appears in the wide intermediate range from the mean-field regime to the quantum Hall regime. We have discussed which excited states largely contribute to the EE from the ES and the emergence of the long-range interaction in the entanglement Hamiltonian. We have numerically demonstrated that the subleading term of the EE scales logarithmically with respect to the number of quantum fluxes and its coefficient is close to $1/4$. We have obtained the subleading term from the Nambu-Goldstone modes, so that the continuous symmetry breaking of vortex lattices is related to the EE.

As an outlook, we may discuss the oscillation of the vortex lattices in binary BECs trapped by the potential. It is of interest to compare the theoretical analysis with the experiment for parallel fields. It is also worthwhile to discuss the oscillation modes for antiparallel fields and an experiment to confirm the rescaling relations.

We have explained that various configurations of vortex lattices appear in binary BECs [17] while only a triangular lattice appears in a scalar BEC. In the case of spin-1 BECs, the ground state has been found to show a rich variety of structures of vortex lattices, which depend on the ratio of two interaction parameters of a spin-1 Bose gas, within the mean-field theory under the LLL approximation [75]. In the present thesis, we have obtained the energy spectra, the quantum depletion, and the quantum correction to the ground-state energy. As we have found a pair of linear and quadratic dispersion

relations which are unique to the binary system, we might obtain the interesting excitation spectra of vortex lattices in spin-1 BECs. We can also discuss whether the powers of the dispersion relations change by controlling the two interaction parameters of a spin-1 Bose gas as in the non-rotating spin-1 BECs [6]. Furthermore, we may consider shifts of the transition points due to quantum fluctuations.

We have found the intercomponent ES with a square-root dispersion relation, which is related to the emergence of the long-range interaction in the entanglement Hamiltonian, for vortex lattices in binary BECs; this result is similar to what was found for the binary homogeneous BECs with a Rabi coupling [30]. For vortex lattices in spin-1 BECs, we might obtain an interesting ES which is related to the long-range interaction in the entanglement Hamiltonian. We have also shown that the behavior of the intercomponent EE in vortex lattices is consistent with the ground-state phase diagram of the binary Bose gases in the quantum Hall regime. By calculating the intercomponent EE of the vortex lattices in spin-1 BECs, we might find features related to the ground state of the rapidly rotating spin-1 bosons in the quantum Hall regime [76].

Appendix A

Details of derivations in Chapter 3

A.1 Detailed derivation of Eqs.(3.14), (3.15) and (3.18)

A.1.1 Equation (3.14)

From the cylindrical symmetry of f and $\int_0^{2\pi} \mathrm{d}\phi\ \cos n\phi = \int_0^{2\pi} \mathrm{d}\phi\ \sin n\phi = 2\pi\delta_{n,0}$ $(n \in \mathbb{Z})$, we find

$$
\begin{aligned}
&\sum_j \int_j \mathrm{d}^3\mathbf{r}\ nf^2 \rho\cdot\mathbf{r}_\perp \simeq \sum \int_j \mathrm{d}^3\mathbf{r}\ f^2\left[n(\mathbf{R}_j)+\rho\cdot\nabla_j n(\mathbf{R}_j)\right]\rho\cdot(\mathbf{R}_j+\rho)\\
&=\sum_j \int \mathrm{d}z\ \int_0^\ell \rho\mathrm{d}\rho\ f^2(\rho)\int_0^{2\pi}\mathrm{d}\phi\ \Bigg[n\rho\left(R_{jx}\cos\phi+R_{jy}\sin\phi\right)+n\rho^2\\
&+\rho^3\left(\frac{\partial n}{\partial R_{jx}}\cos\phi+\frac{\partial n}{\partial R_{jy}}\sin\phi\right)+\rho^2\frac{1+\cos 2\phi}{2}\frac{\partial n}{\partial R_{jx}}R_{jx}+\rho^2\frac{1-\cos 2\phi}{2}\frac{\partial n}{\partial R_{jy}}R_{jy}\\
&+\frac{1}{2}\rho^2\sin 2\phi\left(\frac{\partial n}{\partial R_{jx}}R_{jy}+\frac{\partial n}{\partial R_{jy}}R_{jx}\right)\Bigg]\\
&=\sum_j \int \mathrm{d}z\ \int_0^\ell \rho\mathrm{d}\rho\ f^2(\rho)\int_0^{2\pi}\mathrm{d}\phi\ \rho^2[n(\mathbf{R}_j)+\frac{1}{2}\mathbf{R}_j\cdot\nabla_j n(\mathbf{R}_j)]\\
&=\sum_j \frac{1}{2}\nabla_j\cdot[\mathbf{R}_j n(\mathbf{R}_j)]\int \mathrm{d}z\ \int_j \mathrm{d}^2\mathbf{r}\ \rho^2 f^2.
\end{aligned}
\tag{A.1}
$$

By using the fact that the density slowly varies in the cell, we obtain the integral over the system by connecting the integral over each unit cell. Equation (A.1) becomes

$$
\begin{aligned}
&\frac{1}{2}\sum_j \nabla_j\cdot[\mathbf{R}_j n(\mathbf{R}_j)]\int_j \mathrm{d}^3\mathbf{r}\ \left\langle\rho^2\right\rangle \simeq \frac{1}{2}\int \mathrm{d}^3\mathbf{r}\ \nabla\cdot[\mathbf{r}n(\mathbf{r})]\left\langle\rho^2\right\rangle\\
=&\frac{1}{2}\int \mathrm{d}^3\mathbf{r}\ \nabla\cdot[\mathbf{r}n(\mathbf{r})\left\langle\rho^2\right\rangle]-\frac{1}{2}\int \mathrm{d}^3\mathbf{r}\ \mathbf{r}n(\mathbf{r})\cdot\nabla\left\langle\rho^2\right\rangle,
\end{aligned}
\tag{A.2}
$$

where $\langle g\rangle = \int_j \mathrm{d}^3\mathbf{r}\ gf^2 / \int_j \mathrm{d}^3\mathbf{r}$ is the average of an arbitrary function g within the unit cell j.

A.1.2 Equation (3.15)

The term $\hbar\mathbf{\Omega}_v \cdot (\mathbf{R}_j \times \nabla\phi_j)_z$ in the total energy (3.10) is given by

$$
\begin{aligned}
&\sum_j \int_j \mathrm{d}^3\mathbf{r}\; n f^2 \hbar\mathbf{\Omega}_v \cdot (\mathbf{R}_j \times \nabla\phi_j) \\
&\simeq \sum \int_j \mathrm{d}^3\mathbf{r}\; f^2 \left[n(\mathbf{R}_j) + \rho\cdot\nabla_j n(\mathbf{R}_j)\right] f^2 \hbar\Omega_v \left(R_{jx}\frac{\cos\phi}{\rho} - R_{jy}\frac{\sin\phi}{\rho}\right) \\
&= \sum_j \int \mathrm{d}z \int_0^\ell \rho\mathrm{d}\rho\; f^2(\rho) \int_0^{2\pi} \mathrm{d}\phi \left[\frac{n}{\rho}\left(R_{jx}\cos\phi + R_{jy}\sin\phi\right)\right. \\
&\left. + \frac{1+\cos 2\phi}{2}\frac{\partial n}{\partial R_{jx}}R_{jx} + \frac{1-\cos 2\phi}{2}\frac{\partial n}{\partial R_{jy}}R_{jy} + \frac{1}{2}\sin 2\phi\left(\frac{\partial n}{\partial R_{jx}}R_{jy} + \frac{\partial n}{\partial R_{jy}}R_{jx}\right)\right] \qquad \text{(A.3)} \\
&= \sum_j \int \mathrm{d}z \int_0^\ell \rho\mathrm{d}\rho\; \hbar\Omega_v f^2(\rho) \int_0^{2\pi} \mathrm{d}\phi \left[n(\mathbf{R}_j) + \frac{1}{2}\mathbf{R}_j\cdot\nabla_j n(\mathbf{R}_j)\right] \\
&= \sum_j \frac{\hbar\Omega_v}{2}\nabla_j\cdot\left[\mathbf{R}_j n(\mathbf{R}_j)\right] \int \mathrm{d}z \int_j \mathrm{d}^2\mathbf{r}\; f^2 \simeq \frac{\hbar\Omega_v}{2}\int \mathrm{d}^3\mathbf{r}\; \mathbf{r}_\perp\cdot\nabla n \\
&= \frac{\hbar\Omega_v}{2}\left[\int \mathrm{d}^3\mathbf{r}\; \nabla\cdot(\mathbf{r}n) - \int \mathrm{d}^3\mathbf{r}\; (\nabla\cdot\mathbf{r}_\perp)n\right] = -\hbar\Omega_v\int \mathrm{d}^3\mathbf{r}\; n f^2,
\end{aligned}
$$

where we assume that the density slowly varies in the cell and it is zero at large distance.

A.1.3 Equation (3.18)

The second term of Eq. (3.17) is given by

$$
\begin{aligned}
&\sum_j \int_j \mathrm{d}^3\mathbf{r}\; n(f^2-1) r_\perp^2 \\
&\simeq \sum_j \int_j \mathrm{d}^3\mathbf{r}\; \left[n(\mathbf{R}_j) + \rho\left(\frac{\partial n}{\partial R_{jx}}\cos\phi + \frac{\partial n}{\partial R_{jy}}\sin\phi\right)\right](f^2-1) \\
&\qquad\qquad \times\left[R_j^2 + \rho^2 + 2\rho(R_{jx}\cos\phi + R_{jy}\sin\phi)\right] \\
&= \sum_j \int \mathrm{d}z \int_0^\ell \rho\mathrm{d}\rho\; f^2(\rho) \int_0^{2\pi}\mathrm{d}\phi \left[n(R_j^2+\rho^2) + 2n\rho(R_{jx}\cos\phi + R_{jy}\sin\phi)\right. \\
&+ \rho\left(\frac{\partial n}{\partial R_{jx}}\cos\phi + \frac{\partial n}{\partial R_{jy}}\sin\phi\right)(R_j^2+\rho^2) \\
&\left. + 2\rho^2\left\{\frac{1+\cos 2\phi}{2}\frac{\partial n}{\partial R_{jx}}R_{jx} + \frac{1-\cos 2\phi}{2}\frac{\partial n}{\partial R_{jy}}R_{jy} + \frac{1}{2}\sin 2\phi\left(\frac{\partial n}{\partial R_{jx}}R_{jy} + \frac{\partial n}{\partial R_{jy}}R_{jx}\right)\right\}\right] \\
&= \sum_j \int \mathrm{d}z \int_0^\ell \rho\mathrm{d}\rho\; (f^2-1)\int_0^{2\pi}\mathrm{d}\phi \left[n(\mathbf{R}_j)R_j^2 + \rho^2\left(n + \frac{\partial n}{\partial R_{jx}}R_{jx} + \frac{\partial n}{\partial R_{jy}}R_{jy}\right)\right].
\end{aligned}
\qquad \text{(A.4)}
$$

By using $\frac{\partial n}{\partial R_{jx}} R_{jx} + \frac{\partial n}{\partial R_{jy}} R_{jy} = \mathbf{R}_j \cdot [\nabla_j n(\mathbf{R}_j)] - 2n$, the last expression in Eq. (A.4) is rewritten as

$$\begin{aligned}
&\sum_j \int \mathrm{d}z \int_0^\ell \rho \mathrm{d}\rho \, (f^2 - 1) \int_0^{2\pi} \mathrm{d}\phi \, \left[n(\mathbf{R}_j) R_j^2 + \rho^2 (\mathbf{R}_j \cdot [\nabla_j n(\mathbf{R}_j)] - n) \right] \\
&\simeq \int \mathrm{d}^3\mathbf{r} \, (f^2 - 1) n(\mathbf{r}) r_\perp^2 - \sum_j \int_j \mathrm{d}^3\mathbf{r} \, n(\mathbf{r}) (f^2 - 1) \rho^2 + \int \mathrm{d}^3\mathbf{r} \, \nabla \cdot [\mathbf{r}_\perp n] \left(\langle \rho^2 \rangle - \frac{\ell^2}{2} \right).
\end{aligned} \tag{A.5}$$

Since we can replace f^2 by its average due to the slow variation of the density, the first term in Eq. (A.5) vanishes. By integrating the last term by parts, Eq. (A.5) becomes

$$\begin{aligned}
&- \sum_j \int_j \mathrm{d}^3\mathbf{r} \, n(\mathbf{r}) (f^2 - 1) \rho^2 + \int \mathrm{d}^3\mathbf{r} \, \left\{ \nabla \cdot \left[\mathbf{r}_\perp n \left(\langle \rho^2 \rangle - \frac{\ell^2}{2} \right) \right] - \mathbf{r}_\perp n \cdot \nabla \left(\langle \rho^2 \rangle - \frac{\ell^2}{2} \right) \right\} \\
&= - \sum_j \int_j \mathrm{d}^3\mathbf{r} \, n (f^2 - 1) \rho^2,
\end{aligned} \tag{A.6}$$

since the surface term vanishes as the density is zero at large distance and $\langle \rho^2 \rangle$ does not depend on the position.

A.2 Detailed derivation of elastic constants

In Chap. 3, we introduce the elastic energy density $\mathcal{E}_{\mathrm{el}}(\mathbf{u}_\alpha, \partial_i \mathbf{u}_\alpha)$ of the vortex lattices in binary BECs. We discuss how we can constrain its form as in Eqs. (3.41), (3.43) and (3.44) due to the symmetry of vortex lattices.

The most general form of the elastic energy density is given by the quadratic forms of $\mathbf{w} := (w_1, w_2)^{\mathrm{t}}$ and $\mathbf{u}_-$, such as

$$\mathcal{E}_{\mathrm{el}}^{(+)} = \frac{g n^2}{2} \mathbf{w}^{\mathrm{t}} C \mathbf{w}, \quad \mathcal{E}_{\mathrm{el}}^{(-)} = \frac{g n^2}{2\ell^2} \mathbf{u}_-^{\mathrm{t}} D \mathbf{u}_-, \quad \mathcal{E}_{\mathrm{el}}^{(+-)} = \frac{g n^2}{\ell} \mathbf{w}^{\mathrm{t}} F \mathbf{u}_-, \tag{A.7}$$

where C, D, and F are real 2×2 matrices, whose elements are written as C_{ij}, D_{ij} and F_{ij} $(i, j = 1, 2)$, respectively, and we can assume C and D to be symmetric. We assume that the vortex lattices are symmetric under the coordinate transformation given by

$$\begin{pmatrix} x \\ y \end{pmatrix} \to \begin{pmatrix} x' \\ y' \end{pmatrix} = \Lambda \begin{pmatrix} x \\ y \end{pmatrix}, \tag{A.8}$$

where Λ is a real 2×2 matrix. Under this transformation, we find that $\mathbf{w}$ is transformed by a different matrix $\tilde{\Lambda}$ in general due to the spatial derivative, while $\mathbf{u}_-$ is transformed by the same matrix Λ. To obtain the elastic energy which is invariant under this transformation, the matrices have to satisfy

$$\tilde{\Lambda}^{\mathrm{t}} C \tilde{\Lambda} = C, \quad \Lambda^{\mathrm{t}} D \Lambda = D, \quad \tilde{\Lambda}^{\mathrm{t}} F \Lambda = F. \tag{A.9}$$

To discuss the symmetry of vortex lattices, we consider the following transformations given as

$$\text{Rotation through the angle } \phi: \ \Lambda = R(\phi) = \begin{pmatrix} \cos\phi & -\sin\phi \\ \sin\phi & \cos\phi \end{pmatrix}, \ \tilde{\Lambda} = R(2\phi); \tag{A.10}$$

$$\text{Mirror about the } yz \text{ plane}: \ \Lambda = M_x = \begin{pmatrix} -1 & 0 \\ 0 & 1 \end{pmatrix}, \ \tilde{\Lambda} = \begin{pmatrix} 1 & 0 \\ 0 & -1 \end{pmatrix}; \tag{A.11}$$

$$\text{Mirror about the } xz \text{ plane}: \ \Lambda = M_y = \begin{pmatrix} 1 & 0 \\ 0 & -1 \end{pmatrix}, \ \tilde{\Lambda} = \begin{pmatrix} 1 & 0 \\ 0 & -1 \end{pmatrix}. \tag{A.12}$$

Each lattice structure depicted in Fig. 2.2 (a)-(e) is invariant under the following transformation:

$$\text{(a) } R(\pi/3), M_x \ \text{ (b) } R(2\pi/3), M_x \ \text{ (c) } R(\pi) \ \text{ (d) } R(\pi/2), M_x, M_y \ \text{ (e) } R(\pi), M_x, M_y, \tag{A.13}$$

so that we require Eq. (A.9) for these transformations to obtain constraints on C, D, and F. For instance, we find that (i) $F = 0$ from the invariance under rotation through $\phi = \pi$, which is satisfied by all vortex lattices except (b), since $\Lambda = -I$ and $\tilde{\Lambda} = I$ (identity). (ii) From the invariance under rotation through ϕ, we obtain

$$(C_{11} - C_{22})\sin(2\phi) = C_{12}\sin(2\phi) = (D_{11} - D_{22})\sin\phi = D_{12}\sin\phi = 0. \tag{A.14}$$

We find $C_{11} = C_{22}$ and $C_{12} = 0$ for $\phi \neq n\pi/2$ and $D_{11} = D_{22}$ and $D_{12} = 0$ for $\phi \neq n\pi$ ($n \in \mathbb{Z}$). (iii) From the invariance under the mirror reflection about the yz plane, we find $C_{12} = D_{12} = F_{11} = F_{22} = 0$. (iv) From the invariance under rotation through $\phi = 2\pi/3$, we find $F_{12} = F_{21}$. By combining these results, we obtain Eqs. (3.43) and (3.44) after setting the elastic constants as

$$(C_1, C_2, C_3, D_1, D_2, D_3, F_1) := (C_{11}, C_{22}, 2C_{12}, D_{11}, D_{22}, 2D_{12}, 2F_{12}). \tag{A.15}$$

A.3 Phase correlation function

In this section, we describe the derivation of the phase correlation function (3.75). By substituting the correlator with respect to the phase in Eq. (3.72) into Eq. (3.75), this correlation function is expressed as

$$\langle [\theta_\uparrow(\mathbf{r}) - \theta_\uparrow(\mathbf{0})]^2 \rangle \approx \frac{2}{nF\ell^2} \left[G(\mathbf{0};\alpha) - G(\mathbf{r};\alpha) \right], \tag{A.16}$$

where F is constant, since we are considering overlapping triangular lattices. We obtain a Green's function for two-dimensional Poisson's equation $G(\mathbf{r};\alpha)$ as

$$G(\mathbf{r};\alpha) = \frac{1}{A}\sum_{\mathbf{k}\neq\mathbf{0}} \frac{1}{k^2} \mathrm{e}^{-\alpha k + \mathrm{i}\mathbf{k}\cdot\mathbf{r}} = \frac{1}{A}\sum_{\mathbf{k}\neq\mathbf{0}} \frac{1}{k^2} \mathrm{e}^{-\alpha k + \mathrm{i}kr\cos\theta}, \tag{A.17}$$

where we express the wave vector $\mathbf{k}$ using the polar coordinate (k, θ) with θ which is the angle relative to $\mathbf{r}$. Though the logarithmic behavior of a Green's function for two-dimensional Poisson's equation is standard, we derive it for the present regularization scheme using the convergence factor $\mathrm{e}^{-\alpha k}$.

By differentiating Eq. (A.17) with respect to r, we have

$$-\frac{\partial}{\partial r}G(\mathbf{r};\alpha) = \frac{1}{A}\sum_{\mathbf{k}\neq\mathbf{0}}\frac{-\mathrm{i}\cos\theta}{k}\mathrm{e}^{-\alpha k+\mathrm{i}kr\cos\theta} = \frac{1}{(2\pi)^2}\int_0^{2\pi}\mathrm{d}\theta\int_0^{\infty}\mathrm{d}k\ (-\mathrm{i}\cos\theta)\mathrm{e}^{-k(\alpha-\mathrm{i}r\cos\theta)}$$
$$= \frac{1}{(2\pi)^2}\int_0^{2\pi}\mathrm{d}\theta\frac{-\mathrm{i}\cos\theta}{\alpha-\mathrm{i}r\cos\theta}. \tag{A.18}$$

By defining $z=\mathrm{e}^{\mathrm{i}\theta}$, we can rewrite the last integral as a contour integral along the unit circle, which is given by

$$-\frac{\partial}{\partial r}G(\mathbf{r};\alpha) = \frac{1}{(2\pi)^2}\oint\frac{\mathrm{d}z}{\mathrm{i}z}\frac{z^2+1}{r(z^2+1)+2\mathrm{i}\alpha z} = \frac{1}{(2\pi)^2\mathrm{i}r}\oint\mathrm{d}z\frac{z^2+1}{z(z-z_+)(z-z_-)}, \tag{A.19}$$

where $z_\pm=\mathrm{i}(-\alpha\pm\sqrt{r^2+\alpha^2})/r$ are the locations of poles. Since $|z_+|<1<|z_-|$, the integral picks up the residues at $z=0$ and z_+, leading to

$$-\frac{\partial}{\partial r}G(\mathbf{r};\alpha) = \frac{1}{2\pi r}\left[\frac{1}{z_+z_-}+\frac{z_+^2+1}{z_+(z_+-z_-)}\right] = \frac{1}{2\pi r}\left(1-\frac{\alpha}{\sqrt{r^2+\alpha^2}}\right). \tag{A.20}$$

Therefore, $G(\mathbf{0};\alpha)-G(\mathbf{r};\alpha)$ in Eq. (A.16) can be calculated as

$$G(\mathbf{0};\alpha)-G(\mathbf{r};\alpha) = \frac{1}{2\pi}\lim_{a_0\to0}\int_{a_0}^{r}\mathrm{d}r'\left(\frac{1}{r'}-\frac{\alpha}{r'\sqrt{r'^2+\alpha^2}}\right)$$
$$= \frac{1}{2\pi}\lim_{a_0\to0}\left(\ln\frac{r}{a_0}+\operatorname{arsinh}\frac{\alpha}{r}-\operatorname{arsinh}\frac{\alpha}{a_0}\right) = \frac{1}{2\pi}\left(\ln\frac{r}{2\alpha}+\operatorname{arsinh}\frac{\alpha}{r}\right). \tag{A.21}$$

By substituting the above equation into Eq. (A.16) and taking the limit $r\gg\alpha$, we obtain Eq. (3.75).

Appendix B

Details of calculation of interaction matrix elements

In this chapter, we describe the derivation of the representation of the interaction matrix element (4.10) by calculating Eq. (4.9). We rewrite the LLL magnetic Bloch state (4.2) as

$$\Psi_{\mathbf{k}\alpha}(\mathbf{r}) = \frac{1}{\sqrt{A\zeta(\mathbf{k})}} \sum_{\mathbf{m}} (-1)^{m_1 m_2} \exp\Bigg[-\frac{1}{4\ell^2}(\mathbf{r}^2 + \mathbf{r}_{\mathbf{m}}^2) + \frac{1}{2\ell^2}\mathbf{r}\cdot(\mathbf{r}_{\mathbf{m}} - i\epsilon_\alpha \mathbf{r}_{\mathbf{m}} \times \mathbf{e}_z) + i\mathbf{k}\cdot\mathbf{r}_{\mathbf{m}}\Bigg]. \tag{B.1}$$

The product of the four wave functions in Eq. (4.9) is integrated as

$$\begin{aligned}
&\left[\prod_j \zeta(\mathbf{k}_j)\right]^{1/2} \int d^2\mathbf{r}\ \Psi^*_{\mathbf{k}_1\alpha}(\mathbf{r})\Psi^*_{\mathbf{k}_2\beta}(\mathbf{r})\Psi_{\mathbf{k}_3\beta}(\mathbf{r})\Psi_{\mathbf{k}_4\alpha}(\mathbf{r}) \\
&= \frac{1}{A^2}\sum_{\{\mathbf{m}_j\}} (-1)^{\sum_j m_{j1}m_{j2}} \int d^2\mathbf{r}\ \exp\Bigg[-\frac{1}{\ell^2}\mathbf{r}^2 + \frac{1}{2\ell^2}\mathbf{r}\cdot\sum_j(\mathbf{r}_{\mathbf{m}_j} - i\epsilon_j\mathbf{r}_{\mathbf{m}_j}\times\mathbf{e}_z) \\
&\qquad\qquad - \frac{1}{4\ell^2}\sum_j \mathbf{r}^2_{\mathbf{m}_j} + i\sum_j \tilde{\mathbf{k}}_j\cdot\mathbf{r}_{\mathbf{m}_j}\Bigg] \\
&= \frac{1}{2AN_{\mathrm{v}}}\sum_{\{\mathbf{m}_j\}} (-1)^{\sum_j m_{j1}m_{j2}} \exp\left[F_{\alpha\beta}(\mathbf{r}_{\mathbf{m}_1},\mathbf{r}_{\mathbf{m}_2},\mathbf{r}_{\mathbf{m}_3},\mathbf{r}_{\mathbf{m}_4}) + i\sum_j \tilde{\mathbf{k}}_j\cdot\mathbf{r}_{\mathbf{m}_j}\right],
\end{aligned} \tag{B.2}$$

where we define $(\epsilon_1,\epsilon_2,\epsilon_3,\epsilon_4) := (-\epsilon_\alpha,-\epsilon_\beta,\epsilon_\beta,\epsilon_\alpha)$, $\tilde{\mathbf{k}}_{1,2} := -\mathbf{k}_{1,2}$, $\tilde{\mathbf{k}}_{3,4} := \mathbf{k}_{3,4}$, and

$$F_{\alpha\beta}(\mathbf{r}_{\mathbf{m}_1},\mathbf{r}_{\mathbf{m}_2},\mathbf{r}_{\mathbf{m}_3},\mathbf{r}_{\mathbf{m}_4}) := \frac{1}{16\ell^2}\left[\sum_j(\mathbf{r}_{\mathbf{m}_j} - i\epsilon_j\mathbf{r}_{\mathbf{m}_j}\times\mathbf{e}_z)\right]^2 - \frac{1}{4\ell^2}\sum_j \mathbf{r}^2_{\mathbf{m}_j}. \tag{B.3}$$

After we introduce $\mathbf{n}_j = \mathbf{m}_j - \mathbf{m}_4$ $(j = 1, 2, 3)$, we find that $F_{\alpha\beta}(\mathbf{r}_{\mathbf{m}_1}, \mathbf{r}_{\mathbf{m}_2}, \mathbf{r}_{\mathbf{m}_3}, \mathbf{r}_{\mathbf{m}_4})$ is rewritten as

$$\begin{aligned}
&F_{\alpha\beta}(\mathbf{r}_{\mathbf{m}_1}, \mathbf{r}_{\mathbf{m}_2}, \mathbf{r}_{\mathbf{m}_3}, \mathbf{r}_{\mathbf{m}_4}) \\
&= \frac{1}{16\ell^2}\left[4\mathbf{r}_{\mathbf{m}_4} + \sum_{j=1}^{3}(\mathbf{r}_{\mathbf{n}_j} - i\epsilon_j \mathbf{r}_{\mathbf{n}_j} \times \mathbf{e}_z)\right]^2 - \frac{1}{4\ell^2}\left[\sum_{j=1}^{3}(\mathbf{r}_{\mathbf{m}_4} + \mathbf{r}_{\mathbf{n}_j})^2 + \mathbf{r}_{\mathbf{m}_4}^2\right] \\
&= -\frac{i}{2\ell^2}\mathbf{r}_{\mathbf{m}_4} \cdot \sum_{j=1}^{3}\epsilon_j(\mathbf{r}_{\mathbf{n}_j} \times \mathbf{e}_z) + \tilde{F}_{\alpha\beta}(\mathbf{r}_{\mathbf{n}_1}, \mathbf{r}_{\mathbf{n}_2}, \mathbf{r}_{\mathbf{n}_3}) \\
&= -i\pi \sum_{j=1}^{3}\epsilon_j(m_{41}n_{j2} - m_{42}n_{j1}) + \tilde{F}_{\alpha\beta}(\mathbf{r}_{\mathbf{n}_1}, \mathbf{r}_{\mathbf{n}_2}, \mathbf{r}_{\mathbf{n}_3}),
\end{aligned} \tag{B.4}$$

where we define

$$\begin{aligned}
\tilde{F}_{\alpha\beta}(\mathbf{r}_{\mathbf{n}_1}, \mathbf{r}_{\mathbf{n}_2}, \mathbf{r}_{\mathbf{n}_3}) &:= \frac{1}{16\ell^2}\left[\sum_{j=1}^{3}(\mathbf{r}_{\mathbf{n}_j} - i\epsilon_j \mathbf{r}_{\mathbf{n}_j} \times \mathbf{e}_z)\right]^2 - \frac{1}{4\ell^2}\sum_{j=1}^{3}\mathbf{r}_{\mathbf{n}_j}^2 \\
&= \frac{1}{8\ell^2}\sum_{i<j}\left[(1 - \epsilon_i\epsilon_j)\mathbf{r}_{\mathbf{n}_i} \cdot \mathbf{r}_{\mathbf{n}_j} + i(\epsilon_i - \epsilon_j)(\mathbf{r}_{\mathbf{n}_i} \times \mathbf{r}_{\mathbf{n}_j})_z\right] - \frac{1}{4\ell^2}\sum_{j=1}^{3}\mathbf{r}_{\mathbf{n}_j}^2.
\end{aligned} \tag{B.5}$$

We find that Eq. (B.2) is rewritten as

$$\begin{aligned}
&\frac{1}{2AN_{\mathrm{v}}}\sum_{\mathbf{m}_4,\mathbf{n}_1,\mathbf{n}_2,\mathbf{n}_3}(-1)^{m_{41}m_{42}+\sum_{j=1}^{3}(m_{41}+n_{j1})(m_{42}+n_{j2})}(-1)^{-\sum_{j=1}^{3}\epsilon_j(m_{41}n_{j2}-m_{42}n_{j1})} \\
&\quad \times \exp\left[\tilde{F}_{\alpha\beta}(\mathbf{r}_{\mathbf{n}_1}, \mathbf{r}_{\mathbf{n}_2}, \mathbf{r}_{\mathbf{n}_3}) + i\left(\sum_{j=1}^{4}\tilde{\mathbf{k}}_j\right) \cdot \mathbf{r}_{\mathbf{m}_4} + i\sum_{j=1}^{3}\tilde{\mathbf{k}}_j \cdot \mathbf{r}_{\mathbf{n}_j}\right] \\
&= \frac{1}{2A}\delta^{\mathrm{P}}_{\sum_{j=1}^{4}\tilde{\mathbf{k}}_j,\mathbf{0}}\sum_{\mathbf{n}_1,\mathbf{n}_2,\mathbf{n}_3}(-1)^{\sum_{j=1}^{3}n_{j1}n_{j2}}\exp\left[\tilde{F}_{\alpha\beta}(\mathbf{r}_{\mathbf{n}_1}, \mathbf{r}_{\mathbf{n}_2}, \mathbf{r}_{\mathbf{n}_3}) + i\sum_{j=1}^{3}\tilde{\mathbf{k}}_j \cdot \mathbf{r}_{\mathbf{n}_j}\right],
\end{aligned} \tag{B.6}$$

where $\delta^{\mathrm{P}}_{\mathbf{k},\mathbf{k}'} = \sum_{\mathbf{G}}\delta_{\mathbf{k},\mathbf{k}'+\mathbf{G}}$ is the periodic Kronecker's delta with $\mathbf{G}$ running over the reciprocal lattice vector. The interaction matrix element is given as in Eq. (4.10) with

$$\begin{aligned}
&S_{\alpha\beta}(\mathbf{k}_1, \mathbf{k}_2, \mathbf{k}_3) \\
&= \sum_{\mathbf{n}_1,\mathbf{n}_2,\mathbf{n}_3}(-1)^{\sum_j n_{j1}n_{j2}}\exp[\tilde{F}_{\alpha\beta}(\mathbf{r}_{\mathbf{n}_1}, \mathbf{r}_{\mathbf{n}_2}, \mathbf{r}_{\mathbf{n}_3}) - i\mathbf{k}_1 \cdot \mathbf{r}_{\mathbf{n}_1} - i\mathbf{k}_2 \cdot \mathbf{r}_{\mathbf{n}_2} + i\mathbf{k}_3 \cdot \mathbf{r}_{\mathbf{n}_3}].
\end{aligned} \tag{B.7}$$

We discuss the case of parallel fields ($\epsilon_\uparrow = \epsilon_\downarrow = +1$). In this case, the function $S_{\alpha\beta}(\mathbf{k}_1, \mathbf{k}_2, \mathbf{k}_3)$ does not depend on both α and β, so that we can drop the subscripts α, β. By utilizing

$$4\ell^2\tilde{F}(\mathbf{r}_{\mathbf{n}_1}, \mathbf{r}_{\mathbf{n}_2}, \mathbf{r}_{\mathbf{n}_3}) = -\sum_j \mathbf{r}_{\mathbf{n}_j}^2 + (\mathbf{r}_{\mathbf{n}_2} \cdot \mathbf{r}_{\mathbf{n}_3} + \mathbf{r}_{\mathbf{n}_1} \cdot \mathbf{r}_{\mathbf{n}_3}) - i(\mathbf{r}_{\mathbf{n}_2} \times \mathbf{r}_{\mathbf{n}_3} + \mathbf{r}_{\mathbf{n}_1} \times \mathbf{r}_{\mathbf{n}_3})_z, \tag{B.8}$$

we obtain

$$
\begin{aligned}
S(\mathbf{k}_1,\mathbf{k}_2,\mathbf{k}_3) = &\sum_{\mathbf{n}} (-1)^{n_1 n_2} \exp\left(-\mathbf{r}_\mathbf{n}^2/4\ell^2 + i\mathbf{k}_3\cdot\mathbf{r}_\mathbf{n}\right) \\
&\times \zeta\left(\mathbf{k}_1 + (\mathbf{r}_\mathbf{n}\times\mathbf{e}_z + i\mathbf{r}_\mathbf{n})/4\ell^2\right)\zeta\left(\mathbf{k}_2 + (\mathbf{r}_\mathbf{n}\times\mathbf{e}_z + i\mathbf{r}_\mathbf{n})/4\ell^2\right),
\end{aligned}
\tag{B.9}
$$

where we rewrite the sums over $\mathbf{n}_1$ and $\mathbf{n}_2$ in terms of $\zeta(\mathbf{k})$ given in Eq. (4.3) and change the remaining dummy variable $\mathbf{n}_3$ to $\mathbf{n}$. To rewrite this, we exploit the following property of $\zeta(\mathbf{k})$ for $\mathbf{s}\in\mathbb{Z}^2$ given as

$$
\begin{aligned}
&\zeta\left(\mathbf{k} + (\mathbf{r}_\mathbf{s}\times\mathbf{e}_z + i\mathbf{r}_\mathbf{s})/2\ell^2\right) \\
&= \sum_{\mathbf{m}} (-1)^{m_1 m_2} \exp\left[(-\mathbf{r}_\mathbf{m}^2 + 2\mathbf{r}_\mathbf{m}\cdot\mathbf{r}_\mathbf{s})/4\ell^2 - i(\mathbf{r}_\mathbf{m}\times\mathbf{r}_\mathbf{s})_z/2\ell^2 - i\mathbf{k}\cdot\mathbf{r}_\mathbf{m}\right] \\
&= \sum_{\mathbf{m}} (-1)^{m_1 m_2} \exp\left[-(\mathbf{r}_\mathbf{m}-\mathbf{r}_\mathbf{s})^2/4\ell^2 + \mathbf{r}_\mathbf{s}^2/4\ell^2 - i\pi(m_1 s_2 - m_2 s_1) - i\mathbf{k}\cdot\mathbf{r}_\mathbf{m}\right] \\
&= (-1)^{s_1 s_2}\exp\left(\mathbf{r}_\mathbf{s}^2/4\ell^2 - i\mathbf{k}\cdot\mathbf{r}_\mathbf{s}\right)\sum_{\mathbf{m}}(-1)^{(m_1-s_1)(m_2-s_2)} \\
&\qquad \times \exp\left[-(\mathbf{r}_\mathbf{m}-\mathbf{r}_\mathbf{s})^2/4\ell^2 - i\mathbf{k}\cdot(\mathbf{r}_\mathbf{m}-\mathbf{r}_\mathbf{s})\right] \\
&= (-1)^{s_1 s_2}\exp\left(\mathbf{r}_\mathbf{s}^2/4\ell^2 - i\mathbf{k}\cdot\mathbf{r}_\mathbf{s}\right)\zeta(\mathbf{k}).
\end{aligned}
\tag{B.10}
$$

By setting $\mathbf{n} = 2\mathbf{s} + \mathbf{p}$ with $\mathbf{s}\in\mathbb{Z}^2$ and $\mathbf{p}\in\{0,1\}^2$ and using the property above, Eq. (B.9) is rewritten as

$$
\begin{aligned}
&S(\mathbf{k}_1,\mathbf{k}_2,\mathbf{k}_3) \\
&= \sum_{\mathbf{p}\in\{0,1\}^2}\sum_{\mathbf{s}} (-1)^{p_1 p_2}\exp\Big[-(2\mathbf{r}_\mathbf{s}+\mathbf{r}_\mathbf{p})^2/4\ell^2 + i\mathbf{k}_3\cdot(2\mathbf{r}_\mathbf{s}+\mathbf{r}_\mathbf{p}) + \mathbf{r}_\mathbf{s}^2/2\ell^2 \\
&\qquad\qquad - i(\mathbf{k}_1+\mathbf{k}_2)\cdot\mathbf{r}_\mathbf{s} - i(\mathbf{r}_\mathbf{p}\times\mathbf{e}_z + i\mathbf{r}_\mathbf{p})\cdot\mathbf{r}_\mathbf{s}/2\ell^2\Big] \\
&\qquad \times \zeta\left(\mathbf{k}_1 + (\mathbf{r}_\mathbf{p}\times\mathbf{e}_z + i\mathbf{r}_\mathbf{p})/4\ell^2\right)\zeta\left(\mathbf{k}_2 + (\mathbf{r}_\mathbf{p}\times\mathbf{e}_z + i\mathbf{r}_\mathbf{p})/4\ell^2\right) \\
&= \sum_{\mathbf{p}\in\{0,1\}^2} (-1)^{p_1 p_2}\exp\left(-\mathbf{r}_\mathbf{p}^2/4\ell^2 + i\mathbf{k}_3\cdot\mathbf{r}_\mathbf{p}\right)\tilde{\zeta}\left(\mathbf{k}_1+\mathbf{k}_2-2\mathbf{k}_3 + (\mathbf{r}_\mathbf{p}\times\mathbf{e}_z - i\mathbf{r}_\mathbf{p})/2\ell^2\right) \\
&\qquad \times \zeta\left(\mathbf{k}_1 + (\mathbf{r}_\mathbf{p}\times\mathbf{e}_z + i\mathbf{r}_\mathbf{p})/4\ell^2\right)\zeta\left(\mathbf{k}_2 + (\mathbf{r}_\mathbf{p}\times\mathbf{e}_z + i\mathbf{r}_\mathbf{p})/4\ell^2\right).
\end{aligned}
\tag{B.11}
$$

For antiparallel fields, $S_{\uparrow\uparrow}(\mathbf{k}_1,\mathbf{k}_2,\mathbf{k}_3)$ is given by $S(\mathbf{k}_1,\mathbf{k}_2,\mathbf{k}_3)$ in Eq. (B.11). The other quantities which are given in Eq. (4.13) are obtained by using the relation $\Psi_{\mathbf{k}\downarrow}(\mathbf{r}) = \Psi^*_{-\mathbf{k}\uparrow}(\mathbf{r})$ only for antiparallel fields to $S_{\alpha\beta}(\mathbf{k}_1,\mathbf{k}_2,\mathbf{k}_3)$.

Appendix C

Details of calculation of a long-range interaction potential

We have introduced the long-range interaction potential $U_G(\mathbf{r}-\mathbf{r}')$[1] in Eq. (5.17), which appears in the entanglement Hamiltonian for overlapping triangular lattices. To derive $U_G(\mathbf{r}-\mathbf{r}')$, we set $\mathbf{r}'=\mathbf{0}$ and calculate

$$U_2(\mathbf{r};\alpha)=\sum_{\mathbf{k}\neq\mathbf{0}}\frac{1}{V|\mathbf{k}|}\mathrm{e}^{-\alpha|\mathbf{k}|+\mathrm{i}\mathbf{k}\cdot\mathbf{r}}. \tag{C.1}$$

By taking the infinite-volume limit $V\to\infty$, this is rewritten in the integral form as

$$U_2(\mathbf{r};\alpha)=\int\frac{\mathrm{d}^2\mathbf{k}}{(2\pi)^2}\frac{1}{|\mathbf{k}|}\mathrm{e}^{-\alpha|\mathbf{k}|+\mathrm{i}\mathbf{k}\cdot\mathbf{r}}. \tag{C.2}$$

We obtain $U_2(\mathbf{r})$ by taking the limit $\alpha\to 0^+$.

By introducing the polar coordinate (k,θ), the integral (C.2) is rewriten as

$$U_2(\mathbf{r};\alpha)=\frac{1}{(2\pi)^2}\int_0^{2\pi}\mathrm{d}\theta\int_0^{\infty}\mathrm{d}k\ \mathrm{e}^{-\alpha k+\mathrm{i}kr\cos\theta}=\frac{1}{(2\pi)^2}\int_0^{2\pi}\mathrm{d}\theta\frac{1}{\alpha-ir\cos\theta}. \tag{C.3}$$

By defining $z=\mathrm{e}^{\mathrm{i}\theta}$ to rewrite the last integral in Eq. (C.3) into a contour integral along the unit circle, we obtain

$$U_2(\mathbf{r};\alpha)=\frac{1}{2\pi^2}\oint\mathrm{d}z\frac{1}{r(z^2+1)+2\mathrm{i}\alpha z}=\frac{1}{2\pi^2 r}\oint\mathrm{d}z\frac{1}{(z-z_+)(z-z_-)}, \tag{C.4}$$

where $z_\pm=\mathrm{i}\left(-\alpha\pm\sqrt{r^2+\alpha^2}\right)/r$ give the locations of poles. As the integral picks up the residue at $z=z_+$ due to $|z_+|<1<|z_-|$, this leads to

$$U_2(\mathbf{r};\alpha)=\frac{\mathrm{i}}{\pi r(z_+-z_-)}=\frac{1}{2\pi\sqrt{r^2+\alpha^2}}\to\frac{1}{2\pi r}\ (\alpha\to 0^+). \tag{C.5}$$

From Eq. (C.5), we find the long-range interaction potential $U_G(\mathbf{r}-\mathbf{r}')$ in Eq. (5.17).

[1] The long-range interaction potentials for one- and three-dimensional systems are discussed in App. A of Ref. [30].

Acknowledgements

The works in this thesis were conducted by the author as a Ph.D. student at Prof. Masahito Ueda group in the University of Tokyo. I would like to express my gratitude to my collaborators and colleagues.

First of all, I would like to express my gratitude to Prof. Masahito Ueda, who is my advisor, for encouraging me during my Ph.D. program. I also thank him for reading my thesis with lots of patience and time to improve the quality of the contents and my English.

I would also like to thank my collaborator Prof. Shunsuke Furukawa for discussing with me to accomplish my studies during my Ph.D course. He suggested me many ideas and spent a long time to improve my research through discussions. My thesis cannot be accomplished without his help and endurance. He read and corrected abstracts for conferences and papers so that I could improve my English skill to explain my work. I also thank him for checking my slides so that I can clearly explain my work.

I would like to thank Dr. Sho Higashikawa in discussing the effective-field theory of vortex lattices. With his advice, I obtained many analytical results which made me possible to discuss numerical results.

I would like to thank Dr. Yukio Tanaka and Dr. Yuki Kawaguchi for arranging my visit in Nagoya University. It was a great experience since it broadened my view to physics and I realized many different styles and nature of researchers during the stay. I would like to thank Terumichi Ohashi for many discussions about my research and the other topics as well as for fun chat. I would like to express my gratitude to all the members in Tanaka group for making a kind and comfortable atmosphere.

I am really thankful to Asako Takeuchi for helping me a lot of dealing with paper works. I would like to thank her for making cakes for celebrations and creating a good atmosphere in the room 949.

I would like to express my special gratitude to all the present and former members in the Ueda group, including Prof. Masaya Nakagawa, Prof. Kazuya Fujimoto, Dr. Taiki Haga, Dr. Ulrich Ebling, Dr. Kohaku H. Z. So, Dr. Yusuke Horinouchi, Dr. Yuto Murashita, Prof. Tomohiro Shitara, Dr. Shuhei Yoshida, Prof. Yuto Ashida, Dr. Ryusuke Hamazaki, Dr. Naoto Kura, Dr. Zongping Gong, Kohei Kawabata, Zhikang Wang, Norifumi Matsumoto, Ziyin Liu, Kangqiao Liu, Shoki Sugimoto and Yuki Sakamoto.

I would like to thank my parents for mental, financial and physical substantial supports which were indispensable to complete the Ph.D. course.

Finally, I acknowledge financial supports from the Japan Society for the Promotion of Science (JSPS) through the Program for Leading Graduate Schools “Advanced Leading Graduate Course for Photon Science” (ALPS). I appreciate this program for getting

rid of my worry to economic conditions during a Ph.D. course. I would also like to thank Grant-in-Aid for Scientific Research on Innovative Areas “Topological Materials Science” (KAKENHI Grant No. JP15H05852) for the financial support on my visit to Nagoya University through its domestic exchange program for young researchers.

Bibliography

[1] M. H. Anderson, J. R. Ensher, M. R. Matthews, C. E. Wieman, and E. A. Cornell. Observation of Bose-Einstein Condensation in a Dilute Atomic Vapor. *Science*, 269(5221):198, 1995.

[2] K. B. Davis, M. O. Mewes, M. R. Andrews, N. J. van Druten, D. S. Durfee, D. M. Kurn, and W. Ketterle. Bose-Einstein Condensation in a Gas of Sodium Atoms. *Phys. Rev. Lett.*, 75:3969, 1995.

[3] C. C. Bradley, C. A. Sackett, J. J. Tollett, and R. G. Hulet. Evidence of Bose-Einstein Condensation in an Atomic Gas with Attractive Interactions. *Phys. Rev. Lett.*, 75:1687, 1995.

[4] C. J. Myatt, E. A. Burt, R. W. Ghrist, E. A. Cornell, and C. E. Wieman. Production of Two Overlapping Bose-Einstein Condensates by Sympathetic Cooling. *Phys. Rev. Lett.*, 78:586–589, 1997.

[5] G. Modugno, M. Modugno, F. Riboli, G. Roati, and M. Inguscio. Two Atomic Species Superfluid. *Phys. Rev. Lett.*, 89:190404, 2002.

[6] Y. Kawaguchi and M. Ueda. Spinor Bose–Einstein condensates. *Physics Reports*, 520(5):253 – 381, 2012.

[7] D. M. Stamper-Kurn, M. R. Andrews, A. P. Chikkatur, S. Inouye, H.-J. Miesner, J. Stenger, and W. Ketterle. Optical Confinement of a Bose-Einstein Condensate. *Phys. Rev. Lett.*, 80:2027–2030, 1998.

[8] A. Görlitz, T. L. Gustavson, A. E. Leanhardt, R. Löw, A. P. Chikkatur, S. Gupta, S. Inouye, D. E. Pritchard, and W. Ketterle. Sodium Bose-Einstein Condensates in the $f = 2$ State in a Large-Volume Optical Trap. *Phys. Rev. Lett.*, 90:090401, 2003.

[9] A. Griesmaier, J. Werner, S. Hensler, J. Stuhler, and T. Pfau. Bose-Einstein Condensation of Chromium. *Phys. Rev. Lett.*, 94:160401, 2005.

[10] R. J. Donnelly. *Quantized Vortices in Helium II.* Cambridge University Press, 2005.

[11] M. R. Matthews, B. P. Anderson, P. C. Haljan, D. S. Hall, C. E. Wieman, and E. A. Cornell. Vortices in a Bose-Einstein Condensate. *Phys. Rev. Lett.*, 83:2498, 1999.

[12] K. W. Madison, F. Chevy, W. Wohlleben, and J. Dalibard. Vortex Formation in a Stirred Bose-Einstein Condensate. *Phys. Rev. Lett.*, 84:806, 2000.

[13] A. L. Fetter. Rotating trapped Bose-Einstein condensates. *Rev. Mod. Phys.*, 81:647, 2009.

[14] J. R. Abo-Shaeer, C. Raman, J. M. Vogels, and W. Ketterle. Observation of Vortex Lattices in Bose-Einstein Condensates. *Science*, 292(5516):476, 2001.

[15] P. Engels, I. Coddington, P. C. Haljan, and E. A. Cornell. Nonequilibrium Effects of Anisotropic Compression Applied to Vortex Lattices in Bose-Einstein Condensates. *Phys. Rev. Lett.*, 89:100403, 2002.

[16] V. Schweikhard, I. Coddington, P. Engels, V. P. Mogendorff, and E. A. Cornell. Rapidly Rotating Bose-Einstein Condensates in and near the Lowest Landau Level. *Phys. Rev. Lett.*, 92:040404, 2004.

[17] E. J. Mueller and T. L. Ho. Two-Component Bose-Einstein Condensates with a Large Number of Vortices. *Phys. Rev. Lett.*, 88:180403, 2002.

[18] K. Kasamatsu, M. Tsubota, and M. Ueda. Vortex Phase Diagram in Rotating Two-Component Bose-Einstein Condensates. *Phys. Rev. Lett.*, 91:150406, 2003.

[19] V. Schweikhard, I. Coddington, P. Engels, S. Tung, and E. A. Cornell. Vortex-Lattice Dynamics in Rotating Spinor Bose-Einstein Condensates. *Phys. Rev. Lett.*, 93:210403, 2004.

[20] M. C. Beeler, R. A. Williams, K. Jimenez-Garcia, L. J. LeBlanc, A. R. Perry, and I. B. Spielman. The spin Hall effect in a quantum gas. *Nature*, 498(7453):201, 2013.

[21] Y. J. Lin, K. Jiménez-García, and I. B. Spielman. Spin–orbit-coupled Bose–Einstein condensates. *Nature*, 471:83, 2011.

[22] Y.-J. Lin, R. L. Compton, K. Jimenez-Garcia, J. V. Porto, and I. B. Spielman. Synthetic magnetic fields for ultracold neutral atoms. *Nature*, 462(7273):628, 2009.

[23] S. Furukawa and M. Ueda. Global phase diagram of two-component Bose gases in antiparallel magnetic fields. *Phys. Rev. A*, 90:033602, 2014.

[24] S. Furukawa and M. Ueda. Quantum Hall phase diagram of two-component Bose gases: Intercomponent entanglement and pseudopotentials. *Phys. Rev. A*, 96:053626, 2017.

[25] N. Laflorencie. Quantum entanglement in condensed matter systems. *Physics Reports*, 646:1 – 59, 2016.

[26] M. A. Metlitski and T. Grover. Entanglement entropy of systems with spontaneously broken continuous symmetry. arXiv:1112.5166, 2011.

[27] A. Kitaev and J. Preskill. Topological Entanglement Entropy. *Phys. Rev. Lett.*, 96:110404, 2006.

[28] X.-L. Qi, H. Katsura, and A. W. W. Ludwig. General Relationship between the Entanglement Spectrum and the Edge State Spectrum of Topological Quantum States. *Phys. Rev. Lett.*, 108:196402, 2012.

[29] R. Lundgren, Y. Fuji, S. Furukawa, and M. Oshikawa. Entanglement spectra between coupled Tomonaga-Luttinger liquids: Applications to ladder systems and topological phases. *Phys. Rev. B*, 88:245137, 2013.

[30] T. Yoshino, S. Furukawa, and M. Ueda. Intercomponent entanglement entropy and spectrum in binary Bose-Einstein condensates. arXiv:2009.02949, 2020.

[31] T. Yoshino, S. Furukawa, S. Higashikawa, and M. Ueda. Collective modes of vortex lattices in two-component Bose–Einstein condensates under synthetic gauge fields. *New Journal of Physics*, 21(1):015001, 2019.

[32] K. Kasamatsu, M. Tsubota, and M. Ueda. VORTICES IN MULTICOMPONENT BOSE–EINSTEIN CONDENSATES. *International Journal of Modern Physics B*, 19(11):1835, 2005.

[33] P. Ao and S. T. Chui. Binary Bose-Einstein condensate mixtures in weakly and strongly segregated phases. *Phys. Rev. A*, 58:4836–4840, 1998.

[34] S. T. Chui and P. Ao. Broken cylindrical symmetry in binary mixtures of Bose-Einstein condensates. *Phys. Rev. A*, 59:1473–1476, 1999.

[35] M. Trippenbach, K. Góral, K. Rzazewski, B. Malomed, and Y. B. Band. Structure of binary Bose-Einstein condensates. *J. Phys. B: At. Mol. Opt. Phys. 33 4017*, 2000.

[36] C. J. Myatt, E. A. Burt, R. W. Ghrist, E. A. Cornell, and C. E. Wieman. Production of Two Overlapping Bose-Einstein Condensates by Sympathetic Cooling. *Phys. Rev. Lett.*, 78:586–589, 1997.

[37] D. S. Hall, M. R. Matthews, C. E. Wieman, and E. A. Cornell. Measurements of Relative Phase in Two-Component Bose-Einstein Condensates. *Phys. Rev. Lett.*, 81:1543–1546, 1998.

[38] H.-J. Miesner, D. M. Stamper-Kurn, J. Stenger, S. Inouye, A. P. Chikkatur, and W. Ketterle. Observation of Metastable States in Spinor Bose-Einstein Condensates. *Phys. Rev. Lett.*, 82:2228–2231, 1999.

[39] A. J. Leggett. *Quantum liquids Bose condensation and Cooper pairing in condensed-matter systems*. Oxford University Press, 2006.

[40] D. A. Butts and D. S. Rokhsar. Predicted signatures of rotating Bose–Einstein condensates. *Nature*, 397:327, 1999.

[41] N. R. Cooper. Rapidly rotating atomic gases. *Advances in Physics*, 57(6):539, 2008.

[42] A. A. Abrikosov. On the Magnetic properties of superconductors of the second group. *Sov. Phys. JETP*, 5:1174, 1957. [Zh. Eksp. Teor. Fiz.32,1442(1957)].

[43] J. Dalibard, F. Gerbier, G. Juzeliūnas, and P. Öhberg. *Colloquium* : Artificial gauge potentials for neutral atoms. *Rev. Mod. Phys.*, 83:1523, 2011.

[44] G. Baym and C. J. Pethick. Vortex core structure and global properties of rapidly rotating Bose-Einstein condensates. *Phys. Rev. A*, 69:043619, 2004.

[45] G. Watanabe, S. A. Gifford, G. Baym, and C. J. Pethick. Structure of vortices in rotating Bose-Einstein condensates. *Phys. Rev. A*, 74:063621, 2006.

[46] T. L. Ho. Bose-Einstein Condensates with Large Number of Vortices. *Phys. Rev. Lett.*, 87:060403, 2001.

[47] M. Keçeli and M. Ö. Oktel. Tkachenko modes and structural phase transitions of the vortex lattice of a two-component Bose-Einstein condensate. *Phys. Rev. A*, 73:023611, 2006.

[48] H. Watanabe and H. Murayama. Redundancies in Nambu-Goldstone Bosons. *Phys. Rev. Lett.*, 110:181601, 2013.

[49] S. Moroz, C. Hoyos, C. Benzoni, and D. T. Son. Effective field theory of a vortex lattice in a bosonic superfluid. *SciPost Phys.*, 5:39, 2018.

[50] J. Sinova, C. B. Hanna, and A. H. MacDonald. Quantum Melting and Absence of Bose-Einstein Condensation in Two-Dimensional Vortex Matter. *Phys. Rev. Lett.*, 89:030403, 2002.

[51] A. Aftalion, X. Blanc, and J. Dalibard. Vortex patterns in a fast rotating Bose-Einstein condensate. *Phys. Rev. A*, 71:023611, 2005.

[52] C. J. Pethick and H. Smith. *Bose–Einstein Condensation in Dilute Gases*. Cambridge University Press, 2 edition, 2008.

[53] O. Penrose and L. Onsager. Bose-Einstein Condensation and Liquid Helium. *Phys. Rev.*, 104:576–584, 1956.

[54] C. N. Yang. Concept of Off-Diagonal Long-Range Order and the Quantum Phases of Liquid He and of Superconductors. *Rev. Mod. Phys.*, 34:694–704, 1962.

[55] S. I. Matveenko and G. V. Shlyapnikov. Tkachenko modes and their damping in the vortex lattice regime of rapidly rotating bosons. *Phys. Rev. A*, 83:033604, 2011.

[56] M. P. Kwasigroch and N. R. Cooper. Quantum fluctuations of vortex lattices in ultracold gases. *Phys. Rev. A*, 86:063618, 2012.

[57] E. I. Rashba, L. E. Zhukov, and A. L. Efros. Orthogonal localized wave functions of an electron in a magnetic field. *Phys. Rev. B*, 55:5306, 1997.

[58] A. A. Burkov. Fractional quantum Hall effect and featureless Mott insulators. *Phys. Rev. B*, 81:125111, 2010.

[59] I. Panfilov, A. Patri, Kun Yang, and A. A. Burkov. Chiral spin liquid from magnetic Wannier states. *Phys. Rev. B*, 93:125126, 2016.

[60] J. Zak. Magnetic Translation Group. *Phys. Rev.*, 134:A1602, 1964.

[61] A. M. Perelomov. On the completeness of a system of coherent states. *Theoretical and Mathematical Physics*, 6(2):156, 1971.

[62] G. Baym. Tkachenko modes of vortex lattices in rapidly rotating bose-einstein condensates. *Phys. Rev. Lett.*, 91:110402, 2003.

[63] E. B. Sonin. Vortex oscillations and hydrodynamics of rotating superfluids. *Rev. Mod. Phys.*, 59:87, 1987.

[64] H. Watanabe and H. Murayama. Unified Description of Nambu-Goldstone Bosons without Lorentz Invariance. *Phys. Rev. Lett.*, 108:251602, 2012.

[65] Yoshimasa Hidaka. Counting rule for nambu-goldstone modes in nonrelativistic systems. *Phys. Rev. Lett.*, 110:091601, Feb 2013.

[66] Daisuke A. Takahashi and Muneto Nitta. Counting rule of nambu–goldstone modes for internal and spacetime symmetries: Bogoliubov theory approach. *Annals of Physics*, 354:101 – 156, 2015.

[67] I. Coddington, P. Engels, V. Schweikhard, and E. A. Cornell. Observation of tkachenko oscillations in rapidly rotating bose-einstein condensates. *Phys. Rev. Lett.*, 91:100402, 2003.

[68] S. J. Woo, S. Choi, L. O. Baksmaty, and N. P. Bigelow. Dynamics of vortex matter in rotating two-species bose-einstein condensates. *Phys. Rev. A*, 75:031604, Mar 2007.

[69] P. Calabrese and J. Cardy. Entanglement entropy and quantum field theory. *Journal of Statistical Mechanics: Theory and Experiment*, 2004(06):P06002, 2004.

[70] H. Li and F. D. M. Haldane. Entanglement Spectrum as a Generalization of Entanglement Entropy: Identification of Topological Order in Non-Abelian Fractional Quantum Hall Effect States. *Phys. Rev. Lett.*, 101:010504, 2008.

[71] X. Chen and E. Fradkin. Quantum entanglement and thermal reduced density matrices in fermion and spin systems on ladders. *J. Stat. Mech. Theor. Exp.*, 2013(08):P08013, 2013.

[72] I. Peschel. LETTER TO THE EDITOR: Calculation of reduced density matrices from correlation functions. *J. Physics A: Mathematical and General*, 36:L205–L208, 2003.

[73] I. Peschel and V. Eisler. Reduced density matrices and entanglement entropy in free lattice models. *Journal of Physics A: Mathematical and Theoretical*, 42(50):504003, 2009.

[74] G. Misguich, V. Pasquier, and M. Oshikawa. Finite-size scaling of the Shannon-Rényi entropy in two-dimensional systems with spontaneously broken continuous symmetry. *Phys. Rev. B*, 95:195161, 2017.

[75] J. W. Reijnders, F. J. M. van Lankvelt, K. Schoutens, and N. Read. Rotating spin-1 bosons in the lowest Landau level. *Phys. Rev. A*, 69:023612, 2004.

[76] J. W. Reijnders, F. J. M. van Lankvelt, K. Schoutens, and N. Read. Quantum Hall States and Boson Triplet Condensate for Rotating Spin-1 Bosons. *Phys. Rev. Lett.*, 89:120401, 2002.